ACNP-64611

ELK RIVER REACTOR
OPERATIONS ANALYSIS PROGRAM

Annual Progress Report

July 1, 1963 - June 30, 1964

PREPARED FOR

Chicago Operations Office
U.S. Atomic Energy Commission

Under
Project Agreement No. 1
to
Contract AT(11-1)-1357

by

M.N. Audi
J.R. Fisher
C. Ho
E.D. Kendrick
T.P. Kruzic
A.C. Schafer, Jr.

ALLIS-CHALMERS MANUFACTURING COMPANY
Atomic Energy Division
Bethesda, Maryland

DISCLAIMER

AEC LEGAL NOTICE

DISTRIBUTION

External Copies	
1 - 4	Chicago Operations Office U. S. Atomic Energy Commission 9800 South Cass Avenue Argonne, Illinois Attention: Director, Reactor Engineering Division
5 - 6	Division of Reactor Development U. S. Atomic Energy Commission Washington 25, D. C. Attention: Chief, Water Reactors Branch Civilian Power
7	Division of Reactor Development U. S. Atomic Energy Commission Washington 25, D. C. Attention: Chief, Water Systems Branch Army Reactors
8	Division of Reactor Development U. S. Atomic Energy Commission Washington 25, D. C. Attention: Chief, Reactor Engineering Branch Naval Reactors
9	Dairyland Power Cooperative Association 2615 East Avenue, South (LACBWR Site) La Crosse, Wisconsin Attention: J. Floyd, USAEC Site Representative
10 - 12	Rural Cooperative Power Association Elk River, Minnesota Attention: E. J. Welsh, Manager Nuclear Contract Department
13	Combustion Engineering, Inc. 1000 Prospect Hill Road Windsor, Connecticut Attention: J. M. West

14	Atomic Energy Division Babcock and Wilcox Company Lynchburg, Virginia Attention: J. F. Mumm
15	Atomic Power Department Westinghouse Electric Corporation Post Office Box 355 Pittsburgh 30, Pennsylvania Attention: W. E. Johnson
16 - 35 (plus master)	Division of Technical Information Extension Post Office Box 62 Oak Ridge, Tennessee
36	Consumers Public Power District General Office Post Office Box 477 Columbus, Nebraska
37	Atomics International A Division of North American Aviation, Inc. Post Office Box 309 Canoga Park, California Attention: H. J. Rubinstein
38	City of Piqua Piqua Nuclear Power Facility Piqua, Ohio
39	Dr. J. A. Thie Room 511 2893 Knox Avenue, South Minneapolis 8, Minnesota
40	Nuclear Utility Services, Inc. 1730 M Street, N. W. Washington, D. C. Attention: J. A. Signorelli

CONTENTS

FIGURES

TABLES

1. INTRODUCTION AND SUMMARY

During the report period, integrated operation of the reactor plant was achieved at power levels up to 58.2 Mwt. Initial production of electrical power from the nuclear plant was achieved on August 24, 1963. During power escalation from 5 Mwe to 8.8 Mwe, an irregularity in feedwater flow was observed in Loop No. 1. The cause of this irregularity was found to be hydraulic, and corrective actions were taken. Activity in the off-gas system, caused by tramp uranium on the fuel elements, was a source of operating difficulty which led to operation of the reactor in the "non-vented" condition. With the exception of the aforementioned problems, operation of the plant was satisfactory.

The operations analysis has progressed in accordance with the work outlined on task scoping sheets which were prepared to provide a detailed description of the work scheduled under the program.[1] Data taken during reactor operation have been used in determination of core nuclear characteristics and in areas of core management. Topical reports have been written to describe the determination of the fuel loading for the second core and to describe the control rod analysis. A summary of the work covered in the topical reports is included in this report.

Operating data have also been used to provide a reference for comparing and evaluating the performance of the Plant Energy Transfer and Primary Auxiliary Systems. The performance of these systems has agreed generally with the design parameters. The results of heat balance calculations and overall heat transfer coefficients are included within this report.

Several miscellaneous evaluations were undertaken during the report period, including a study of the long-term-decontamination and waste-disposal requirements, cask handling and storage and control rod disposition. Significant changes in the plant equipment during the report period are described so that the reader may be kept up to date with the reactor plant covered by the analysis.

The Elk River Reactor (ERR) Operations Analysis Program was initiated in November of 1962, under contract with the Atomic Energy Commission. The program technically analyzes and evaluates plant performance in support of the primary objective of the reactor plant, which is to demonstrate a high plant availability factor, consistent with concurrent objectives of low-cost power generation and safe operation.

This annual report covers the activities for the period July 1, 1963 to June 30, 1964 and is in lieu of two semiannual reports covering the same period. The reader is referred to the first semiannual progress report (ACNP-63605) for a detailed description of the overall program responsibilities and for a reasonably detailed description of the reactor plant.

Task scoping sheets were prepared for the Chicago Operations Office, USAEC, to describe the tasks to be performed under the contract. The task scoping sheets provide a description of the work currently in progress and of the program work scheduled for the near future. Frequent reviews allow continuation or curtailment of the work or redirection and expansion to new objectives without undue loss of effort or continuity. New tasks are added from

time to time as directed by the Chicago Operations Office, USAEC, or as recommended by the Allis-Chalmers project staff. A listing of the presently scoped tasks and their objectives is given in Appendix A of this report.

2. REACTOR OPERATING SUMMARY

A tabular summary of the operation of the Elk River Reactor for this report period is given in Table 1. The emergency and test (E&T) condenser was used as a heat sink during power testing throughout July and most of August, 1963. In July, a new leakproof exhaust duct with an in-line blower was installed to replace the original furnace-type duct. In August, sodium pentaborate solution was substituted for boric acid solution in the boron poison system.

TABLE 1
ERR OPERATING HISTORY*

month	reactor heat generation (Mwd)	average power (Mwt)	maximum power (Mwt)	net electrical generation (kwhr)	plant heat rate** (Btu/kwhr)
July 1963	83.3	3.48	35.4***	---	---
Aug. 1963	51.6	2.15	34.9***	136,200	15,000(4)
Sept. 1963	50.4	2.18	20	343,890	14,900(6)
Oct. 1963	0	0	0	---	---
Nov. 1963	0	0	0	---	---
Dec. 1963	14.1	0.59	18.24	68,576	14,600(1)
Jan. 1964	349.7	13.04	25	3,114,500	13,100
Feb. 1964	1295.0	44.7	58.2	12,165,826	10,800
Mar. 1964	1001.5	32.3	58.2	9,286,861	10,930
Apr. 1964	0	0	0	---	---
May 1964	0	0	0	---	---
June 1964	0	0	0	---	---

* From Monthly Operational Reports - Elk River Reactor
** Number in parentheses indicates days of operation over which plant heat rate is calculated
*** Operation with Emergency and Test Condenser (E&T)

The superheater and turbine were placed in service on August 24, 1963, and an electrical output of 5 Mw was achieved. On August 25, the output was raised to 8.8 Mwe. As the level was being established at the higher power, an irregularity in feedwater flow was observed in Loop No. 1. Accompanying this behavior was a rise and fall in primary pressure. The turbine output, however, remained constant. The transient occurred regularly at about

2-min intervals and was pulse-like rather than oscillatory. Since this behavior could not be explained, the plant was shut down. Pertinent variables were wired for readout on the Offner Recorder and additional operations were conducted to investigate the cause of the difficulty.

Most of the operation time during September 1963 was spent in studying the pulsing problem and in accumulating subcooling data. The cause of the problem was determined to be hydraulic and was apparently caused by a horizontal run of pipe in the feedwater return downcomer, beyond the evaporator. It was postulated that this horizontal run of pipe had trapped steam below the condensed water and that periodic venting of this steam back to the water box of the evaporator had caused the observed pulse-like flow of condensate. A concurrent problem which hampered operations was tramp uranium on the fuel elements, causing rubidium activity in the off-gas system that resulted in off-gas duct damper closure.

The reactor was not operated during October, November, and most of December. The outage was for a general safety review prior to the continuation of the Elk River Reactor Test Program.

On December 30, 1963, the power level was increased to 18 Mwt and remained at this level to the beginning of January. Operation at this level indicated no appreciable concentration of radiolytic gases in the primary system, even though the reactor was operated in the non-vented condition. The reactor was operated through January 15 at power levels up to approximately 24 Mwt, in accordance with a planned program. Throttling of the primary feedwater return valves maintained a sufficient water level in the downcomer to prevent pulsing.

On February 11 the ERR achieved full-power operation. A 28-day warranty run was started on February 17, and continued uninterrupted through the end of the month. The run was terminated in March, when the reactor was shut down in order to make the required plant modifications. The reactor was not operated during the months of April, May, and June, while changes were made in the primary feedwater piping and the off-gas system. During this shutdown period, a primary-to-secondary leak in Evaporator No. 1 was located and the leaking tubes were plugged. A stainless-steel liner was installed in the fuel element storage well and the primary relief valves were repaired.

3. NUCLEAR CHARACTERISTICS

3.1 REACTIVITY HISTORY (Task 102)

The objective of this task is to determine the amounts of total reactivity left as a function of time and to determine the reactivity in temperature, voids, xenon, and burnup as a function of time.

3.1.1 Normalized One-dimensional Model

The excess reactivity of the Elk River core at 68 F was measured during the atmospheric

testing program, using the fuel-addition and boric-acid-addition methods.[1] The reactivity was not directly measured at conditions of higher temperature. The experimental information available at these temperatures consists of the measured critical 13-rod (and sometimes 12-rod*) bank position and the differential reactivity worths of the rod banks for incremental displacements about the critical position. A simplified, iterative normalization procedure has been developed that can obtain, from this experimental information, the excess reactivity of the core and the effective poison cross-section of the control-rod bank. The core model used in this iterative procedure is a one-dimensional, axial representation that uses the WANDA-4[13] code with a window-shade mockup of the control rods.

The iterative normalization procedure is as follows: From a set of Westcott-type, two-group cross sections for the core and reflector, a set of values is chosen for the core absorption cross section ($\sum a^{core}$). For each value of $\sum a^{core}$, execute, using the WANDA-4 code, a criticality search for the effective poison cross-section of the 13-rod bank ($\sum p^{13\ rods}$), which gives $k_{eff} = 1.0$ with the control-rod bank at the measured critical position. By using this poison cross-section and slightly displacing the control-rod bank, the differential rod worth is obtained around the critical position. This procedure is repeated until the measured differential worth of the 13-rod bank is reproduced. When a measured critical 12-rod-bank position and differential worth is also available, this procedure is repeated as a check. Using the $\sum a^{core}$ and $\sum p^{13\ rods}$ previously determined, a criticality search is executed for the effective poison cross-section of the center rod ($\sum p^{1\ rod}$) below the 12-rod-bank critical position. Slight displacement of the rod bank yields the differential worth around the critical position. Each value of $\sum a^{core}$ uniquely determines a $\sum p^{13\ rods}$, $\sum p^{1\ rod}$, and the 12- and 13-rod-bank differential worths.

The above normalization procedure is used directly to determine the excess reactivity and the reactivity in temperature for any non-voided core condition in which a measured critical bank position and a measured differential rod worth are available. This model has been used successfully in generating rod calibration curves and in investigating reactivity insertion rates (see Sec. 5.3).

The normalization procedure was applied to four core conditions (68 F, 300 F, 470 F, and 537 F) to obtain the reactivity at each temperature. The measured critical rod-bank positions and differential worths are given in Table 2, along with the deduced k_{eff} for each case.

3.1.2 GAM-TEMPEST-PDQ Model

The methods described in Sec. 3.1.1 permit the normalization of a simple and economical core model to a previously measured condition. However, to evaluate core conditions and modes of operation that have not been measured requires a more detailed and exact core model. Such a model is necessary, for example, in the calculations required for the specifications of the second core feed enrichment (Task 205) and the replacement control rods

* The 12-rod bank here refers to the case with the center control rod fully inserted.

TABLE 2

MEASURED VALUES OF CRITICAL POSITION AND DIFFERENTIAL ROD WORTH

	critical position (in. of withdrawal)		differential rod worth (¢/in.)		deduced k_{eff}
	13 rods	12 rods	13 rods	12 rods	
68 F	12.5		149		1.117
300 F	13.6		142		1.1198
470 F	15.4	17.70	132	96.5	1.114
537 F	16.53		124		1.106

(Task 204) and in the investigation of the effects of any core condition changes, such as fuel burnup, on the available reactivity. Accordingly, a core model has been developed which has given good agreement with the measurements and which will be used for all detailed calculations in this program. A description of the geometric and nuclear aspects of this model follows.

Three geometric models have been used in the program: the cell model, the quarter core model and the whole-core model.

A control cell is defined as four fuel elements and the associated zirconium shroud, water gap, zirconium posts, and control rods or zirconium-rod followers. Figure 1 shows a typical cell. In the cell model, the zirconium posts, shroud, control rods or followers, and the water gap are represented explicitly. The material inside the shrouds, i.e., the fuel, cladding, and moderator are homogenized into one region. This configuration is represented by a basic 40 x 40 mesh in PDQ 2-90[2] calculations and is generally used for comparative calculations of the effects of changes in material parameters and dimensions.

The quarter core model represents one-fourth of the core (see Fig. 2 and assumes quarter-core symmetry. As in the cell model, the shrouds, posts, water gaps, and control rods or followers are represented explicitly, the fuel elements inside the shrouds being homogenized as one region. This model, which uses the maximum mesh available (73 x 73) for the PDQ 2-90, is used for all core conditions that have quarter-core symmetry.

All calculations have been performed with either three or four neutron-energy groups, using the two-dimensional diffusion theory code (PDQ 2-90) on the IBM 7090. The neutron-energy groups comprise those listed in Table 3.

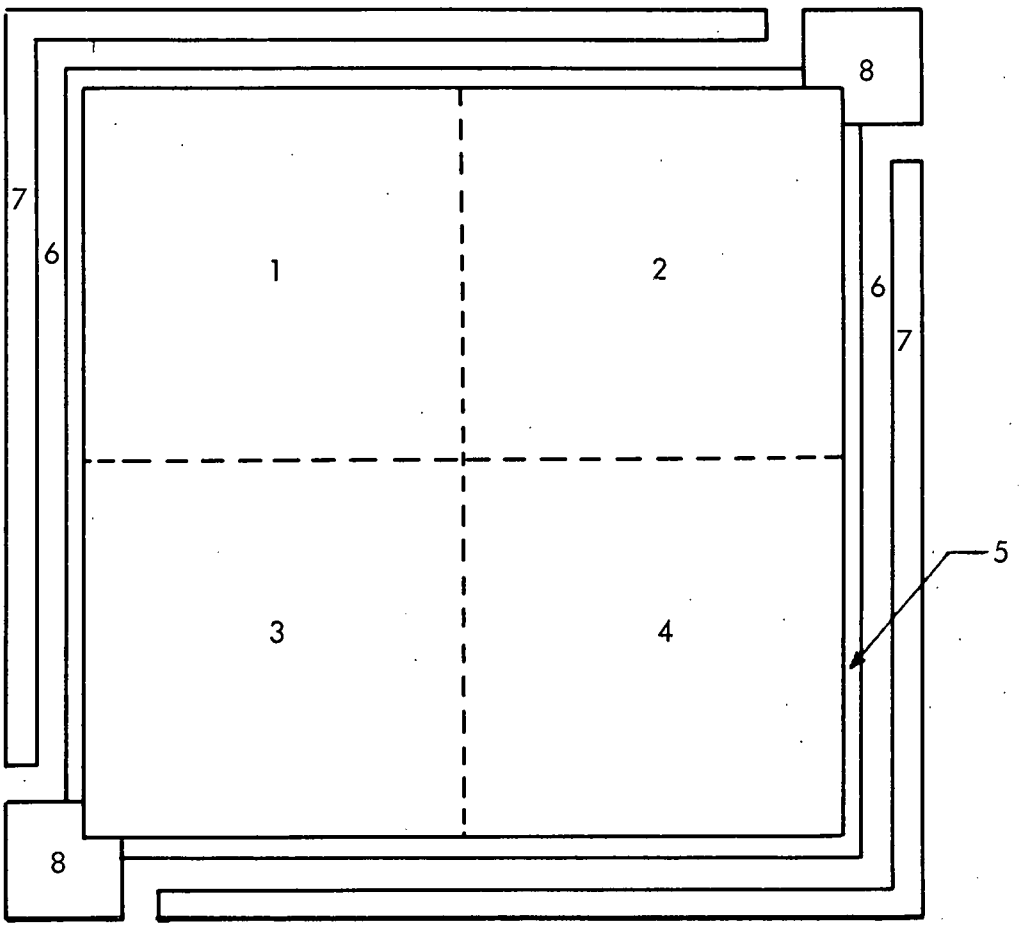

1
2
3
4 } Fuel Elements

5 Zr Shrouds
6 Water Channel
7 Control Rod or Zr Follower
8 Zr Posts

CONTROL CELL LAYOUT

FIG. 1

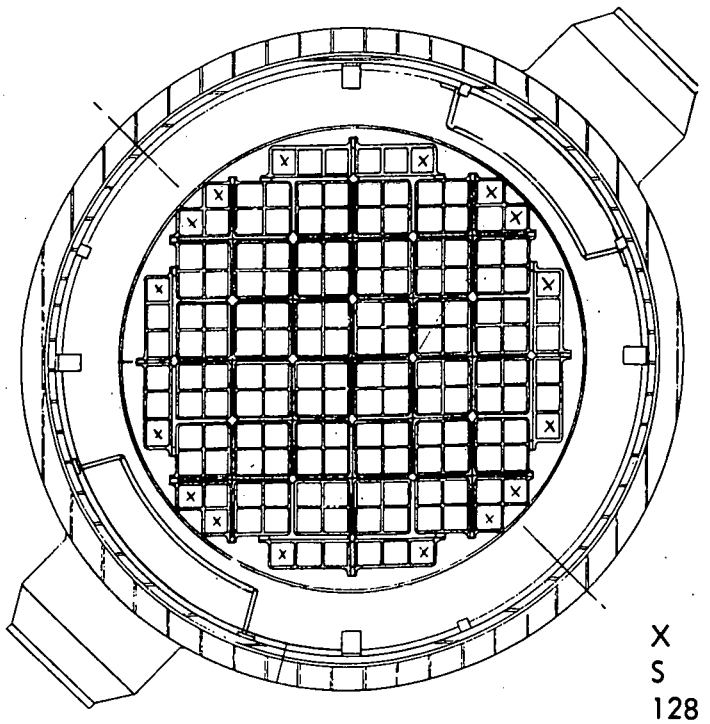

LEGEND

X	denotes dummy elements
S	denotes spiked elements
128	regular elements enriched 4.3%
20	spiked elements enriched 5.2%

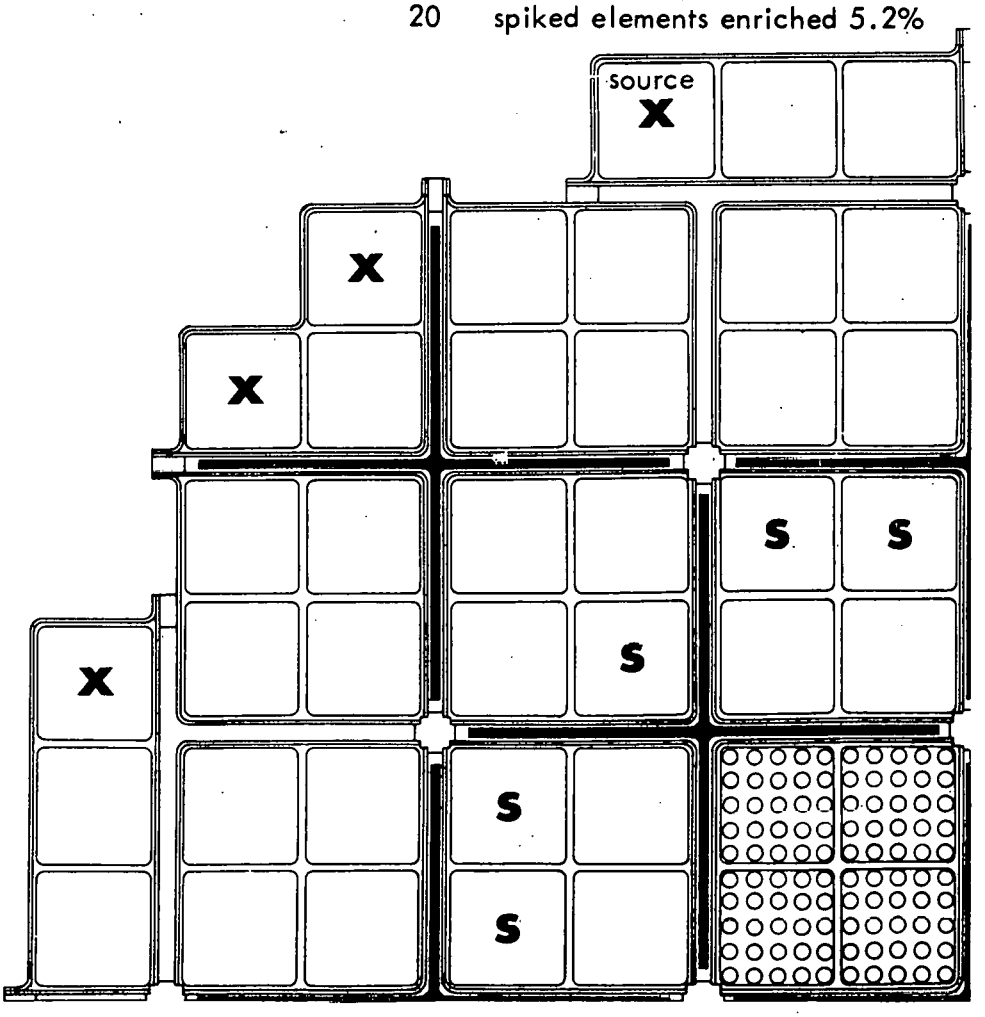

CORE LOADED WITH REGULAR AND SPIKED ELEMENTS

FIG. 2

TABLE 3.

NEUTRON ENERGY GROUPS

three group		four group	
(1)	10^7 ev - 5.53×10^3 ev	(1)	10^7 ev - 454 ev
(2)	5.53×10^3 ev - 0.625 ev	(2)	454 ev - 4 ev
(3)	0.625 ev - 0 ev	(3)	4 ev - 0.625 ev
		(4)	0.625 ev - 0 ev

The energy-averaged diffusion parameters over the fast (>0.625 ev) groups are obtained from the GAM[3] code for all materials other than control rods, and energy-averaged thermal parameters are obtained directly from the TEMPEST-II[4] code except in the case of the control-rod materials and the fuel region inside the shrouds.

3.1.3 Comparison of GAM-TEMPEST-PDQ Model with Experiment

To test the validity of the GAM-TEMPEST-PDQ model, the model values were compared with measurements that were done during the initial startup of the Elk River Reactor. Two unrodded cores were calculated, one containing 148 regular elements and the other containing 128 regular elements and 20 spiked elements. Table 4 lists the deduced and calculated excess reactivities.

TABLE 4

EXCESS REACTIVITIES FOR TWO UNRODDED CORES

	k_{eff}		reactivity (%Δk/k)	
	deduced	calculated	deduced	calculated
148 regular	1.103	1.095	9.32	8.68
128 regular 20 spiked	1.117	1.112	10.5	10.1

3.1.4 Intracell Flux Distributions

In all calculations using the PDQ 2-90 code, the fuel assemblies inside the shrouds have been treated as a homogenized region. To account for the actual intracell flux distribution, the thermal constants in the fuel region are weighted with thermal flux ratios for the fuel pins, cladding, and moderator, to give the correct thermal utilization. The thermal utilization in the fuel region is given by:

$$f = \frac{\int_E \int_V^{\text{fuel}} \Sigma_a(r,E)\, \phi(r,E)\, dV\, dE}{\int_E \int_V^{\text{cell}} \Sigma_a(r,E)\, \phi(r,E)\, dV\, dE}$$

which is sometimes approximated by

$$f \sim \frac{(\bar{\Sigma}_a \bar{\phi} V)_o}{\sum_i (\bar{\Sigma}_a \bar{\phi} V)_i}, \quad i = 0, 1, 2$$

where,

$\bar{\Sigma}_a^i$ is the average macroscopic cross section for the i^{th} material,

$\bar{\phi}_i$ is the average flux in the i^{th} material,

V_i is the volume of the i^{th} material, and

i the material index, is 0, 1, or 2 for fuel moderator or for cladding.

The average cross section, $\bar{\Sigma}_a^i$, is averaged over the thermal spectrum determined by the Wigner-Wilkins equation. The relative fluxes, $\bar{\phi}_i$, are determined from these cross sections, using one of several available approximations to the transport equation. The use of this approximate form of the thermal utilization for the Elk River core, however, yields calculated reactivities higher than the measurements. Consequently, a better prescription for the thermal utilization was developed that could be used quickly and inexpensively.

The weakness of the old approximation was not in the conventional determination of the average cross section $(\bar{\Sigma}_a^i)$ or of the corresponding average flux, but in the assumption that the two quantities could be separately averaged. Accordingly, the following prescription was used:

$$f \simeq \frac{\sum_j \left[\Sigma_a(E_j)\right]_o \bar{\phi}_o(E_j) V_o \int_{E_j} \phi(E)\, dE}{\sum_i \left(\sum_j \left[\Sigma_a(E_j)\right]_i \bar{\phi}_i(E_j) V_i \int_{E_j} \phi(E)\, dE \right)}$$

where,

i = material index,

j = energy index

$\sum_a(E_i)$ is the absorption cross section at energy E_i,

$\bar{\phi}(E_i)$ is the relative spatial averaged flux at energy E_i,

V is the volume, and

$\int_{E_i} \phi(E)\,dE$ is the integrated flux in interval dE.

A comparison of the two methods of obtaining the thermal utilization is given in Table 5. The thermal utilization determined by the old approximation is designated as Method $\left[(\bar{\sum})(\bar{\phi})\right]$ and the new prescription is designated as Method $\left[\bar{\sum}\bar{\phi}\right]$. The subscripts (P_3) and (C&P) identify the approximation used for the transport equation. The first subscript (P_3) denotes the standard P_3 approximation in cylindrical geometry[6]; the second (C&P) denotes the Carlvik & Pershagen method.[7,8] The Carlvik & Pershagen method has been compared with solutions of the transport equation by numerical integration (i.e., S_n approximation) and by the spherical harmonics method (P_n approximation) and, in general, has been shown superior to a P_5 approximation and slightly less accurate than an S_8 approximation.

TABLE 5

THERMAL UTILIZATION METHOD RESULTS

method	f	%△f/f
$\left[(\bar{\sum})(\bar{\phi})\right]_{C\&P}$	0.78420	2.03
$\left[\sum\bar{\phi}\right]_{C\&P}$	0.76824	
$\left[(\bar{\sum})(\bar{\phi})\right]_{P_3}$	0.78941	1.78
$\left[\sum\bar{\phi}\right]_{P_3}$	0.77535	

Results using the two prescriptions are also shown in Fig. 3 for reactivity versus moderator temperature, where the values of k_{eff} deduced from the measurements (see Table 2) are plotted along with the k_{eff} calculated by both the old and new methods of obtaining the thermal utilization. For convenience in comparison, the calculations have been normalized to the measured k_{eff} at 68 F. The new method follows more closely the variation of reactivity with temperature.

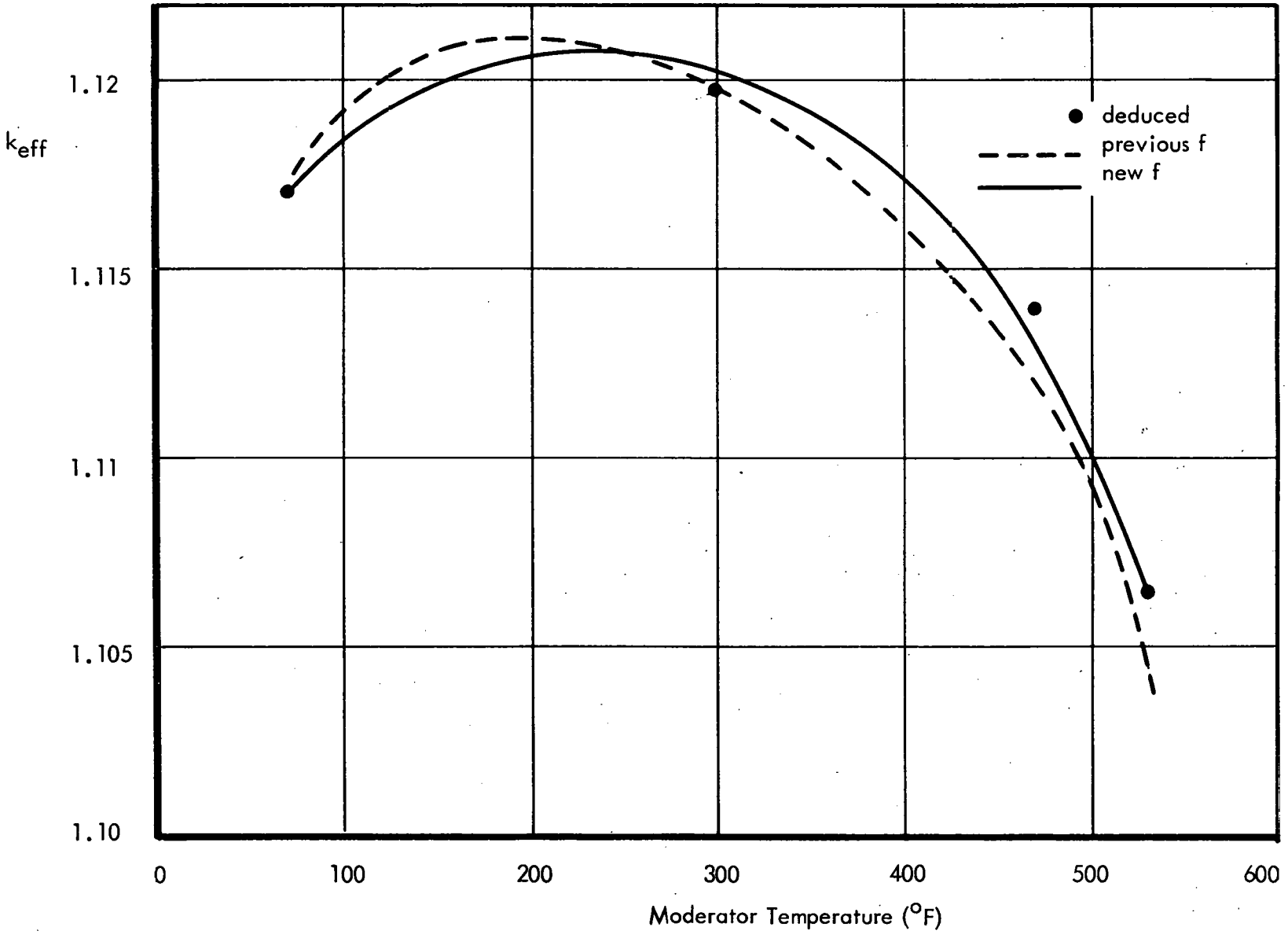

THERMAL UTILIZATION RESULTS WITH OLD AND NEW METHODS

FIG. 3

3.1.5 Xenon Buildup to Equilibrium

Xenon buildup to equilibrium has been calculated for full power and has been compared with the observed movement of the center rod. The resulting calibration of the center rod enables the reactivity resulting from exposure during the 28-day power run to be determined. The core-average value of the neutron flux cannot be used directly in calculating the xenon buildup in a reactor, since the neutron flux distribution is not uniform. This non-uniformity causes a higher rate of xenon buildup than would be predicted by use of the average flux. This effect has previously been investigated in a study of non-uniform reactivity effects in the Elk River core.[9] From the xenon reactivity calculated in this study (2.31 percent Δk), a non-uniform, corrected average flux may be obtained:

$$\left.\frac{\Delta k}{k}\right|_{Xe}^{Nu} = \frac{f_1 - f(Xe)}{f_1}$$

$$\phi^{Nu} = \frac{\lambda_{Xe} + \Delta\frac{1}{f}\sigma_a}{0.069\ \sigma_f \sigma_{Xe} - \Delta\frac{1}{f}\sigma_a \sigma_{Xe}}$$

where $\Delta\frac{1}{f} = \frac{1}{f_1} - \frac{1}{f(Xe)}$

Using this flux and the relation:

$$N_{Xe} = 0.00768\left[(1 + 0.8325\, e^{-(\phi\sigma + \lambda)t}) - 1.8325\, e^{-2.9t}\right]$$

where t is the time in seconds.

The xenon buildup to equilibrium may be calculated. Table 6 gives the results of the calculations. Figure 4 shows a plot of the xenon worth, along with the observed center-rod movement, which yields a calibration of the center-rod worth versus position.

The deduced value of worth of equilibrium xenon at full power is 2.5 percent Δk (see Sec. 3.1.7).

3.1.6 Reactivity with Burnup

A calculation has been performed of reactivity versus time for the first 100 full-power days. Each isotopic contributor was determined individually, with the assumption that all other contributors remained unperturbed. The total reactivity change was obtained by summing the reactivity contributions from the individual isotopes. A plot of the reactivity versus full-power days is shown in Fig. 5.

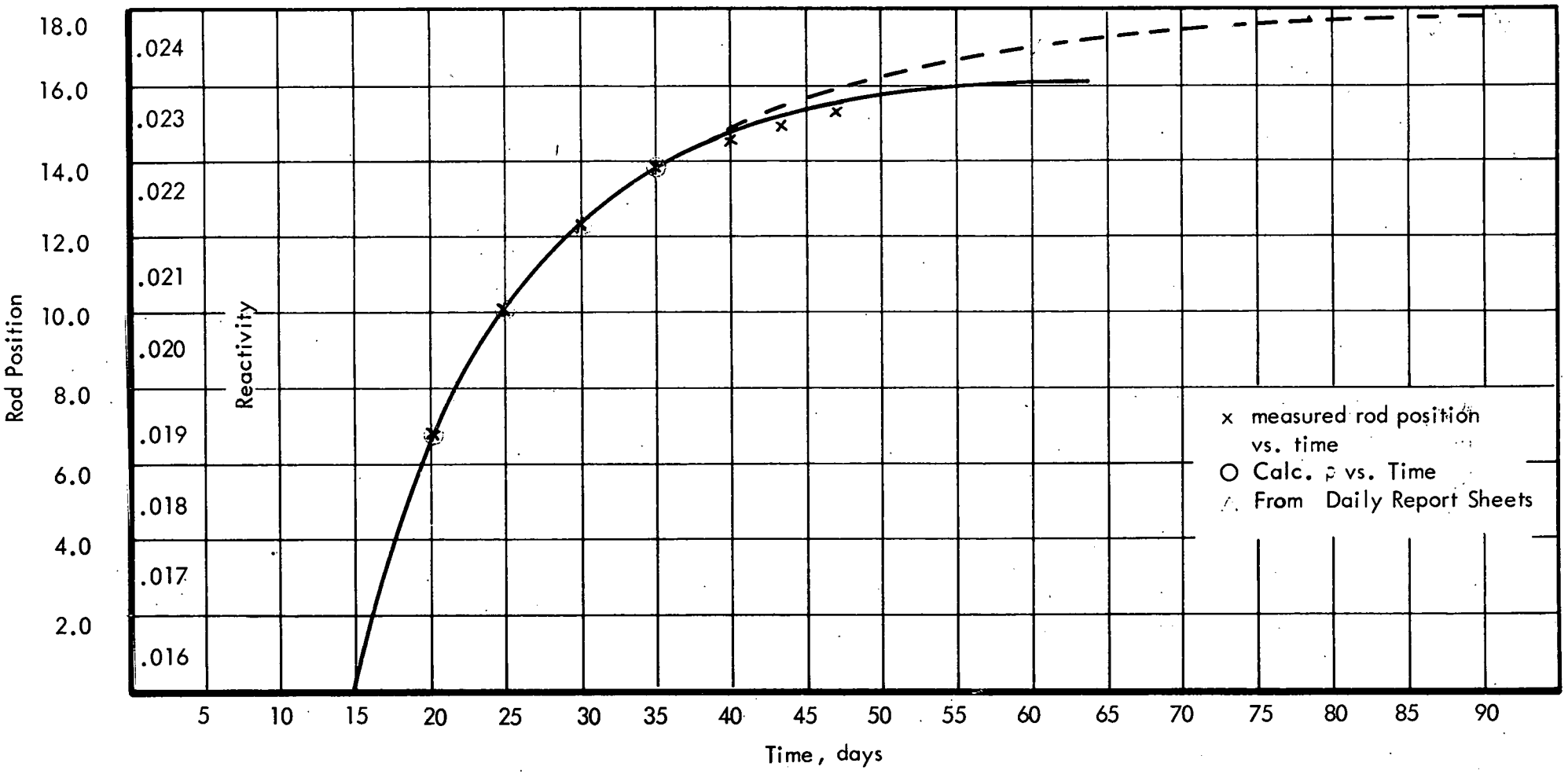

RODS MOVEMENT & Xe BUILDUP

FIG. 4

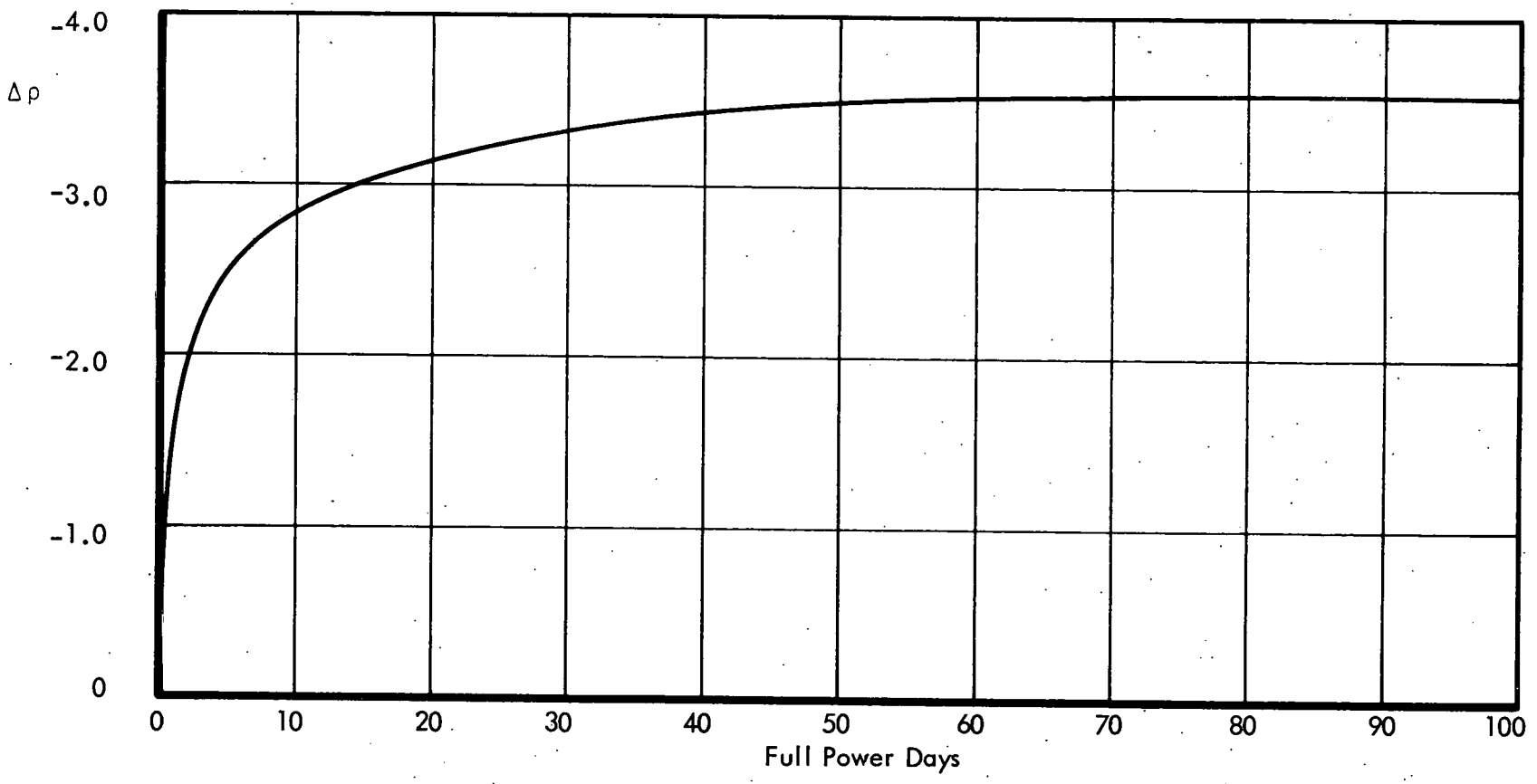

CHANGE IN REACTIVITY VS. FULL POWER DAYS

FIG. 5

TABLE 6

RESULTS OF EQUILIBRIUM CALCULATIONS

time (hours)	N_{Xe}	ρ_{Xe} % $\Delta k/k$
5	0.00148	0.44
10	0.00344	1.05
15	0.00499	1.52
20	0.0062	1.86
25	0.0067	2.02
30	0.00707	2.14
35	0.0073	2.21
45	0.00755	2.28
55	0.076	2.31
∞		2.33

As noted in Sec. 3.1.4, the movement of the center rod was calibrated as a function of xenon buildup. This calibration has been extended to cover the 28-day power run. Figure 6 shows the center rod position and inferred reactivity versus full-power days.

At the end of the 28-day power run, the reactor was shut down for a three-month period. Reactor shutdown causes a reactivity gain because of protactinium decay and the resultant U-233 buildup. The calculated increase was 57 cents and the measured increase was 59 cents.

3.1.7 Reactivity Inventory at Full Power (58.2 Mwt)

The center rod in the control-rod configuration at full power (58.2 Mwt) and for equilibrium xenon is raised to approximately 16 in. from the bottom of the core; all other rods are fully withdrawn. The reactivity losses to xenon, temperature, voids, and Doppler effects are listed in Table 7.

TABLE 7

REACTIVITY LOSSES AT FULL POWER

	ρ deduced (Δk)	ρ predicted (Δk)
Temperature	0.010	0.0128
Equilibrium xenon[14]	0.025	0.023
Voids plus Doppler effect[10]	0.043	0.035
	0.078	0.071

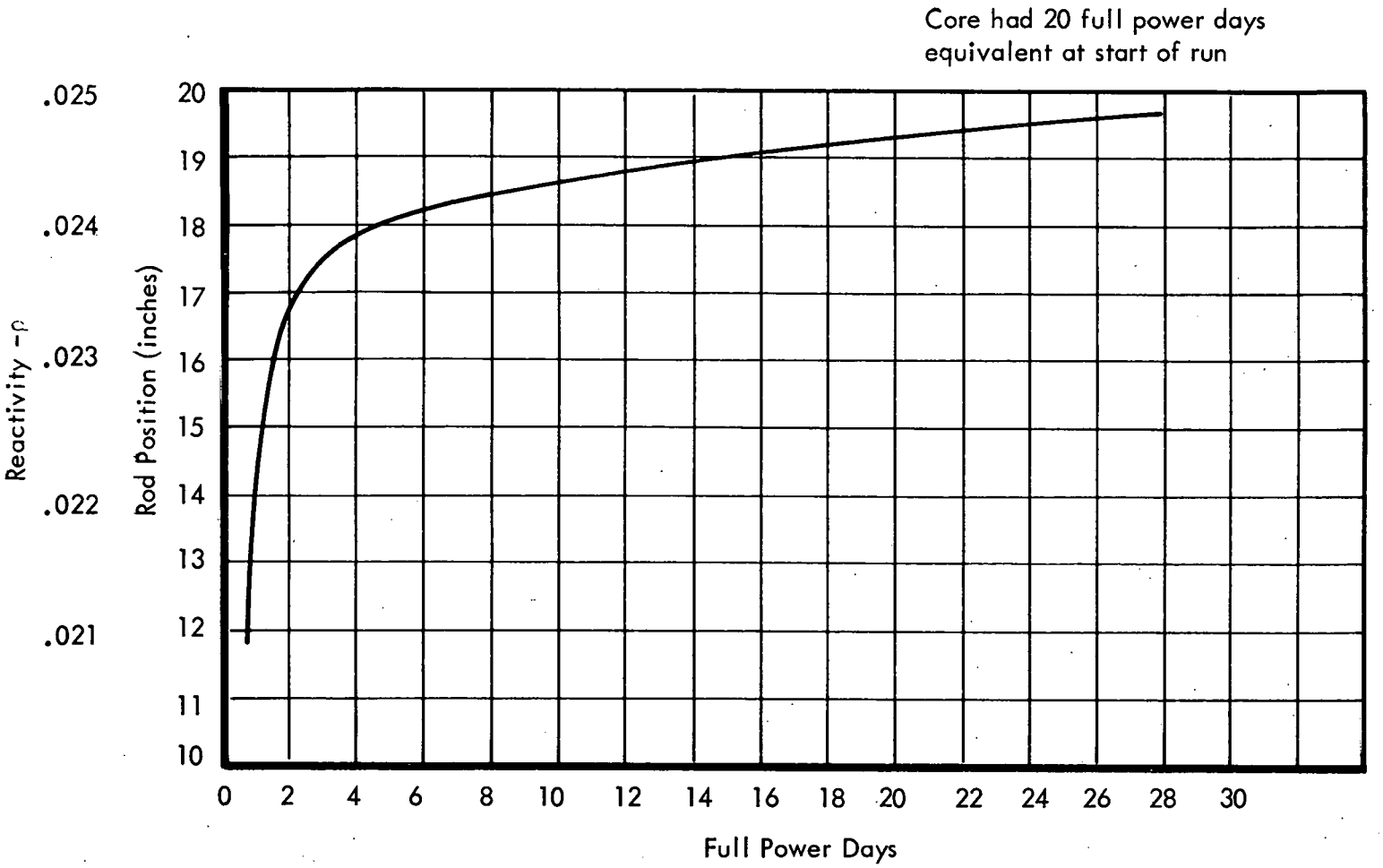

CENTER ROD POSITION DURING 28-DAY RUN

FIG. 6

The predicted value of 3.5 percent Δk for voids plus the Doppler effect is based on a 21 percent core-average void. The deduced value of 4.3 percent Δk indicates about a 24 percent core-average void. However, the 4.3 percent Δk includes the reactivity loss from the increased rod worth of the center rod, which is about 0.5 percent Δk. Therefore, the reactivity for voids plus Doppler effect is about 3.8 percent Δk, which corresponds to about a 23 percent core-average void.

The cold, clean k_{eff} equals 1.117, and, hence, the reactivity available for samarium, protactinium, and lifetime is 3.9 percent Δk. Since 6 percent Δk is held by burnable poisons in the fuel cladding, the total reactivity available at full power, after equilibrium xenon, is about 10 percent Δk.

3.2 POWER DISTRIBUTIONS (Task 103)

The objective of this task is to obtain the power distributions as a function of time and rod positions and to recommend changes in rod operation if distributions indicate they may be necessary.

3.2.1 Three-Dimensional Power Distributions

A three-dimensional, semi-empirical computer code has been obtained which allows the mockup of a boiling water core in which the coupled effects of flow, power, and voids are represented. Each control rod can be represented independently and the code has a burnup option. This code should be valuable in following the three-dimensional power distributions closely, throughout the operation of the reactor core; in obtaining reactivity coefficients and control-rod-worth variations; in following the core burnup; and in fuel-cycle calculations. The advantages that this code has over other three-dimensional codes -- its simplicity in internal calculations and its semi-empirical nature -- greatly reduce computer time.

For economical operation, the code requires that all spatially-independent or control-cell-averaged quantities be generated peripherally and presented to the code as curve fits. The code iterates between the coupled equations for the macroscopic three-dimensional power and for the void and burnup distributions and then converges on an eigenvalue (k_{eff}). The averaged control-cell quantities were determined using two-dimensional, x-y cell calculations. These cell calculations used the new thermal diffusion parameters averaged for space and energy in the fuel region determined under Task 102 (see Sec. 3.1.1). Shrouds, water gaps, posts, rod followers and control rods were all represented explicitly. Each control cell contains four fuel elements and half of two control rods (or rod followers), together with the associated structures. Three different rodded conditions are, therefore, possible -- unrodded, one rod inserted, and two rods inserted. Each of these three conditions must be calculated to yield the k_{∞} of the four fuel elements. These cell calculations must be done for each temperature and void condition of interest. At present, only the room temperature condition (68 F) and the operating conditions (537 F versus void fraction) have been calculated. The results of these cell calculations are shown in Figs. 7, 8, and 9 for fuel enriched to 4.3 percent and 5.2 percent.

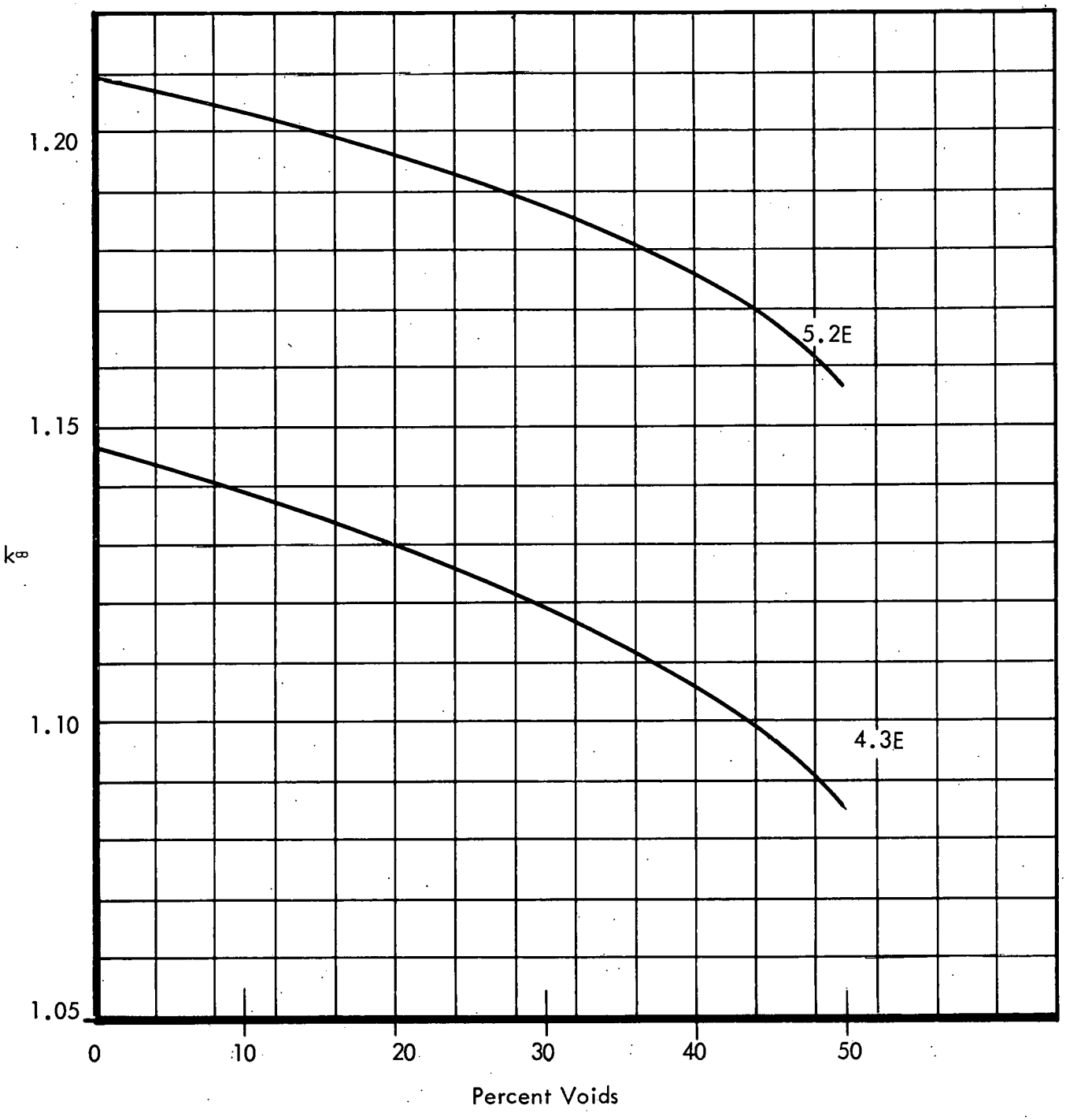

UNRODDED k_∞ VS. PERCENT VOIDS

FIG. 7

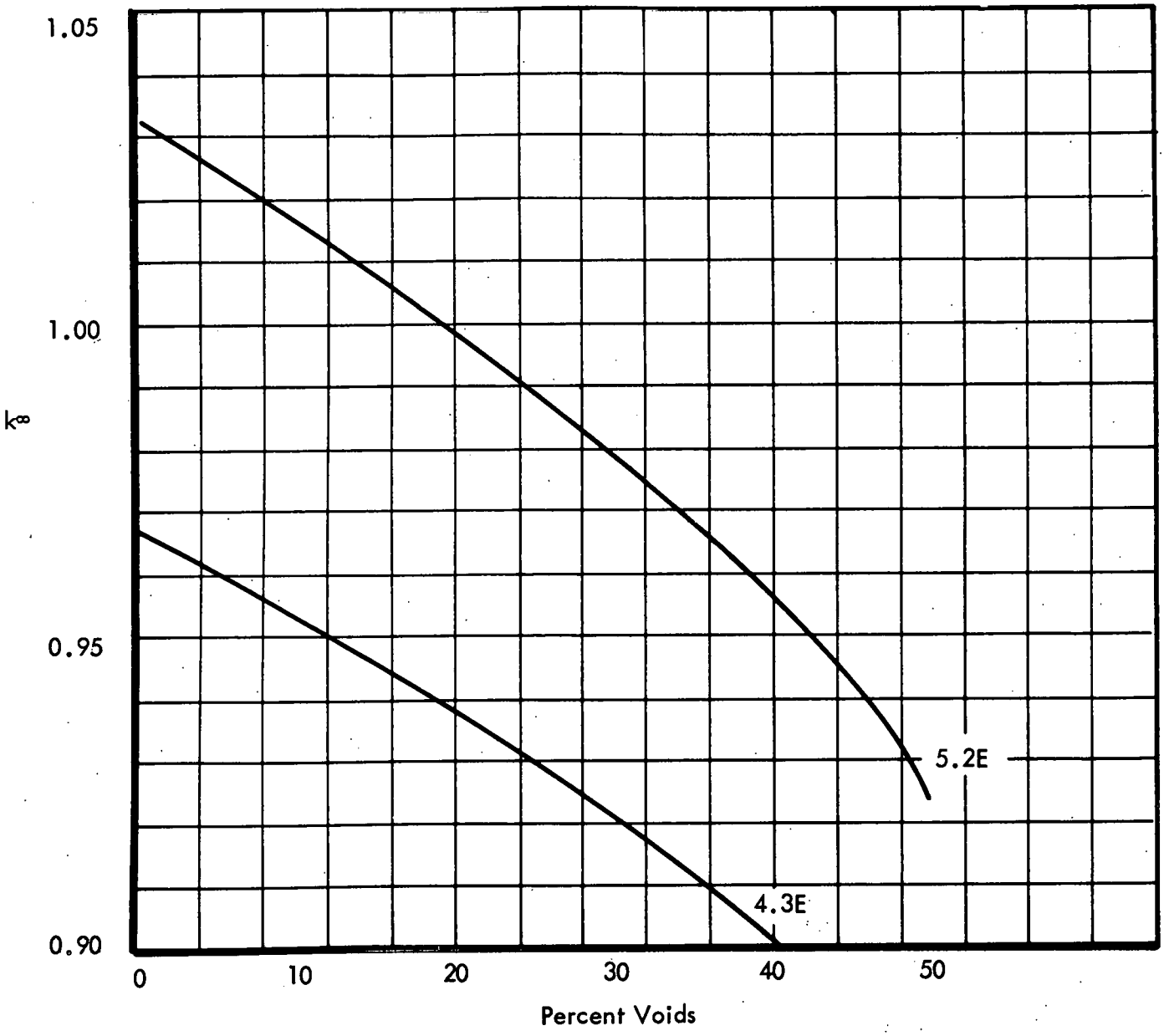

HALF-RODDED k_∞ VS. PERCENT VOIDS

FIG. 8

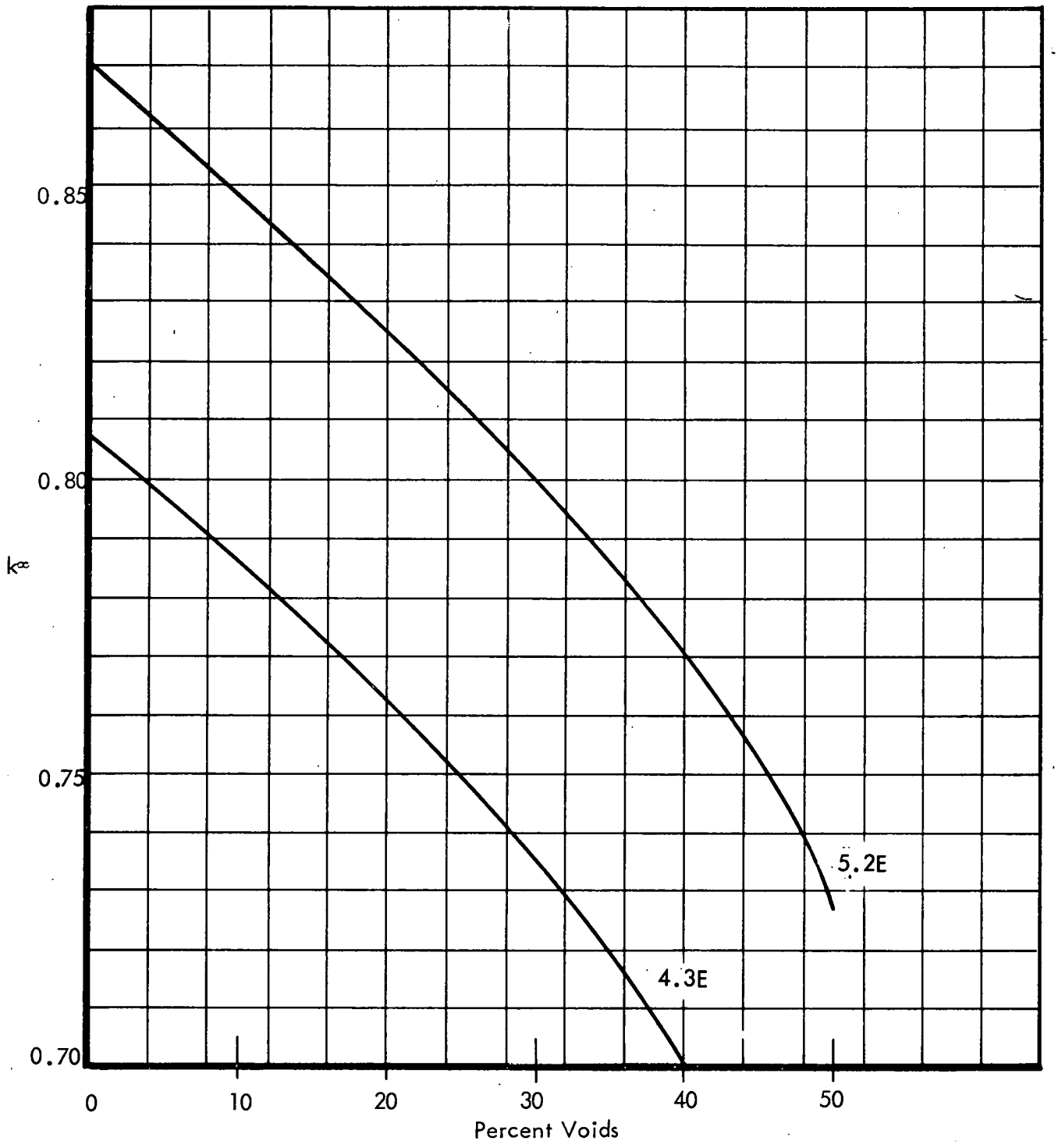

FULLY-RODDED k^{∞} VS. PERCENT VOIDS

FIG. 9

Four initial test cases have been run to determine the effect of various transport kernels on the calculated reactivity. The core considered was the unrodded core, of 148 regular fuel elements, at room temperature. The choice of this core was based on the reliability of the measured excess reactivity (9.32 percent ρ) and the absence of complicating factors such as control rods and voids. Four cases were run, comparing three different transport kernels and a combination of two of the kernels. An estimated reflector albedo was used. The results are given in Table 8.

TABLE 8

EFFECT OF VARIOUS TRANSPORT KERNELS ON CALCULATED REACTIVITY

	calculated				measured
kernel:	I	II	III	IV	
Reactivity (% ρ)	7.20	6.79	6.98	7.70	9.32

Kernel IV yields a value within 0.4 percent of the measured reactivity. A tentative choice of transport kernels was made. The optimum kernel for the room temperature condition is not necessarily the optimum for the hot, voided condition; thus the choice of kernels is tentative, pending comparison at other conditions. Following the selection of a transport kernel, several other room temperature cases were set up to test the control-rod representation, based on conditions measured in the core of 148 regular fuel elements. These conditions included: all rods in; 13-rod bank at critical position; and center rod removed. The results of these cases will be compared with the measured reactivities and power distributions.

The first series of operating cases is also being calculated. The first condition under investigation is the full-power (58.2 Mwt) operating condition with equilibrium xenon. These cases will give the excess reactivity* of the core, the reactivity worth of the center rod, and the power distributions at operating conditions. Since ERR operates as a natural circulation system, and since there are some uncertainties in flow distributions, subcooling, etc., selected ranges of these variables will be investigated.

3.2.2 Effects of Rod Programming

The present mode of ERR operation (12 control rods withdrawn and with the center (regulating) rod inserted to maintain criticality) has been examined in terms of the effect on power distribution. The conclusion was that the power distributions, as calculated by the project staff[10] for this mode of operation, are sufficient to demonstrate no adverse pealing will occur. No further problems were foreseen for this mode of operation.

*Which can be compared with the deduced values listed in Sec. 4.1.7.

3.3 REACTIVITY COEFFICIENTS (Task 104)

The three-dimensional core model utilized under Task 103 - Power Distributions (see Sec. 3.2) is also applicable in determining the temperature and void coefficients as a function of time. When this core model is completely checked out, it will be used to record reactivity in temperature and voids versus operating history. Until then, the normalized, one-dimensional approach, (see Sec. 3.1) based on critical rod-bank positions and differential rod worths will be used. The deduced points on the curve of k_{eff} versus moderator temperature (Fig. 3 are obtained by this one-dimensional approach. Analysis of data from the site will continue and the reactivity coefficient curves will be recalculated according to the current state of operation.

4. CORE MANAGEMENT

4.1 FUEL CYCLE STUDIES (Task 201)

During the next six months, effort will be concentrated on a detailed analysis of a fuel management program for ERR. Based on the feed enrichment of Core II and on the replacement control rods that will be available, various fuel loading patterns and control-rod programs will be investigated to determine a fuel management program which best meets the objectives of high exposure for the Core-II assemblies and of demonstrating the thoria-urania recycle. The primary objective of the reactor plant is the demonstration of a high plant availability factor, consistent with low power-generation costs and safe operation.

A generalized fuel management program was postulated for Task 205 (Fuel Loading for Second Core)[11] (see Sec. 4.4) to estimate probable exposures of the Core-II assemblies. Based on reloading in core batches of one-third, this program assumed a uniform loading pattern. Under Task 201, specific loading patterns will be examined in conjunction with various rod programming schemes for their effect on power distributions, reactivity, and discharge exposures. It is expected that the three-dimensional core model being developed under Task 103 (see Sec. 3.2.1) will be extensively used in the examination of loading patterns and rod programs.

4.2 CONTROL-ROD ANALYSIS (Task 204)

The objective of Task 204 is to investigate the types and sizes of control rods that might be used as replacement rods and to determine the advantages and disadvantages of various rod types. Information is to be provided for use in preparing detailed procurement specifications for replacement control rods. The following areas have been investigated regarding this objective:

1. The change in rod worth caused by use of different poison materials (i.e., Ag-In-Cd, Hafnium, and B_4C)

2. The effect of the rod span on rod worth

3. The effect of blade thickness and the density of the absorbing material on rod worth.

4. The effect of burnup on the nuclear life of the rod

A topical report[12] has been issued that covers the analysis and conclusions from this task. The methods used and the results obtained are summarized below.

4.2.1 Methods of Analysis

Four materials were selected for the physics investigations for replacement control rods:

1. boron-stainless steel (presently in the reactor)
2. boron-carbide
3. silver-indium-cadmium
4. hafnium

A control rod worth calculation was done for each of the materials, assuming a uniformly loaded core with an unrodded reactivity of 12 percent (the maximum reactivity available in the second core). The different materials were made to conform to the spatial limitations of the present core. A description of the rod geometries is given in this section (see Fig. 10.). Rod-worth calculations were made by a four energy group, two-dimensional method. Two geometric models were used in the analysis of rod worth -- the cell model and the whole-core model.

Cell Model

The cell model comprises four fuel elements, a zirconium shroud, portions of the zirconium support posts, and the associated control blades. (The blades are absorber sections for the rodded cases and zirconium followers for the unrodded cases.) Figure 1 shows a typical cell. In the cell model, the zirconium post, the shrouds, and the control section are represented explicitly. The material inside the shrouds, i.e., the fuel, the cladding, and the water are homogenized and treated as one region. This configuration was represented by a 40 x 40 mesh in the PDQ 2-90 program and was used for all comparative calculations.

Whole-Core Model

The whole-core model comprises 148 fuel elements, 13 control rods or followers, and 16 dummy elements (stainless-steel cans) (see Fig. 11). Because of the size of whole-core model, there cannot be as much geometric detail as in the cell model. The regions inside the shrouds are homogenized and treated as one region; the zirconium shrouds and a portion of the posts were homogenized with the water that is between the shroud and control blades; the control blades (followers for rods-out cases) are represented explicitly. This configuration uses the maximum mesh available (73 x 73) in the PDQ 2-90. The whole-core model was used in calculating absolute shutdown margins for the fully rodded core and for the "stuck rod" condition.

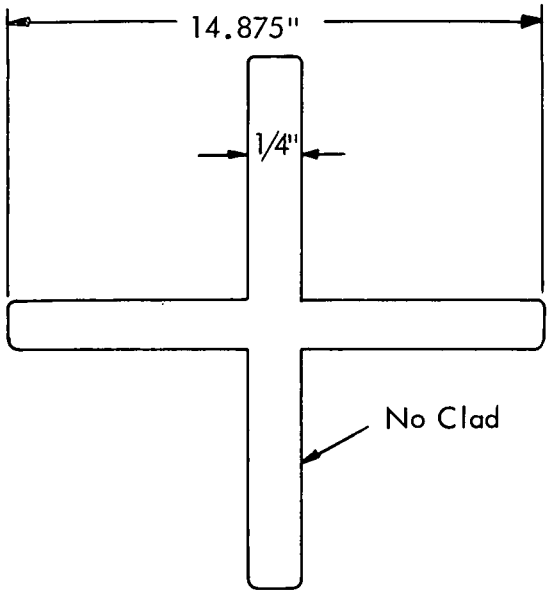

(a) Boron-Stainless Steel Rod

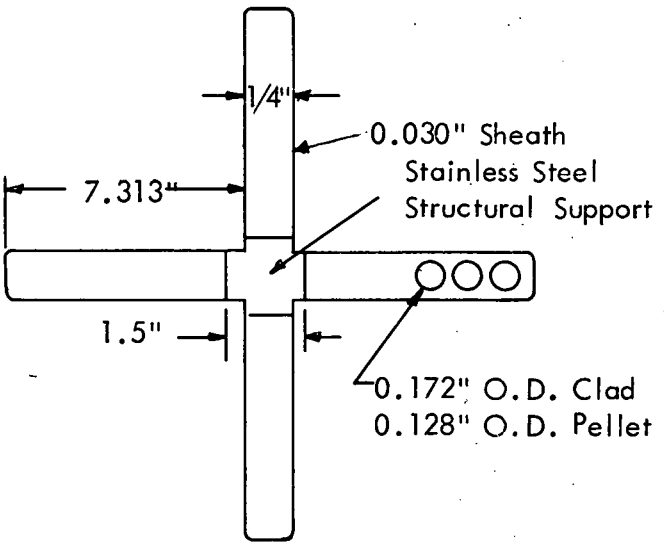

(b) B_4C Rod

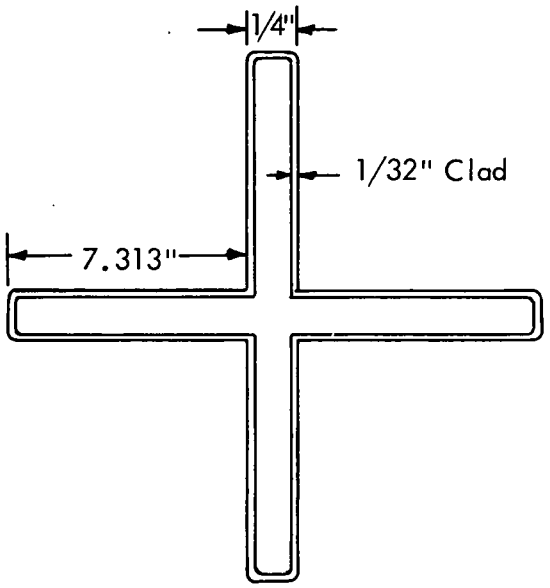

(c) Ag - In - Cd Rod

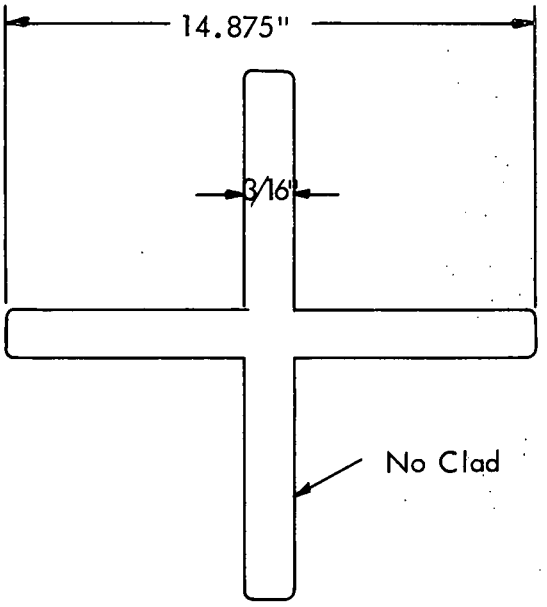

(d) Hafnium Rod

ROD GEOMETRIES

FIG. 10

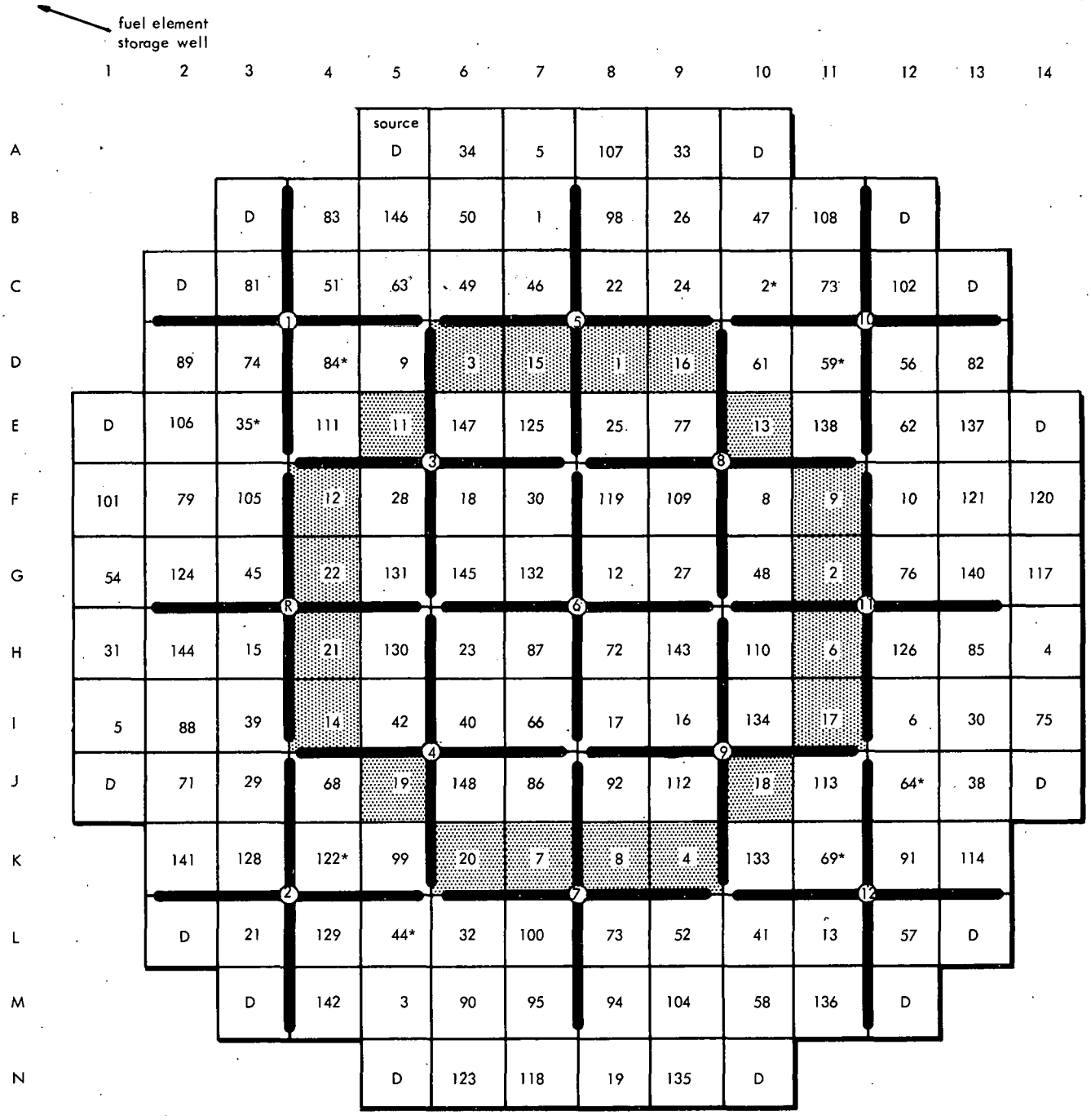

ERR CORE LAYOUT

FIG. 11

The nuclear representation of the absorbing portion of the rods was done by two methods suggested by Henry[5]:

1. By using equivalent diffusion parameters obtained as follows:

$$\Sigma_a = \frac{\sqrt{\langle\alpha\rangle\,\langle\beta\rangle}}{2t} \ln\left[\frac{1+\sqrt{\frac{\langle\alpha\rangle}{\langle\beta\rangle}}}{1-\sqrt{\frac{\langle\alpha\rangle}{\langle\beta\rangle}}}\right]$$

$$D\Sigma_a = \langle\alpha\rangle\langle\beta\rangle$$

where

$$\langle\alpha\rangle = \frac{\int_{u_o}^{u_g} \frac{\alpha(u)\,du}{1+c\alpha(u)}}{\int_{u_o}^{u_g} \frac{du}{1+c\alpha(u)}}$$

$$\langle\beta\rangle = \frac{\int_{u_o}^{u_g} \frac{\beta(u)\,du}{1+c\beta(u)}}{\int_{u_o}^{u_g} \frac{du}{1+c\beta(u)}}$$

$$c \simeq \sqrt{3}$$

$$\alpha(u) = \frac{J^+ + J^-}{\phi^+ + \phi^-} = \frac{1-2E_3(Z)}{2\left[1+3E_4(Z)\right]}$$

$$\beta(u) = \frac{J^+ - J^-}{\phi^+ - \phi^-} = \frac{1+2E_3(Z)}{2\left[1-3E_4(Z)\right]}\,; \quad Z = 2\Sigma_a(u)\,t$$

2. By using the extrapolated boundary condition:

$$\frac{\frac{d\phi}{dY}}{\phi} = d$$

where $\frac{d}{D} = \langle \alpha \rangle$

In general, the first method was utilized for full-core calculations and the second for the cell calculations.

A variation in the first method was incorporated in the full core calculations. The absorption cross section and diffusion coefficients for the absorber section in Groups 1 and 2 were taken directly from GAM, as was the diffusion coefficient for Group 3. The absorption cross sections for Groups 3 and 4 were obtained as described, but with $\langle \beta \rangle$ defined as follows:

$$\langle \beta \rangle = \frac{\int_{u_o}^{u_g} \alpha(u)\, \beta(u)\, \phi(u)\, du}{\langle \alpha \rangle \int_{u_o}^{u_g} \phi(u)\, du}$$

The diffusion theory parameters obtained from GAM are compared in Table 9 with those obtained by the above methods for a 1/4-in., 2.2 w/o boron-stainless-steel rod.

TABLE 9

COMPARISON OF DIFFUSION THEORY PARAMETERS

Group	Σ_a		D	
	Henry	GAM	Henry	GAM
1	0.0049	0.0065	8.45	0.929
2	0.1870	0.1803	0.234	0.314
3	0.7173	0.9313	0.054	0.185

The absorption values are quite close for the upper two energy groups. In the lower energy group, the GAM value tends to be higher, as expected, since the spatial self-shielding is not accounted for. The diffusion coefficients show a wider variation, and the decision was made to combine the two sets of constants in the manner explained above.

To test the validity of the calculational model for control-rod calculations, several cases were calculated using measured core conditions. The cases chosen for calculation were:

1. 128 regular elements, 20 spiked elements (no rods in)
2. 128 regular elements, 20 spiked elements (all rods in)
3. 128 regular elements, 20 spiked elements (12 rods in and the center rod removed)

Table 10 lists the deduced and the calculated reactivity values. The calculated values agree well with the deduced values in all three cases.

TABLE 10

DEDUCED AND CALCULATED REACTIVITIES

description	k_{eff}		$\%\Delta k/k = \frac{k_1 - k_2}{k_1}$	
	deduced	calc.	deduced	calc.
no rods in	1.117	1.1.12	10.5	10.1
13 rods in	0.92	0.9173	-17.9	-17.6
12 rods in, center rod out	0.94	0.9386	-15.9	-15.8

In earlier work (see Sec. 4.3, Task 205) for the specification of the second-core fuel loading, the calculated value of the "stuck rod" was thought to be conservative, and it was stated that this value was to be investigated further. As explained in Sec. 4.2.1, two methods for representing the absorber section of the control rods are currently being utilized. In the earlier work, the extrapolated boundary condition was used in a full-core calculation for all energy groups. This procedure yielded severe flux discontinuity across the rods and erratic source distributions and, hence, erratic eigenvalues. If the equivalent diffusion parameters are used, as explained in Sec. 4.2.1, the continuity of flux and current is preserved and the agreement between the calculated and deduced rod worth is good, as shown in Table 10.

4.2.2 Rod Description

Four absorbing materials were considered for rod replacement:

1. boron-stainless-steel
2. boron-carbide
3. silver-indium-cadmium
4. hafnium

The thickness of the various materials was determined from design considerations and the spatial limitations of the existing reactor.

4.2.2.1 Boron-Stainless-Steel: The boron-stainless-steel material is of the same thickness (0.25 in.) as the present rods (Fig. 10). The boron content is 2.2 w/o of natural boron. The rod is unclad and has a zirconium follower 1/4-in. thick, with a span of 14-7/8 in.

4.2.2.2 Boron Carbide: The boron carbide was assumed to be in the form of pellets inside a 0.172-in.-OD tube. The tubes are in a linear array and are covered with a 30-mil sheath of stainless steel. The outside dimension of the rod is 0.25 in., and the diameter of the boron carbide pellets 0.128 in. (Fig. 10). The zirconium follower is 1/4-in. thick, with a span of 14-7/8 in.

4.2.2.3 Silver-Indium-Cadmium: The silver-indium-cadmium was assumed to be 80 percent silver, 15 percent indium and 5 percent cadmium. The absorber material is 3/16-in. thick and is clad with 1/32-in. of stainless steel (Fig. 10). The zirconium follower is 1/4-in. thick, with a span of 14-7/8 in.

4.2.2.4 Hafnium: For purposes of the calculation, the hafnium was assumed to have the same thickness (3/16 in.) as the silver-indium-cadmium (Fig. 10). The zirconium follower also was assumed to be 1/4-in. thick, with a 14-7/8 in. span.

4.2.3 Material Comparison

The material comparison utilized the cell method, and the designs were limited to the restrictions of the existing spaces. The comparative values for the different materials are given in Table 11.

TABLE 11

RELATIVE ROD WORTHS

material	cell rod worth $\rho = \frac{k_1 - k_2}{k_1 k_2}$	relative rod worth normalized to boron-stainless steel
boron-stainless steel	24.4	1.0
hafnium	26.0	1.066
silver-indium-cadmium	27.2	1.115
boron carbide	30.0	1.230

These values of rod worth are not the absolute value of the rod worth in the whole core but of that based on a cell calculation, and they are used for comparison purposes only. Since the core is not rodded at the periphery, the full core rod worths are somewhat less than these values. But all of the other materials afford an increase in rod worth over the

present boron-stainless steel, and the boron carbide affords a substantial increase over the other materials. The hafnium thickness was assumed the same as that of the Ag-In-Cd (3/16 in.). However, it is not necessary to clad hafnium, and an actual thickness of 1/4 in. can be used. This greater thickness would increase the worth by about 6 percent, making it slightly more than Ag-In-Cd but still less than B_4C.

4.2.4 Effect of Boron Density in Boron-Stainless Steel and B_4C Rods

Effect of boron density in the boron-type rods has been investigated using (α) values (the current-to-flux ratio at the rod surface). The values of α, as functions of theoretical B_4C density for the three upper energy groups, are shown in Figs. 12, 13, and 14. The results shown in Fig. 17 are generalized to be applicable to any boron rods whose boron content is expressed in percent of B_4C theoretical density ($\rho_{th}^{B_4C}$). The actual calculated points for Fig. 14 are given in Table 12.

TABLE 12

EFFECT OF SPAN AND DENSITY VARIATION

case	material	percent of theoretical density (pellet OD = 0.128 in.) A	span, in. B	B_4C pellet OD at 72% theoretical density, in. C	cell rod worth, $\%\rho$ D
1	boron-stainless-steel		14-7/8		24.4
2	boron carbide	72	14-7/8	0.128	30.0
3	boron carbide	60	14-7/8	0.107	28.8
4	boron carbide	31	14-7/8	0.055	24.4
5	boron carbide	10	14-7/8	0.018	19.8
6	boron carbide	72	12	0.128	24.9

Case 1 is the reference, which is based on the present ERR control rods. In Cases 2 through 5, Columns A and D give the variation of worth versus B_4C density, and Columns C and D give the variation of worth versus pellet diameter.

Figure 15 shows that the worth of boron rods is very much dependent on boron density in the low-density range, but, after reaching a certain density value, is fairly insensitive to change of boron density. The dotted portion of the curve was not calculated, simply being an extrapolation of zero.

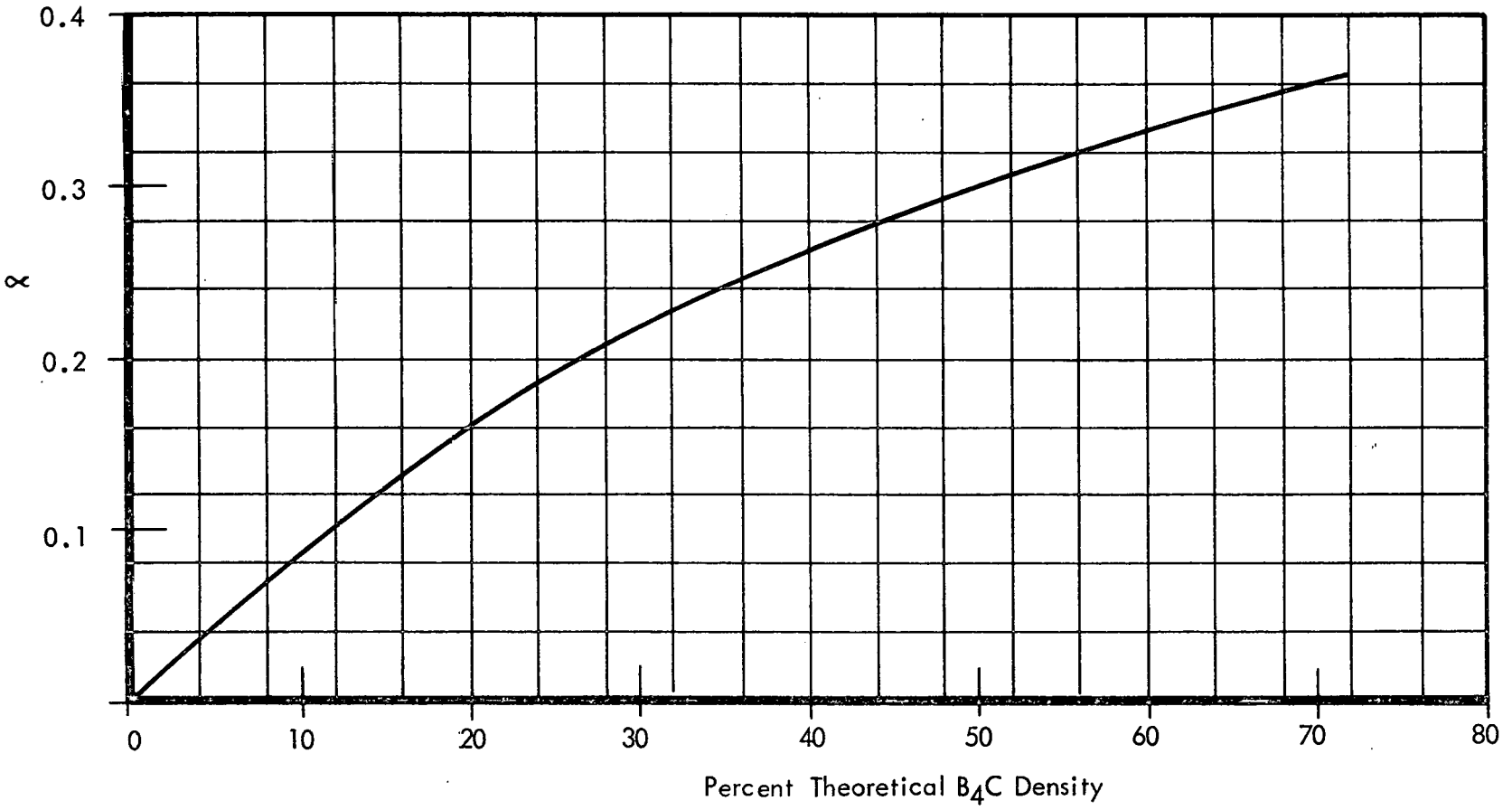

αVALUES VS. BORON CONCENTRATION IN B_4C RODS, 0.625 ev $\leq$ E $\leq$ 4.0 ev

FIG. 12

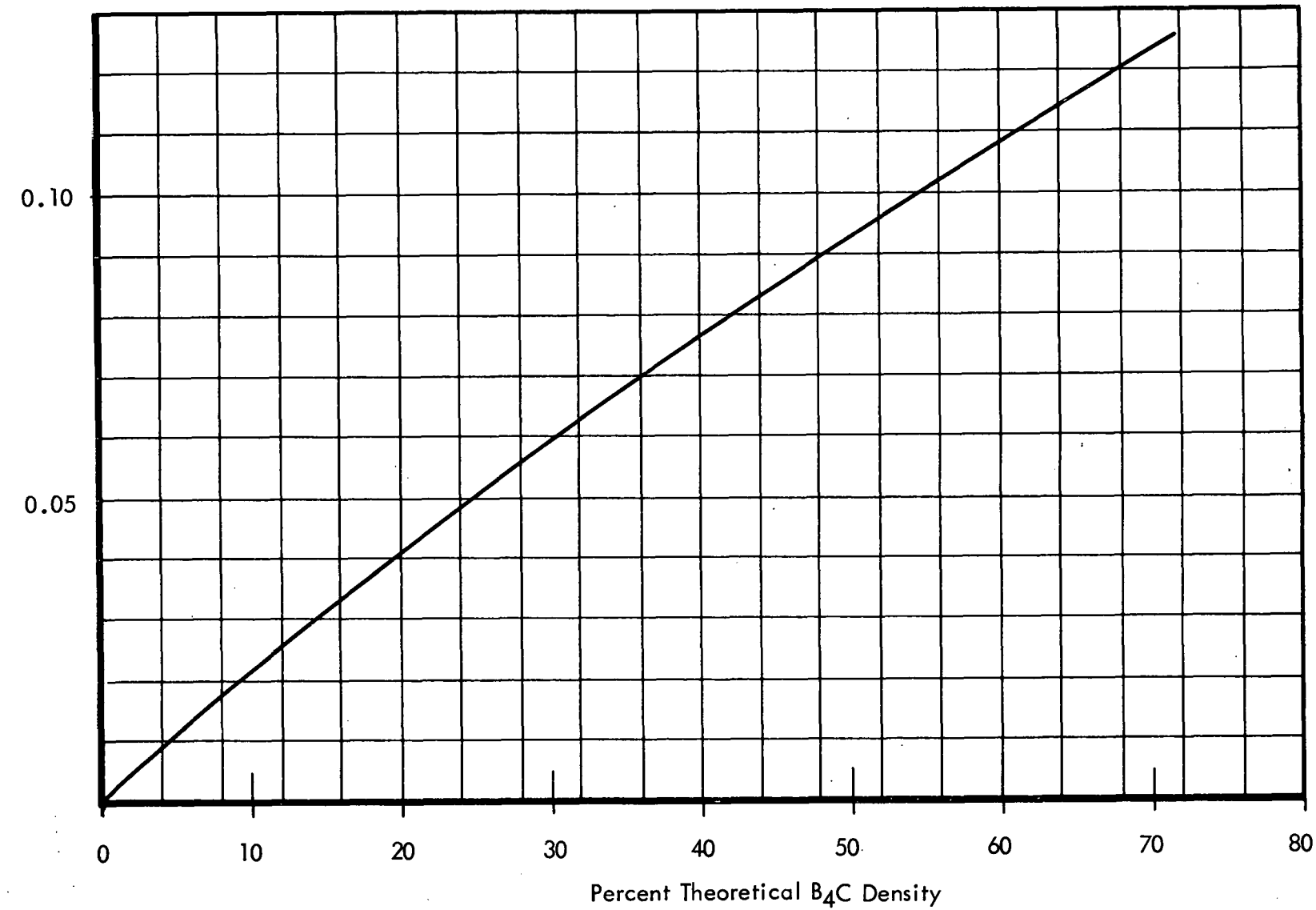

α VALUES VS. BORON CONCENTRATION IN B_4C RODS, 4.0 ev $\leq$ E $\leq$ 454 ev

FIG. 13

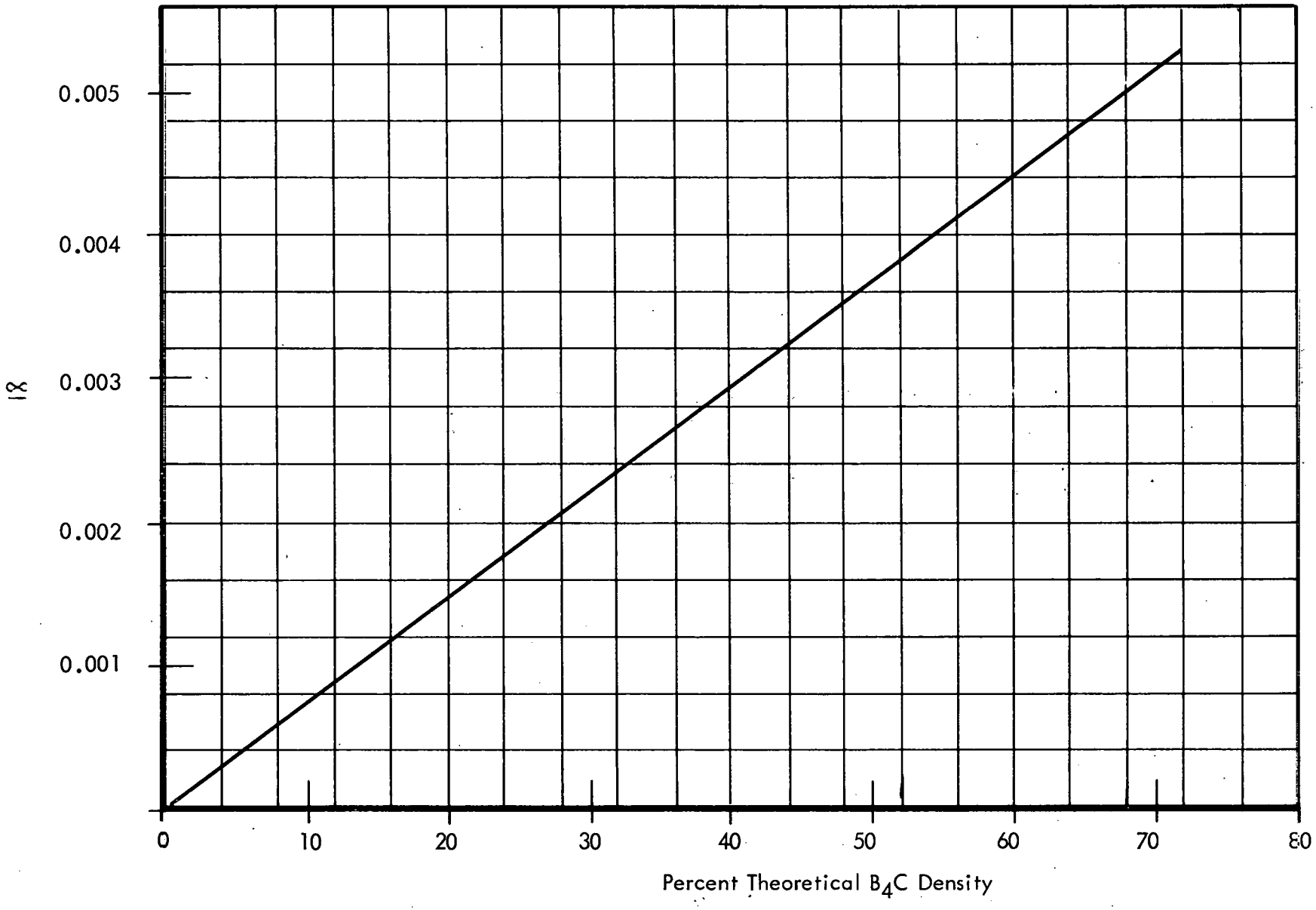

α VALUES VS. BORON CONCENTRATION IN B_4C RODS, $454 \text{ ev} \leq E \leq 10^7 \text{ ev}$

FIG. 14

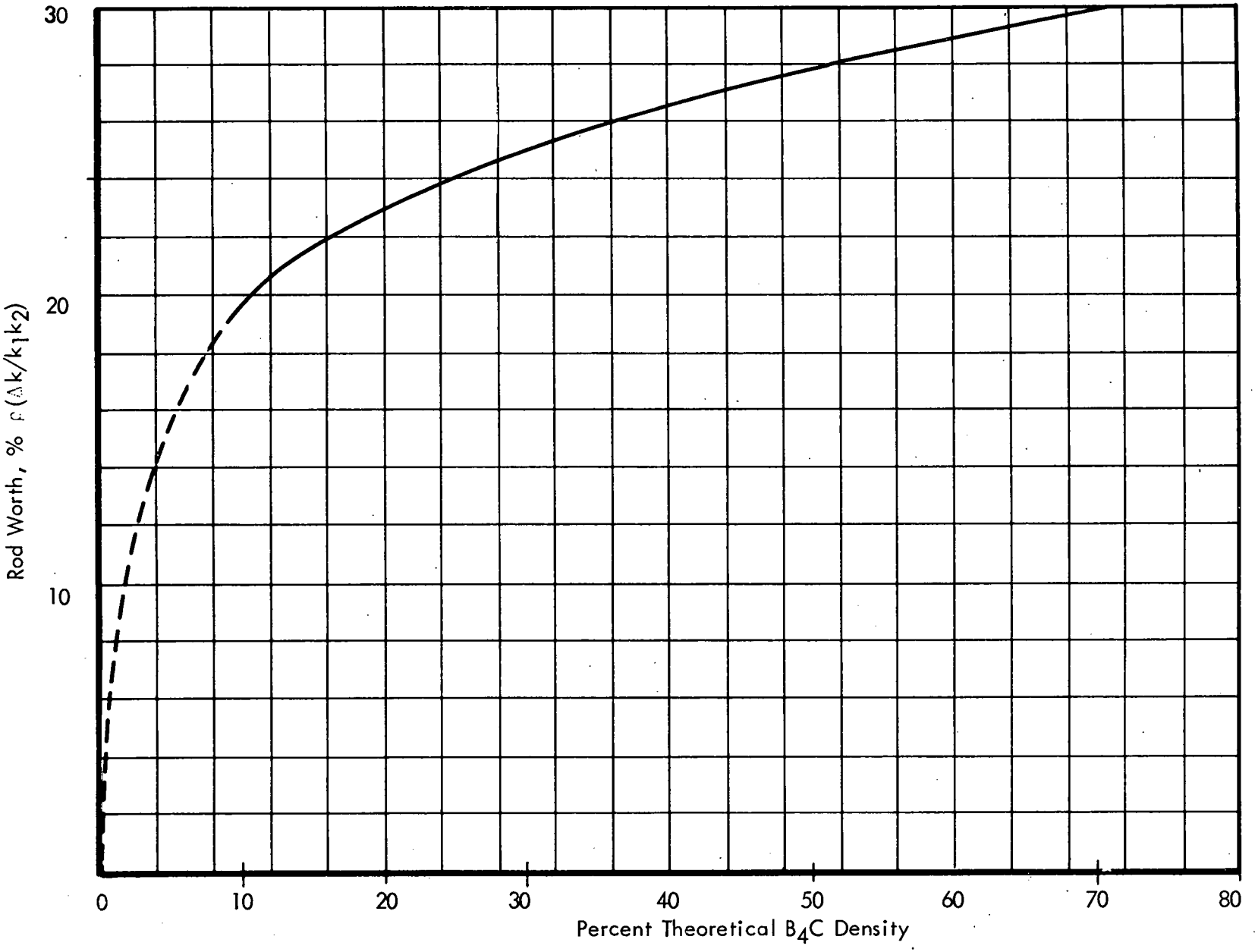

CALCULATED ROD WORTH VS. BORON CONCENTRATION, ERR - Regular Core

FIG. 15

4.2.5 Depletion of Absorbing Isotopes

In order to investigate the rod-worth change caused by burnup or time-depletion of boron, it was assumed that the rods must control an average of 3 percent reactivity for 3 years at full-power operation. This assumption establishes the total number of neutrons that the rods must absorb and, hence, the number of boron atoms that are destroyed.

The total worth of the boron carbide rods (i.e., the cold rod-worth) will decrease by approximately 0.1 percent ρ at the end of three full-power years, if the depletion is uniformly distributed among 13 rods. If, however, single-rod operation is used, as in the present core, this individual rod will lose 37 percent of its boron-10, corresponding to a decrease of approximately 0.2 percent ρ in the rod worth, assuming uniform rod burnout. The change in B_4C rod-worth is negligible for the 3-year period.

Based on the same assumptions, the worth of 13 boron-stainless-steel rods will decrease by 0.2 percent after 3 years of full-power operation. If a single rod is used for control, the worth of the rod will decrease by approximately 20 percent, or approximately 0.5 percent ρ. Burnup in the boron-stainless rods during required shutdowns is, therefore, not a problem, the only concern being local depletion effects. It should be pointed out that, in the present ERR core, the average reactivity to be controlled by the rods is about half that assumed in this study for the same period.

In the calculation of the Ag-In-Cd-rods depletion, the maximum effect was assumed to be the 100 percent depletion of cadmium in the rods. The recalculated α_4 value for the thermal group, without cadmium contribution, was about 10 percent less than the original value for the three components. The contribution of cadmium, in terms of total rod worth, was found to be less than 1 percent of ρ for ERR. Therefore, the decrease in rod worth caused by burnup is negligible in the Ag-In-Cd rods. The hafnium worth is assumed to be unaffected by the isotopic depletion from neutron absorption. Table 13 gives the effects that depletion of absorbing materials has on rod worth. The depletion effect on total rod worth can be considered negligible for all materials for a minimum of 3 full-power years after installation.

TABLE 13

DEPLETION EFFECTS ON ROD WORTH

material	change in total rod worth in 3 years	change in single-rod worth in 3 years
boron-stainless steel	< 0.5%	~ 0.5%
silver-indium-cadmium	< 0.5%	< 0.5%
boron carbide	< 0.1%	< 0.3%
hafnium	0.0	0.0

4.2.6 Reactivity Insertion Rates

The reactivity insertion rates of the center (No. 6) rod were calculated for B_4C and boron-stainless-steel rods in a core with a maximum reactivity of about 15 percent ρ. The calculated reactivity insertion rates are given in Table 14.

TABLE 14

REACTIVITY INSERTION RATES OF BORON CENTER ROD

boron concentration $\%, \rho^{B_4C}_{th}$	reactivity insertion rate (¢/in.) for core k_{eff}	
	1.15	1.102
72	50.96	
50	46.37	
31 (equivalent to boron-stainless-steel rod currently in ERR)	36.16	23

Since the total rod worths of the B_4C rods (72 percent $\rho^{B_4C}_{theoretical}$) and the boron-stainless-steel rods represent the highest and lowest values among the four types of rods examined, the reactivity insertion rates of the Ag-In-Cd rod and of the hafnium rod will be between 50.96 ¢/in. and 36.16 ¢/in.

For a core with a reactivity of only 12 percent ρ, the reactivity insertion rate of the center rod should be less than the values given in the above table. Extrapolation from available results shows that the maximum reactivity insertion rate for a B_4C center rod (72 percent $\rho^{B_4C}_{th}$) should be around 40 ¢/in. for a core having approximately 12 percent reactivity.

4.2.7 Effect of Decreased Span

The possibility of reducing the control-rod span was considered during the study. Using B_4C as the reference material (since it affords the most rod worth) the span of the rod was reduced by a cell calculation, to determine what B_4C-rod span would yield the same total rod worth as the boron-stainless steel. The analysis showed that a 23 percent reduction in rod span yields a 24 percent reduction in rod worth. Based on this result, a B_4C rod with a 12-in. span would have the same total rod worth as a boron-stainless rod with a 14-7/8 in. span. However, a shortened span is not recommended because of the flexibility needed in the fuel cycle and in the operating rod configurations because of the uncertainty in projected reactivities.

4.2.8 Effect of Varying the Diffusion Coefficients in Region Adjacent to Rod

During the reliability investigation of the rod analysis, a calculation was done to determine the rod-worth effect of varying the diffusion coefficients in the water channels adjacent to the rods. Table 15 lists the values of the diffusion coefficients and the associated rod worths. The variation of the diffusion coefficient had only a minor effect on rod worth.

TABLE 15

DIFFUSION COEFFICIENTS AND ASSOCIATED ROD WORTHS

Array	40 x 40	20 x 20	20 x 20
Diffusion coefficient, D_4	0.176	0.176	0.1207
Unrodded k	1.1274	1.1279	
Rodded k	0.88418	0.88226	0.87902

The effect of the number of mesh points on the eigenvalue was also investigated since the number of mesh points must be reduced in going from a cell calculation to a full-core calculation. The same cell was calculated by 1600 mesh points and by 400 mesh points The results, shown in Table 17, indicate the number of mesh points has little effect on the cell calculation.

4.2.9 Effect of Varying the Rod Parameters

There is some uncertainty in the epithermal parameters of strong absorbers, especially of resonance absorbers such as hafnium and Ag-In-Cd. To determine the effect these uncertainties have on the calculated rod worth, a series of cell calculations were done for Ag-In-Cd, where the α values (i.e., current-to-flux ratio) for the various energy groups were varied. Table 16 shows the various α values and their effect on k and ρ.

TABLE 16

α VALUES FOR SILVER-INDIUM-CADMIUM

Case	α_1	α_2	α_3	α_4	k	ρ
1	0.0032	0.1060	0.4080	0.4750	0.8531	0.286
2	0.0032	0.1060	0.4080	0.4317	0.8555	0.282
3	0.0032	0.1060	0.4080	0	0.9813	0.132
4	0.0032	0.1060	0.0986	0.475	0.8752	0.255
5	0.0032	0.085	0.4080	0.475	0.8592	0.277
6					1.127	

A 20 percent variation in the α for Group 2 changes k by only 0.61 percent and a 10 percent variation in α for Group 4 changes k by 0.24 percent. A variation of 400 percent in the α of Group 3 changes k by only 2.2 percent. Thus, uncertainties of only 10 or 15 percent in the epithermal cross sections will have little or no effect on the calculated worths.

Case 3 of Table 17 shows the effect of setting α thermal equal to zero. This case represents only epithermal captures in the rod, and, as shown, the epithermal contribution is 46 percent of the total rod worth.

4.2.10 Recommendations

Based on the above results, boron carbide is the best rod material, from a physics viewpoint, for ERR. The spatial constraints do not, as the data show, present any disadvantages (e.g., reduced rod worth or rapid depletion) to the B_4C. It is prudent to design for the maximum rod worth achievable within the constraints since this design: provides greater fuel-cycle flexibility; enhances the possibility of continuing, for the second core, the present mode of operation; helps to compensate for uncertainties in the projected second core reactivities; and increases the possibilities for longer fuel burnup, since the nuclear life of these rods will last through much of the third core cycle.

Therefore, a full-spanned rod (14-7/8 in.), whose absorbing material is B_4C, of a diameter not less than 1/8 in., was recommended for the replacement control rods.

4.3 FUEL LOADING FOR SECOND CORE (Task 205)

The Core-II fuel-procurement schedule for ERR required that the weight percent of U-235 in thoria be determined prior to full-power reactor operation. To fulfill the task objectives, therefore, it was necessary to predict the excess reactivity in the full-power core by additional computer calculations. The time schedule necessitated establishment of the following criteria for the calculations:

1. Three zones are assumed for this particular loading.
2. Twelve full power months are assumed before reloading, for a burnup of about 5500 Mwd/MT in the first core as a basis.
3. The maximum enrichment to be specified is consistent with the present control rods.
4. The present boron-clad spares can be used in reloading if required for shutdown margin.
5. Present experimental data is to be extrapolated to full power by best estimates.

A topical report[11] covered the task analysis and conclusions in detail. The task methods and results are summarized in the following subsections.

4.3.1 Core Definition for the Analysis

Each fuel assembly consists of 25 fuel tubes in a 5 x 5 array. The general configuration of the fuel assemblies is similar to that in Core I. The fuel assembly* is constructed as

* Fig. 16 prepared from drawings supplied by the United Nuclear Corporation

shown in Fig. 16. There are two Inconel-X spacers per assembly, in the form of box grids that divide the assembly in thirds. The spacer strips for each assembly are 0.031-in. thick, 1.125-in. wide, weigh 0.848 lb per assembly, and are attached to four tubes by brazed collars of Type-348 stainless steel. Table 17 gives other data, pertinent to the Core-II fuel assembly, which, together with the foregoing criteria in Sec. 3, define the core for analytic purposes.

TABLE 17

CORE-II FUEL-ASSEMBLY DATA

Weight of U and Th as urania and thoria	26.545 kg
Fuel cladding material	Type-348 stainless steel
Cladding thickness	0.020 in.
Pellet density	94.5 ± 1.5% of theoretical
Pellet diameter	0.406 in.
Pellet column length	60 ± 0.25 in.
Impurity content	<20 ppm equiv. of natural boron

4.3.2 Method of Approach

The basic data required for this task are the excess reactivity and the reactivity in temperature, voids and xenon at full power (58.2 Mwt). When the full-power experimental data are analyzed, the reactivity for temperature, voids, and xenon and, hence, the remaining operating reactivity will be inferred. However, no experimental data beyond 25 Mwt was available for this task, so a calculated value of 2.55 percent $\Delta k/k$ for the operating reactivity was used. Full-power data now indicate that the reactivity is between 2.5 percent and 3.5 percent $\Delta k/k$.

A non-uniform, lifetime calculation, including axial and radial non-uniform burnup effects, was normalized to the calculated value of the operating reactivity, yielding the Core-I fuel-assembly reactivity-burnup curve shown in Fig. 17.

From the ground rules, it was assumed that Core I operates for one equivalent full-power year, after which approximately one-third of the Core-I fuel assemblies (those with the highest exposure) will be removed from the core and replaced with Core-II feed-fuel assemblies. The Core-I fuel assemblies are selected according to calculations of the relative exposure of individual fuel assemblies. These calculations also yield the relative burnup of the remaining assemblies, giving the exposure and isotopic composition of the Core-I fuel assemblies that remain in the reactor after the first burnup interval.

A range of enrichments was tentatively chosen for the Core-II feed-fuel assemblies, and three-group core constants were generated for Core-II feed assemblies with these enrichments and for exposed Core-I assemblies with the isotopic composition of one burnup interval. The initial excess reactivity and control-rod worths were then calculated for conditions with Core-I exposed assemblies and Core-II feed assemblies in the ratio of two to one. These

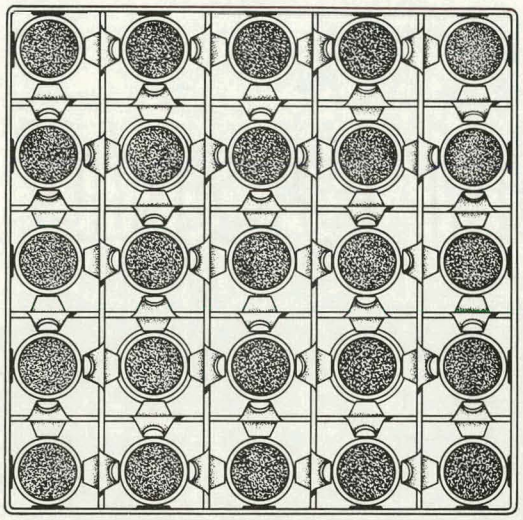

PLAN VIEW OF FUEL PIN SPACER ASSEMBLY

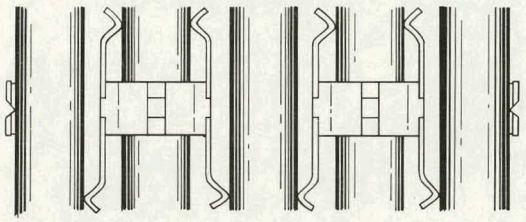

SECTION SHOWING COLLARS

ERR
FUEL ELEMENT ASSEMBLY

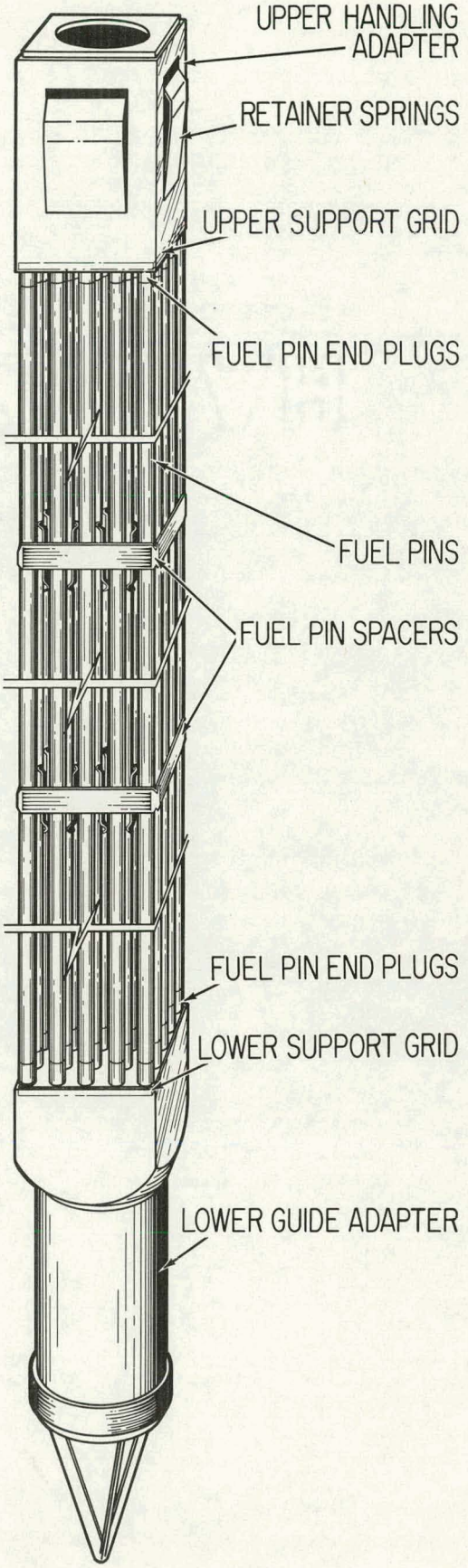

ERR FUEL ELEMENT ASSEMBLY

FIG. 16

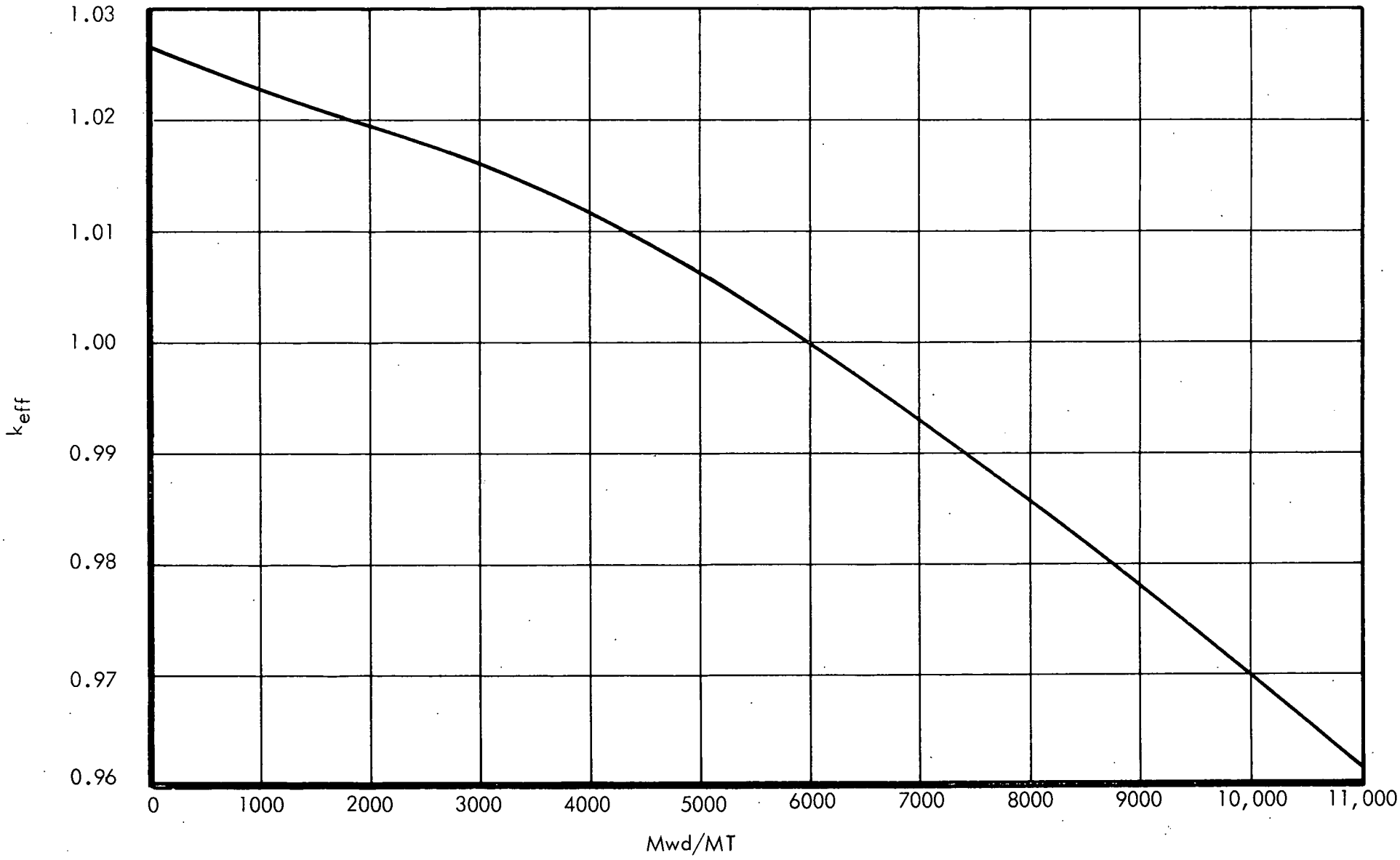

k_{eff} vs. NONUNIFORM BURNUP FOR CORE I FUEL ASSEMBLIES

FIG. 17

calculations gave parametric curves of reactivity and shutdown margin as functions of feed enrichment for the first reloading.

The exposure of the remaining Core-I assemblies for the next two burnup intervals and the exposure of the Core-II assemblies were estimated. Using the reactivity burnup curve for the Core-II fuel assemblies that was generated for this estimate, together with the similar curve for Core-I assemblies, the exposures of Core I and Core II fuel assemblies were estimated.

A local-peaking calculation determined the peaking in a cell with one Core-II feed-fuel assembly and three Core-I exposed-fuel assemblies. The results were compared with the present core, where each cell contains one Core-I assembly of 5.2 w/o enrichment and three Core-I assemblies of 4.3 w/o enrichment. Since the peaking was found to be more severe in the present core, it is not a problem in the second core.

4.3.3 Results and Conclusions

The study shows that, for feed enrichments between 4.4 w/o and 4.8 w/o, the expected average exposures and calculated minimum stuck-rod shutdown margins are as given in Table 18.

TABLE 18

CORE-II AVERAGE EXPOSURE AND MINIMUM SHUTDOWN MARGIN

feed enrichment w/o	average exposure Mwd/MT	minimum shutdown margin $\%\Delta k/k$
4.4	14,800	-1.0
4.6	16,300	-0.4
4.8	17,500	+0.2

The calculated shutdown margins were quite conservative since they correspond to a stuck-rod worth of 5.4 percent $\Delta k/k$. Based on values inferred from ERR measurements, this calculated stuck-rod worth was known to be high. The conservative values were used in the recommendation because the completion schedule of the analysis did not allow time to resolve the high value of the calculated stuck-rod worth. The stuck-rod worth was later resolved under Task 204 - Control Rod Analysis (see Sec. 4.3).

The final selection of loading (4.4 w/o U-235) was influenced by additional factors not mentioned in the statement of the objective. Table 19 gives values for enrichments of 4.4, 4.6, and 4.8 w/o.

TABLE 19

TYPICAL FUEL CYCLES FOR VARYING FEED ENRICHMENTS

feed enrichment (w/o)	maximum cold reactivity during cycle (% Δ k/k)	minimum stuck-rod shutdown margin (% Δ k/k)	Core-I exposure average (Mwd/MT)	Core-I exposure maximum (Mwd/MT)	projected Core-II exposure average (Mwd/MT)	projected Core-II exposure maximum (Mwd/MT)
4.4	11.9	-1.0	9,800	13,000	14,800	15,400
4.6	12.5	-0.4	10,200	13,900	16,300	17,000
4.8	13.1	+0.2	10,800	14,900	17,500	18,000

5. PLANT ENERGY TRANSFER SYSTEMS

During July and August of 1963, plant activities were directed toward execution of the power testing program, the emergency and test condenser being utilized as a heat sink. Preparations for integrated plant operation were also continuing. The superheater and turbine were put into service on August 24, and the plant achieved an electrical output of 5 Mw. Delays occurred subsequently because of the following problems: primary feedwater pulsing; high airborne activity in the containment building resulting from valve leaks; and radiolytic gases. The first operating data for the integrated plant were obtained in January 1964. Full-power operating data were obtained in February and March.

5.1 REACTOR PRIMARY SYSTEM (Task 301)

5.1.1 System Performance

Data collected during January were used to calculate the heat transferred in the evaporators and subcoolers during reactor operation at 18 Mwt and 24 Mwt. These initial heat balances were quite poor because of inaccuracies in the instrumentation. The calculated secondary-system heat gain was consistently greater than the calculated heat removal from the primary system, indicating inaccuracies in the primary-system flowmeters. Heat balance calculations are expected to be accurate within ± 5 percent on the basis of the installed instruments. If accuracies on the order of ± 0.5 percent were desired, special instrumentation and carefully controlled tests would be required. Subsequent to these calculations, the instrumentation was checked and recalibrated.

February data evaluation showed a good agreement between the primary and secondary heat balances calculated. Reactor power was gradually increased from 35 Mwt to full power (58.2 Mwt), which was achieved for the first time at 12 midnight, February 10, 1964. The heat transfer data at 35 Mwt and 58.2 Mwt for the individual components are given in Tables 20 and 21. The values calculated for the heat transferred and the overall heat transfer coefficients showed excellent agreement with the measured values everywhere except for the No. 2 subcooler at 35 Mwt. This discrepancy may be attributed to an adjustment that was made in the subcooler outlet valve (PF1-2) when temperature readings were taken. While these data

TABLE 20

RESULTS OF HEAT BALANCE CALCULATIONS

	Heat Transferred, Btu/hr	
N-5 Power Level	35 Mwt	58.2 Mwt
Date Data Taken	2-5-64	2-20-64
Evaporator No. 1 Calculations		
Based on primary system data	4.52×10^7	8.74×10^7
Based on secondary system data	4.55×10^7	8.44×10^7
Average	4.53×10^7	8.59×10^7
Deviation from average, %	±0.11	±1.75
Evaporator No. 2 Calculations		
Based on primary system data	4.27×10^7	8.60×10^7
Based on secondary system data	4.54×10^7	8.29×10^7
Average	4.44×10^7	8.445×10^7
Deviation from average, %	±3.82	±1.83
Subcooler No. 1 Calculations		
Based on primary system data	9.35×10^6	1.28×10^7
Based on secondary system data	9.83×10^6	1.39×10^7
Average	9.59×10^6	1.335×10^7
Deviation from average, %	±2.5	±4.1
Subcooler No. 2 Calculations		
Based on primary system data	8.46×10^6	1.3×10^7
Based on secondary system data	9.76×10^6	1.37×10^7
Average	9.11×10^6	1.335×10^7
Deviation from average, %	±6.03	±3.37
Total Heat Transferred		
Based on primary system data	10.57×10^7	19.92×10^7
Based on secondary system data	10.98×10^7	19.49×10^7

TABLE 21

CALCULATED OVERALL HEAT TRANSFER COEFFICIENTS

	Btu/hr $(ft^2)(^oF)$	
N-5 Power Level	35 Mwt	58 Mwt
Date Data Taken	2-5-64	2-19-64
Evaporator No. 1 Calculations		
Based on primary system data	357	616
Based on secondary system data	355	595
Average	356	605.5
Deviation from average, %	±0.3	±1.73
Evaporator No. 2 Calculations		
Based on primary system data	337	608
Based on secondary system data	336	585
Average	336.5	596.5
Deviation from average, %	±0.15	±1.93
Subcooler No. 1 Calculations		
Based on primary system data	407	600
Based on secondary system data	443	627
Average	425	613.5
Deviation from average, %	±4.23	±2.2
Subcooler No. 2 Calculations		
Based on primary system data	369	610
Based on secondary system data	440	616
Average	403.5	613
Deviation from average	±9.3	±0.5

were taken, the evaporator blowdowns were closed, and the evaporator outlet-line moisture separators removed 3.4 gpm for Evaporator No. 1 and 6.0 gpm for Evaporator No. 2, as determined by the difference between the secondary feedwater inlet and steam outlet flows. The secondary-steam quality, as determined by an Ellison steam calorimeter, ranged between 99.8 percent and 100 percent.

The 28-day warranty run commenced on February 17, 1964, and ended on March 20, when the reactor plant was shut down for piping modifications and maintenance repairs. The performance data at full power for the evaporators and subcoolers showed excellent agreement with the design values (see Table 22).

TABLE 22

COMPARISON OF THERMAL DUTIES

	actual, Btu/hr	design, Btu/hr	deviation, %
evaporators	8.23×10^7	8.5×10^7	1.41
subcoolers	1.32×10^7	1.34×10^7	1.50

Data compiled and computed for operation during March (Tables 23 to 26) were used in computing heat transfer duties and overall heat transfer coefficients. The calculated secondary-system heat gain is, again, greater than the calculated heat removal from the primary system. The secondary-system thermal power is used for calibration purposes at the site for the following reasons:

1. A more accurate calculation of flow can be obtained, since five flowmeters are available for measuring secondary flows, but only two for primary flows.

2. The steam quality delivered to the superheater can be measured easily.

3. Thermocouple-jack temperature points are more accessible, which makes temperature checks by an L&N bridge possible.

4. The turbine heat rate can be compared with the manufacturer's curve and the Boiler No. 3 measured heat rate.

The component reliability file shows 32 primary-system entries for the report period. Some of the major problems were discussed in the foregoing sections. Analysis and correction of these difficulties were handled by the Allis-Chalmers Operations Project as part of the responsibility in plant startup and are reported here only to present the overall plant operating picture. These items are covered in more detail in the ERR Monthly Operational Reports. Small steam leaks in the primary valves continued to be a source of operating difficulty during the report period. The component reliability file shows 27 entries involving valve leaks. These leaks could often be repaired by replacing the valve packing. The primary

TABLE 23

RESULTS OF HEAT BALANCE CALCULATIONS
(3-3-64)

	Heat Transferred, Btu/hr		
Power Level	58.2 Mwt		
Date & Time Data Taken	3-3-64 1740	3-3-64 2241	3-4-64 0335
Evaporator No. 1 Calculations			
Based on primary system data	8.19×10^7	8.16×10^7	8.34×10^7
Based on secondary system data	8.62×10^7	8.58×10^7	8.64×10^7
Average	8.40×10^7	8.37×10^7	8.49×10^7
Deviation from average, %	±2.62	± 2.5	±1.77
Evaporator No. 2 Calculations			
Based on primary system data	8.11×10^7	8.12×10^7	8.28×10^7
Based on secondary system data	8.51×10^7	8.43×10^7	8.56×10^7
Average	8.31×10^7	8.28×10^7	8.42×10^7
Deviation from average, %	±2.41	±1.81	±1.66
Subcooler No. 1 Calculations			
Based on primary system data	1.25×10^7	1.25×10^7	1.23×10^7
Based on secondary system data	1.40×10^7	1.39×10^7	1.39×10^7
Average	1.33×10^7	1.32×10^7	1.31×10^7
Deviation from average, %	±5.26	±5.26	±6.12
Subcooler No. 2 Calculations			
Based on primary system data	1.30×10^7	1.28×10^7	1.23×10^7
Based on secondary system data	1.38×10^7	1.36×10^7	1.37×10^7
Average	1.34×10^7	1.32×10^7	1.30×10^7
Deviation from average, %	±2.98	±3.03	±5.38
Total Heat Transferred			
Based on primary system data	18.85×10^7	18.81×10^7	19.08×10^7
Based on secondary system data	19.91×10^7	19.75×10^7	19.96×10^7

TABLE 24

RESULTS OF HEAT BALANCE CALCULATIONS
(3-19-64)

	Heat Transferred, Btu/hr		
Power Level		58.2 Mwt	
Date & Time Data Taken	3-19-64 1357	3-19-64 1550	3-19-64 1848
Evaporator No. 1 Calculations			
Based on primary system data	8.28×10^7	8.26×10^7	8.24×10^7
Based on secondary system data	8.54×10^7	8.54×10^7	8.57×10^7
Average	8.41×10^7	8.40×10^7	8.41×10^7
Deviation from average, %	±1.55	±1.67	±1.9
Evaporator No. 2 Calculations			
Based on primary system data	8.2×10^7	8.22×10^7	8.17×10^7
Based on secondary system data	8.5×10^7	8.5×10^7	8.5×10^7
Average	8.35×10^7	8.36×10^7	8.33×10^7
Deviation from average, %	± 1.8	±1.67	±2.04
Subcooler No. 1 Calculations			
Based on primary system data	1.21×10^7	1.27×10^7	1.26×10^7
Based on secondary system data	1.387×10^7	1.387×10^7	1.39×10^7
Average	1.3×10^7	1.33×10^7	1.33×10^7
Deviation from average, %	± 6.9	± 4.5	± 4.5
Subcooler No. 2 Calculations			
Based on primary system data	1.29×10^7	1.26×10^7	1.28×10^7
Based on secondary system data	1.35×10^7	1.35×10^7	1.35×10^7
Average	1.32×10^7	1.30×10^7	1.32×10^7
Deviation from average, %	± 2.2	± 3.8	± 2.3
Total Heat Transferred			
Based on primary system data	18.98×10^7	19.01×10^7	18.95×10^7
Based on secondary system data	19.78×10^7	19.78×10^7	19.81×10^7

TABLE 25

CALCULATED OVERALL HEAT TRANSFER COEFFICIENTS
(3-3-64)

Btu/hr $(ft^2)(^oF)$

Power Level		58.2 Mwt	
Date & Time Data Taken	3-3-64 1740	3-3-64 2241	3-4-64 0335
Evaporator No. 1 Calculations			
Based on primary system data	513	548	610
Based on secondary system data	546	579	631
Average	530	564	620
Deviation from average, %	±3.02	±2.66	±1.77
Evaporator No. 2 Calculations			
Based on primary system data	515	547	606
Based on secondary system data	539	568	627
Average	527	558	617
Deviation from average, %	±2.27	±1.79	±1.47
Subcooler No. 1 Calculations			
Based on primary system data	502	510	580
Based on secondary system data	561	568	654
Average	532	539	617
Deviation from average, %	±5.45	±5.38	± 6.0
Subcooler No. 2 Calculations			
Based on primary system data	542	537	600
Based on secondary system data	577	571	668
Average	560	554	634
Deviation from average, %	±3.04	±3.07	±5.37

TABLE 26

CALCULATED OVERALL HEAT TRANSFER COEFFICIENTS
(3-19-64)

Btu/hr $(ft^2)(^\circ F)$

Power Level		58.2 Mwt	
Date & Time Data Taken	3-19-64 1357	3-19-64 1550	3-19-64 1848
Evaporator No. 1 Calculations			
Based on primary system data	546	532	522
Based on secondary system data	562	548	542
Average	554	540	532
Deviation from average, %	±1.45	±1.48	±1.88
Evaporator No. 2 Calculations			
Based on primary system data	541	528	518
Based on secondary system data	561	547	539
Average	551	537.5	528.5
Deviation from average, %	±1.82	±1.77	±1.98
Subcooler No. 1 Calculation			
Based on primary system data	569	600	588
Based on secondary system data	652	655	650
Average	610	628	619
Deviation from average, %	± 6.9	± 4.3	± 5.0
Subcooler No. 2 Calculations			
Based on primary system data	615	593	576
Based on secondary system data	643	636	607
Average	629	621.5	591.5
Deviation from average, %	± 2.2	± 2.3	± 2.6

relief valves that had been leaking during operation were removed from the system and returned to the vendor for flanging. Previously, these valves were welded to the system and could not easily be removed for repair, resetting or retesting. These valves were reinstalled with flanged connections for easier maintenance.

5.1.2 System Analysis

The heat-transfer relationship of the evaporators is shown in Fig. 18, which is a plot of heat flux (q/A) versus the temperature difference between the primary and secondary steam (Δt_b). The scattering in the data is mainly attributed to the flow meter inaccuracies mentioned in this report. Component behavior was rated on a thermodynamic heat exchanger efficiency, which is defined as the ratio of the actual amount of heat removed from a fluid to the maximum amount that could be removed (by an exchanger with infinite surface).

The calculated efficiencies compare favorably with the design values, as shown in Table 27.

TABLE 27

COMPARISON OF ACTUAL AND DESIGN HEAT EXCHANGER EFFICIENCIES

	actual	design	deviation
Evaporators	0.512	0.553	-0.041
Subcoolers	0.683	0.605	+0.078
Overall (evaporators & subcoolers)	0.818	0.825	-0.007

A reactor power of approximately 0.4 to 0.5 Mwt was found to be required to maintain the reactor temperature at 537 F and primary pressure at 922.6 psig. This power compensates for the system heat losses, which are less than 1 percent of the primary output. Of this heat loss, approximately one-half is discharged to the river via the purification and shield coolers. The other 1/2 percent is attributed to environmental heat losses, a factor that compares favorably with conventional power plants. A more accurate calculation will be made, which will utilize a shield-cooling water meter. However, the present approximations indicate the proposed 20-ton air conditioner for the reactor containment building is necessary for a total air-conditioning capacity of 60 tons.

5.2 SUPERHEATER (Task 303)

5.2.1 System Performance

The pertinent operating characteristics of the separately-fired superheater are shown in Figs. 19 and 20. The curves, which were drawn from operating data, show the shape expected for normal operation. Typical operating data (taken on March 19) are compared with initial design data in Table 28.

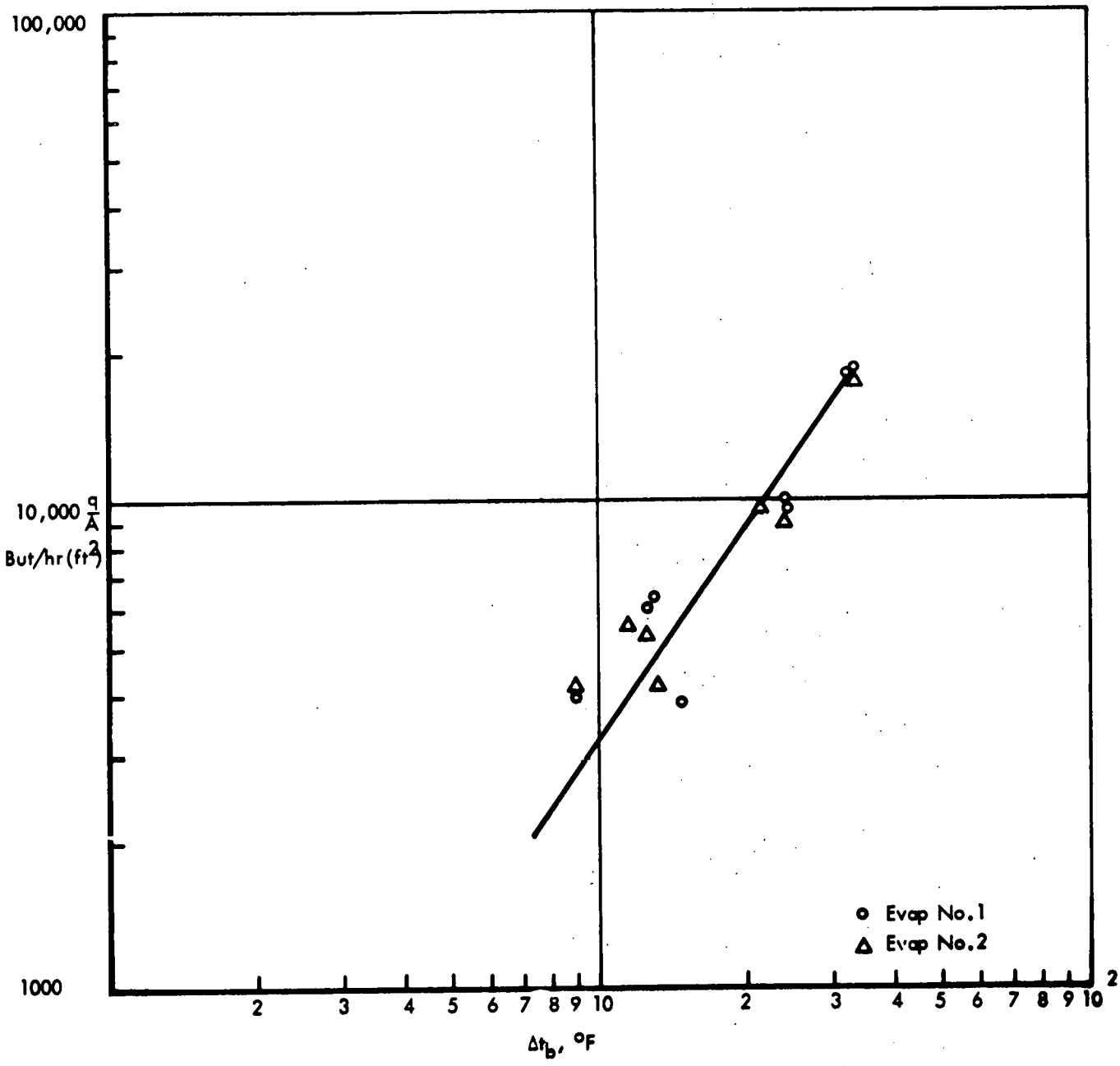

HEAT-TRANSFER RELATIONSHIP OF EVAPORATORS

FIG. 18

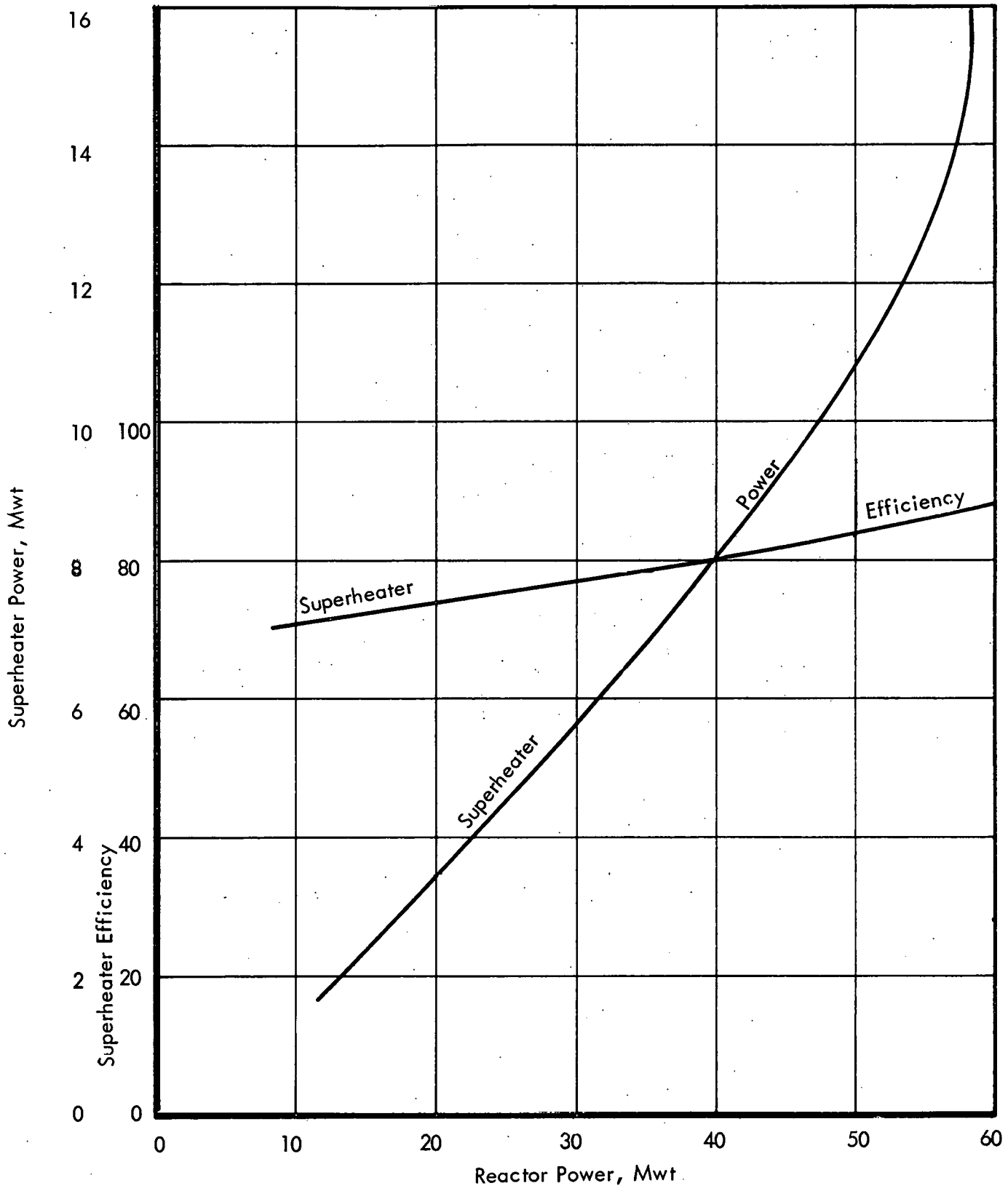

ERR SUPERHEATER OPERATING CHARACTERISTICS
JAN - FEB (1964)

FIG. 19

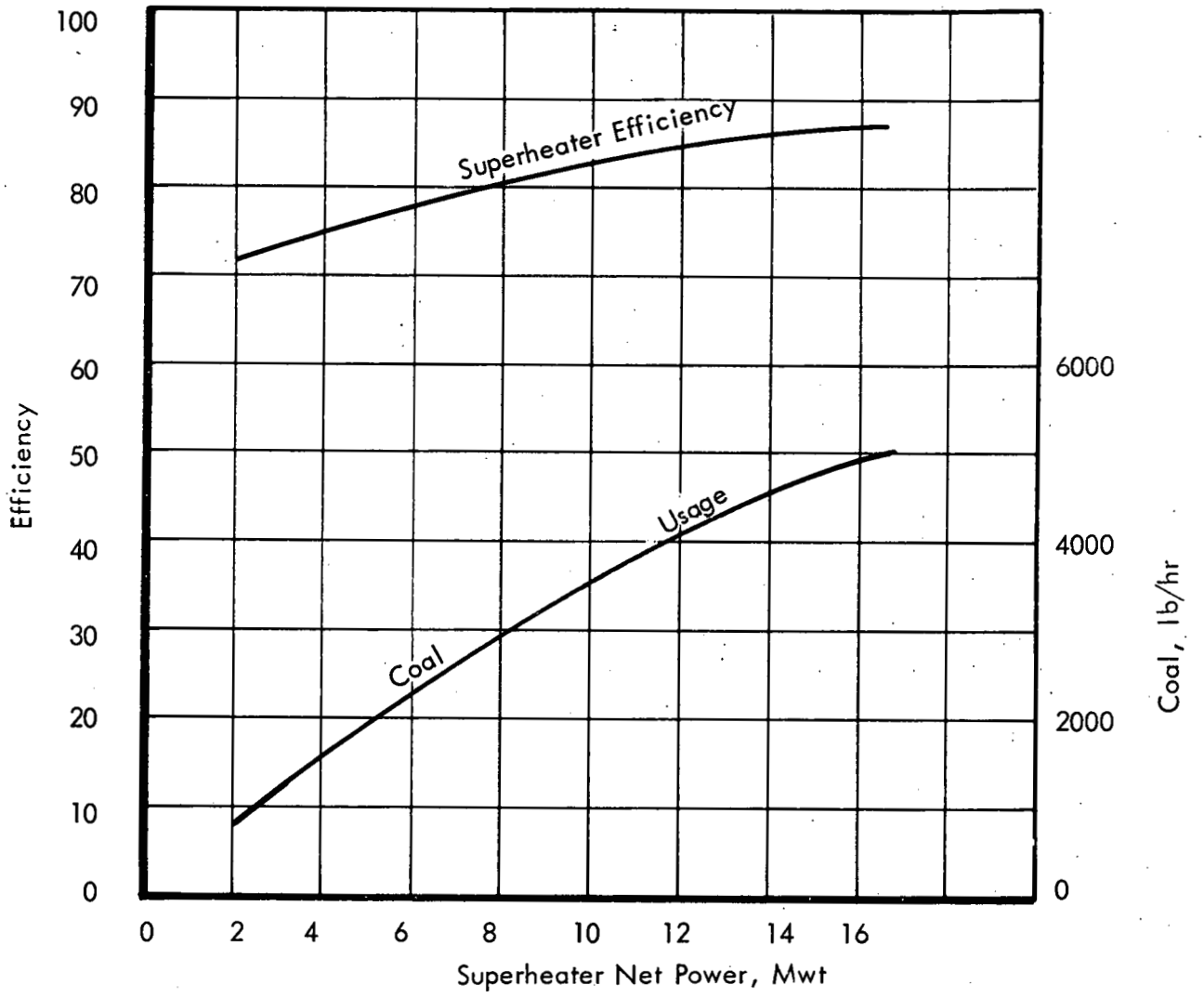

ERR SUPERHEATER OPERATING CHARACTERISTICS
JAN - MAR (1964)

FIG. 20

TABLE 28

COMPARISON OF MEASURED AND DESIGN SUPERHEATER DATA

	design	measured
Superheater inlet temperature, °F	503	500
Superheater inlet pressure, psig	684	690
Superheater outlet temperature, °F	830	824
Superheater outlet pressure, psig	620	620
Steam flow, inlet meters, lb/hr	225,000	229,400
Steam flow, outlet meter, lb/hr	225,000	229,833
Coal fired, lb/hr	4,573	4,654
Heating value of coal, Btu/lb	12,730	12,400
Steam quality inlet, %	99.75	100
Enthalpy of steam (inlet) Btu/lb	1198.23	1202.95
Enthalpy of steam (outlet) Btu/lb	1421.98	1420.23
Superheater duty, Btu/hr	50.3×10^6	49.8×10^6
Overall thermal efficiency, %	87	86.3
Net thermal power, Mwt	14.75	14.6
Calculated plant heat rate, Btu/kw-hr	11,230	10,350

Superheater temperatures indicated satisfactory operation and no hot spots. Thermocouple readings were obtained by an L&N bridge, and typical values are shown in Fig. 21. A typical temperature profile is given in Fig. 22 showing the temperature increase between inlet and outlet sections.

The component reliability file shows 26 entries during the report period. Most of the repairs required were minor and could be considered normal for putting new equipment on the line. The fan blades in the pulverizer required repositioning to achieve design steam temperatures without overloading the pulverizer mill. Repositioning of the fan blades toward the outer edge of the fan rotor increased the velocity through the mill, causing a better coal flow and less load on the motor. Five file records showed difficulties in lighting the superheater torches. Adjustment of the flame rod remedied the deficiency.

5.2.2 System Analysis

The overall performance of the separately-fired superheater was generally excellent. Under normal, base-load conditions, a balanced draft and stabilized coal feed were the only essentials for steady-state operation. The outlet steam temperature was easily maintained at 825 F, and the interstage desuperheating spray-water was not used. The unit thermal efficiency was close to the design value of 87 percent. The design efficiency should be achieved when final adjustments are made and operating techniques are finalized.

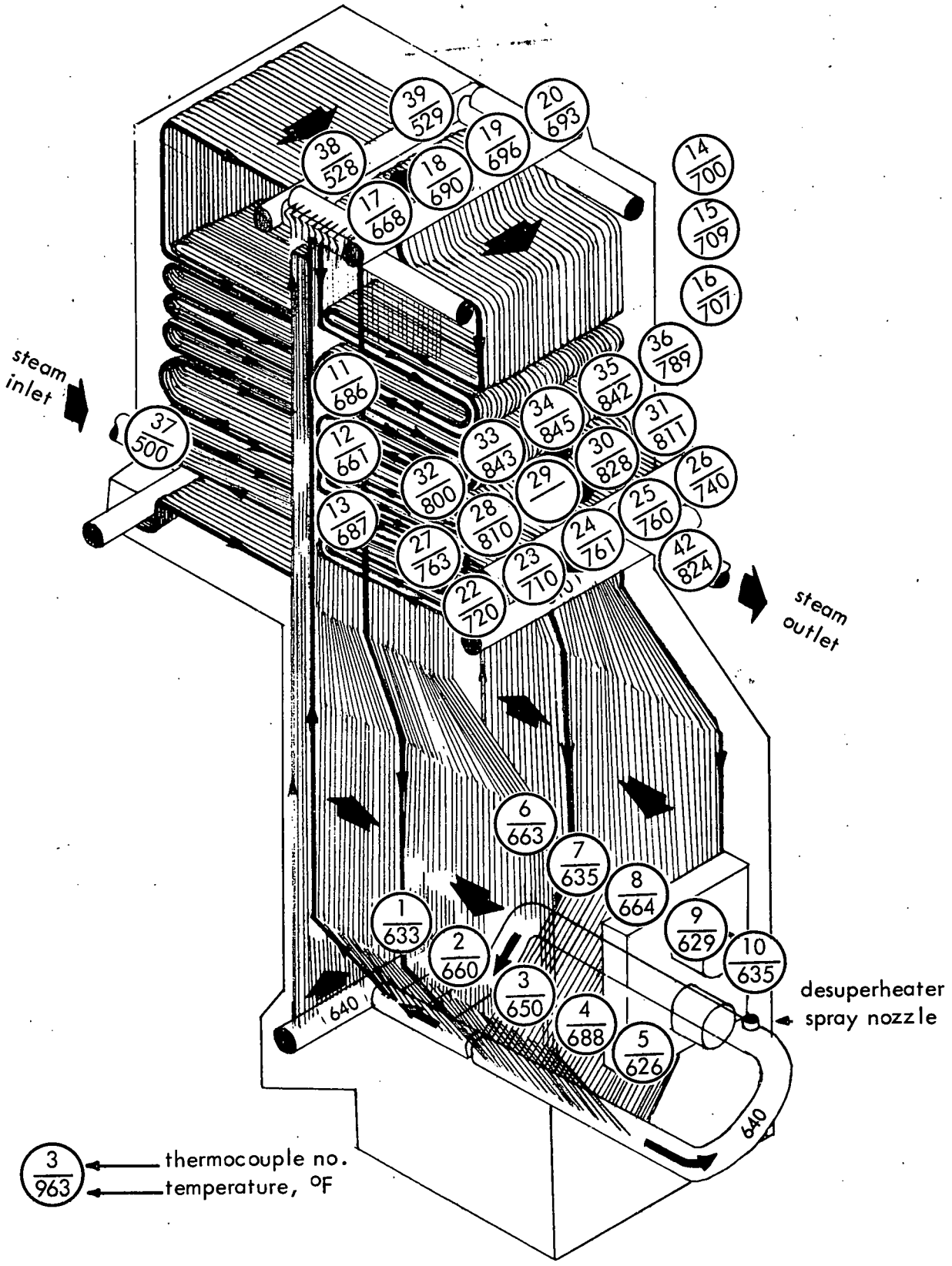

ERR SUPERHEATER

FIG. 21

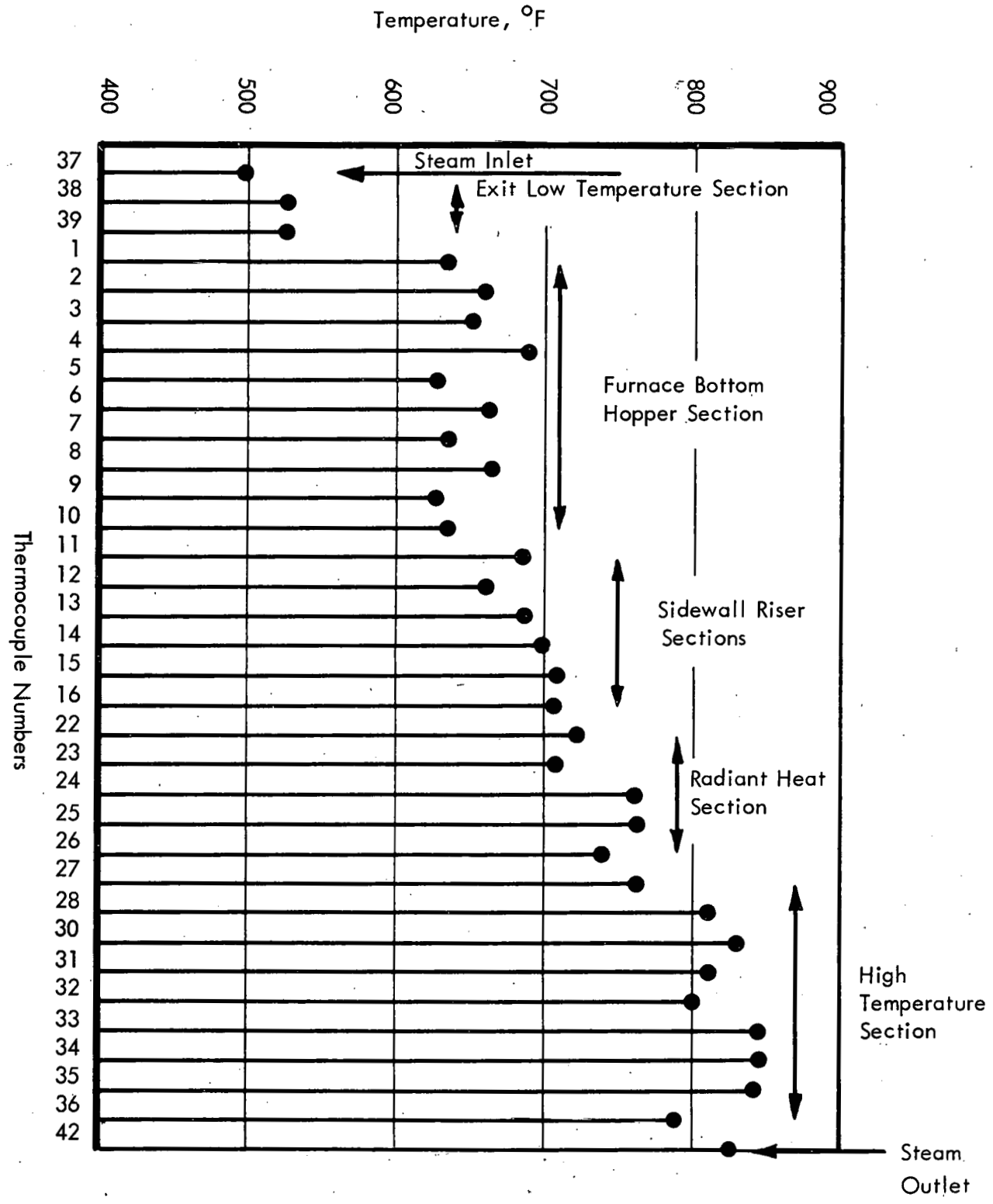

ERR SUPERHEATER TEMPERATURE PROFILE

FIG. 22

The steam cooling valve opens automatically whenever the reactor scrams, and continued steam flow prevents superheater overheating upon sudden shutdown. In a typical instance, the outlet temperature rose only 20 deg after scram. Within 2 min, the outlet temperature was gradually decreasing, while the internals absorbed stored heat. The internal temperature had leveled off at about 725 F before overall cooldown commenced. Recorded temperature points indicated that all superheater elements operated within safe temperature limits.

5.3 REACTOR GROSS POWER AND PLANT HEAT BALANCE (Task 304)

The objective of this task is to determine the gross power of the reactor and the overall thermal efficiencies of the entire plant, during steady-state operating conditions. The net power output of the reactor and superheater are to be compared with the heat energy available to the steam turbine and are to be related to the electrical output of the plant.

5.3.1 System Performance

Evaluation of the system performance has been somewhat hampered by inaccuracies in the plant-flow and temperature transmitters and recorders. These difficulties, which were mentioned in the report, show the need for accurate data in analyzing plant performance. In order to obtain reasonably accurate heat balances, the instruments must be recalibrated at frequent intervals. The data have shown that heat balances are good immediately after instrument calibration. These inaccuracies also affect the calculation of reactor power level, which is used to calculate fuel burnups. Presently, the most accurate measurement of thermal output is based on measurements of secondary-system temperatures, pressures, and flows (see Sec. 5.1.1).

Table 29 shows results of the overall heat balances for two power levels. Figure 23 illustrates the measured flows and temperatures in the plant transfer system from data taken at full power. These values are compared to the design values in Table 30 (see Fig. 6.1 of Ref. 15). In general, the thermal performance of the plant is better than was predicted.

Considerable difficulty was experienced in maintaining high-quality secondary steam to the superheater inlet at all power levels. Steam quality is maintained at the desired 99.75 percent by adjusting the water level on the shell side of the evaporators. At intermediate power levels, the water level must be lowered to maintain steam quality. At power levels below approximately 22 Mwt and above approximately 54 Mwt, optimum performance is obtained at a higher water level.

The above characteristics may be attributed to the operation of the centrifugal-type steam separators according to the following postulations:

1. At low power levels, the vapor velocity in the evaporator shell is low and there is very little moisture entrainment. Therefore, the quality of steam entering and leaving the separator is good even though the separator efficiency is low because of low vapor velocity.

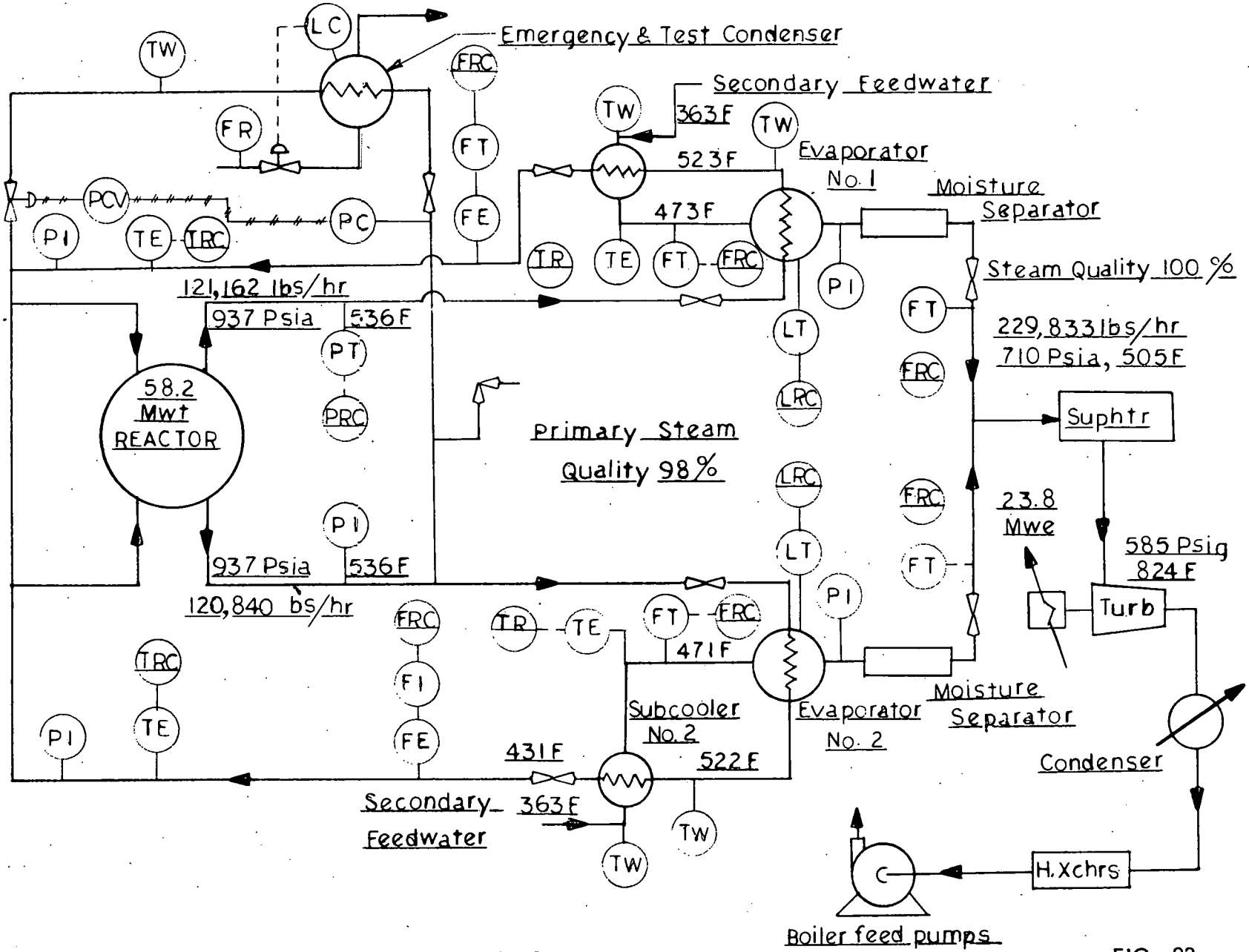

PLANT ENERGY TRANSFER SYSTEM PERFORMANCE

FIG. 23

TABLE 29

OVERALL SYSTEM HEAT BALANCE

	Date 2-5-64	3-3-64
Percent of full power	56	99.6
Reactor thermal power, Mwt	32.6	58.0
(1) Basis, primary system	31.2	56.6
(2) Basis, secondary system	32.2	57.6
evaporators	26.6	49.6
subcoolers	5.6	8.0
(3) Total heat loss	0.40	0.40
purification system	0.08	0.24
shield cooling system	0.05	0.04
unaccountable	0.27	0.12
Superheater thermal power, Mwt		
(1) Coal Input	8.18	16.53
(2) Gas input	1.01	0.38
(3) Steam output	7.82	14.52
(4) Efficiency	85.1	85.8
Turbine generator gross output, Mwe	13.8	24.3
Turbine heat rate, Btu/kwhr	10,130	10,150
Plant thermal efficiency, %	33	32.4

TABLE 30

COMPARISON OF MEASURED AND DESIGN FLOWS AND TEMPERATURES

primary system	design	measured
Reactor power, Mwt	58.2	58.2
Steam pressure, psia	936	937
Steam temperature, °F	536	536
Steam quality, %	-	98
Steam flow, Loop 1, lb/hr	129,000	121,162
Steam flow, Loop 2, lb/hr	129,000	120,840
Feedwater temperature, °F	450	431
Evaporator No. 1 outlet, °F	536	523
Evaporator No. 2 outlet, °F	536	522
secondary system	**design**	**measured**
Steam pressure, evaporator outlet, psia	714	710
Steam temperature, evaporator outlet, °F	506	505
Steam flow, superheater outlet, lb/hr	225,000	229,833
Steam pressure to turbine, psig	600	585
Steam temperature to turbine, °F	825	824
Feedwater to subcoolers, °F	350	363
Feedwater to evaporator No. 1, °F	464	473
Feedwater to evaporator No. 2, °F	464	471
Turbine generator output, Mwe	22	23.8

2. As the power is increased, the vapor velocity in the evaporator shell increases, and moisture entrainment becomes appreciable, which lowers the quality of steam leaving the evaporator. At these velocities, the centrifugal separator is not yet operating at peak efficiency, and the exit steam quality is low. Lowering the apparent water level in the evaporators allows more space for moisture de-entrainment, which increases the quality of steam going to the separators.

3. As full power is approached, moisture entrainment increases even more. The size of entrained droplets also increases. The velocity is high enough so that the centrifugal separator approaches peak efficiency. Therefore, even though the steam quality entering the separator is poor, the exit steam quality is good.

The manufacturer's information on the steam separators indicates that, at the capacities of interest, the steam separator will remove more than 95 percent of the entering droplets. Theoretically, however, the separation efficiency depends on particle size. Separation efficiencies for particle sizes less than 10μ are usually appreciably lower than those for larger particle sizes. To better understand the actual cause of the phenomenon, instrumentation would have to be added to determine: (1) the steam quality leaving the evaporator, and (2) the flow rate of water leaving the steam separators.

Since the characteristics encountered here could also be attributed to other factors (e.g., foaming), they will be the subject of a continuing evaluation.

Judicious lowering of the normal water level in the evaporators has eliminated moisture carryover, and would seem to be acceptable in operating the reactor as a base-load plant. Extreme steam purity is necessary since troublesome turbine-blade deposits may occur with surprisingly low (0.6 ppm) total-solids contamination in the steam. In the 500 - 900 psi range, however, these deposits are usually water soluble and can be removed by periodic washing.

5.4 CORROSION SAMPLES AND TESTS - EVAPORATOR WATER BOXES (Task 615)

In April 1964, the ERR-OAP project recommended that corrosion specimens be inserted into the ERR evaporator water boxes. This recommendation was made from results of the analysis of primary-steam radiolytic gas for non-vented reactor operation (see Sec. 5.5). This analysis showed that the oxygen concentrations in the primary steam leveled off to about 300 ppm at full power. Chlorides in the primary water were non-detectable. Because of the lack of corrosion data for these operating conditions, corrosion test specimens were installed into the primary system in order to obtain the corrosion data of particular interest to ERR operation.[16]

A specimen-mounting clamp mechanism was designed and fabricated to project the test specimens into the fluid flow in the upper and lower evaporator water boxes. The first two sets of corrosion test samples were installed in Evaporator No. 2 on May 27, and the second two sets were installed in Evaporator No. 1 on June 8. The corrosion specimens were prepared in accordance with Recommended Practice for Conducting Plant Corrosion Tests,

ASTM A224-46. The four corrosion-sample test fixtures were fabricated in accordance with Allis-Chalmers Drawing 43-401-523-501 (Fig. 24).

The fixture consists of two rings, one of which is welded into the handhole of the evaporator. The other, removable ring, which contains the corrosion samples, is held in place by a set of ears that protrude into the first ring. The handhole covers, when welded in position, provide a positive lock for the removable ring.

The corrosion samples, mounted on an extended rod, form an integral part of the removable ring. Each fixture contains nine 2-in. x 2-in. x 1/16-in.-thick unstressed coupons of Type-304 stainless steel and one 3/4-in. x 1/4-in.-thick stainless-steel U-bend bar. The mounted samples are fastened to the holding ring by a 1/4-in., Type-304 stainless-steel rod. Spacers separate the nine coupons. The samples are locked in place by a 1/4-in. stainless-steel nuts.

The 2-in. x 2-in. test coupons were sheared from a single sheet of cold-rolled, Type-304 Armco stainless steel. One-third of the samples are in the "as rolled" condition; one-third were annealed at 1800 F for 30 min and then water quenched; the remaining third were sensitized by furnace cooling from 1800 F. Surface discoloration was removed by washing with isopropyl alcohol and water and by washing with alcohol and demineralized water after pickling in an inhibited nitric-acid solution at 170 F. The samples were weighed prior to assembly. Lint-free gloves were used at all times in handling the samples.

Work on the first set of samples should complete the task. Since the two primary loops are symmetrically arranged, examination and testing of the samples will be done after 1 year for one evaporator and after 2 years for the other evaporator.

5.5 RADIOLYTIC GAS SAMPLING PROGRAM (Task 616)

On December 30, 1963, a planned program of power escalation to 25 Mwt was undertaken. This program included a test to determine the partial pressures of hydrogen and oxygen, at selected sample points in the primary system, during reactor operation in the non-vented condition (Test 1001).[16] The test was performed to ensure that the primary system did not contain a combustible mixture of gases. The test results showed that a combustible mixture did not exist in the primary system and that the steam contained oxygen as much as 300 ppm. Chemical analysis of primary water samples taken from a sampling point ahead of the purification system showed an average O_2 concentration of 1.2 ppm.

The volume-percent or mole-percent of oxygen concentration in the water is directly proportional to the partial pressure of oxygen in the steam. Equilibrium between oxygen in the liquid and oxygen in the vapor is established in accordance with Henry's Law, i.e.:

$$K = \frac{P}{X}$$

where K is the constant of Henry's Law,
P is the partial pressure of oxygen in vapor, and
X is the mole fraction of oxygen in water.

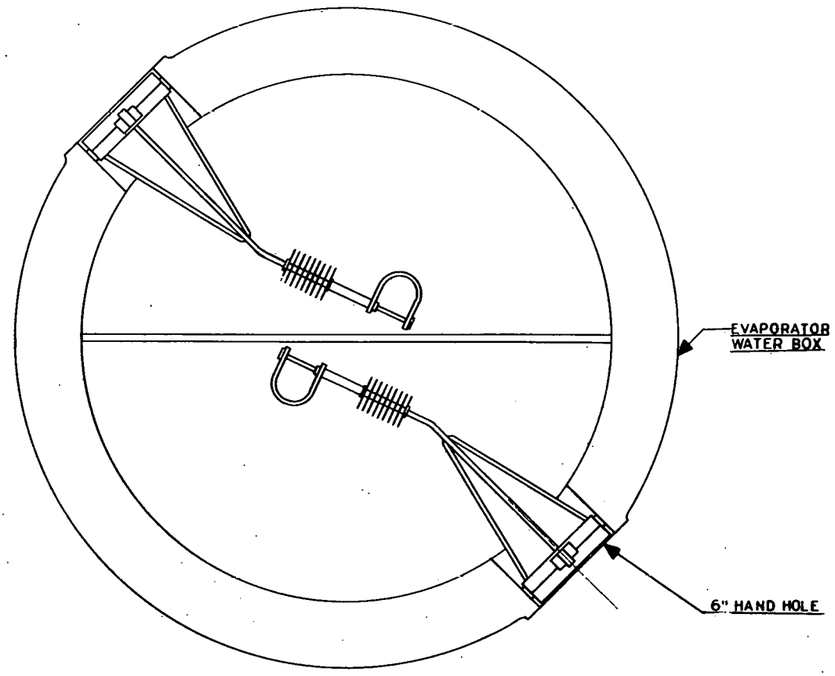

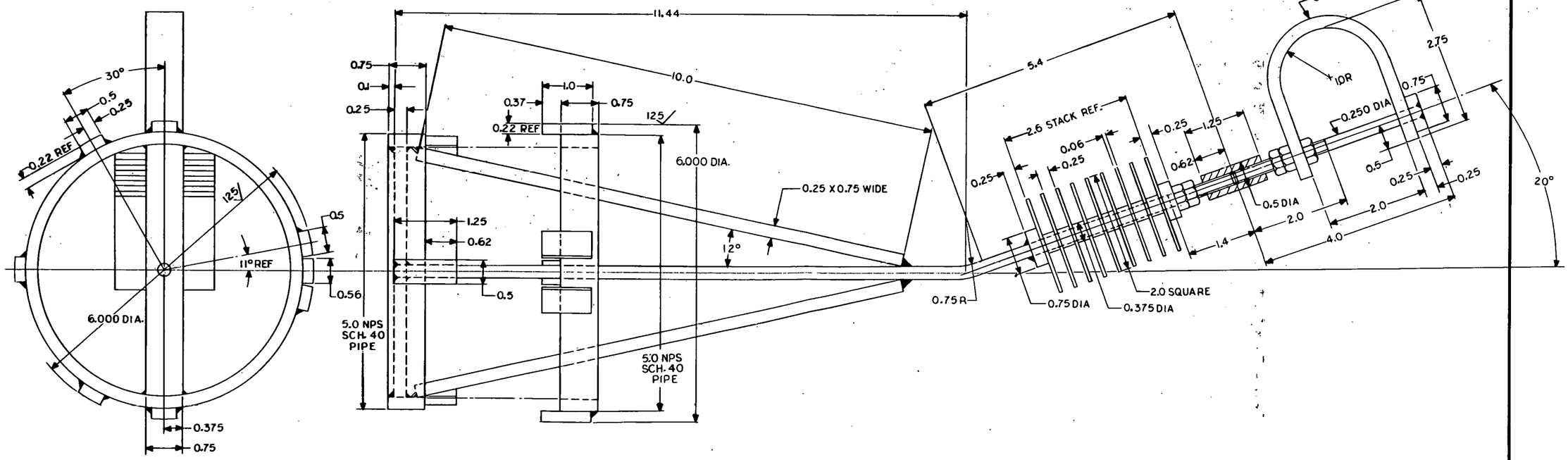

FIG. 24

01	6-19-64
02	7-13-64 GWB

UNLESS OTHERWISE NOTED DIMENSIONS ARE IN INCHES & MACHINING TOLERANCES ARE:

DIMENSIONS	UP TO 6 INCL.	OVER 6 TO 24 INCL.	OVER 24
FRACTIONAL	±	±	±
DECIMAL	±	±	±

ANGLES ±

— Confidential — Property of ALLIS-CHALMERS MFG. CO., Milwaukee, Wis.

DEPT. NUCLEAR POWER

DRN. HFH 6-19-64 CHKD.

APPD. TRC 7-15-64

SIMILAR TO:

SCALE 3/16 SIZE

CORROSION TEST SPECIMEN

43-401-523-501

43-401-523-501

A-C REPR. DOC., MILWAUKEE, WIS. FORM NO. 51744

Under operating conditions of 935 psia and 536 F, the oxygen concentration in the steam was found to be 288 ppm (i.e., 0.2 psia). By Henry's Law, the oxygen content in the water was calculated to be 1.56 ppm, which agrees well with the 1.2 ppm determined by chemical analysis.

It is possible that hydrogen and oxygen are recombining in the primary system, since analysis shows that the hydrogen and oxygen concentrations level off with time. An unresolved factor in the analysis is that the measured gas concentrations in the reactor head are close to the measured gas concentrations in the evaporator water boxes. The primary system downcomer piping to the subcoolers has been sloped to eliminate feedwater pulsing. The slope of the pipe is believed to have a bearing on the gas concentration in the steam line and evaporator water box. Additional tests for gas content in the steam and evaporator water boxes are to be conducted. A mass flow balance for radiolytic gas will be attempted with the new data on gas concentrations. Improvement in sampling and data analysis should result in a better correlation between gas content in the steam and water boxes.

It is generally accepted that stainless-steel stress corrosion occurs for a high oxygen content in the presence of a chloride concentration above 0.1 ppm. Weekly chemical analyses ensure that chloride concentrations in the reactor water remain below 0.1 ppm; thus far, these analyses show chloride concentrations to be less than 0.035 ppm. Serious corrosion is not anticipated for O_2 contents of 1.2 ppm and chloride concentrations less than 0.035 ppm. Although the steam has a high oxygen content, the chlorides, since they are not volatile, are practically non-existent in the steam. Chloride concentration in 98 percent quality steam, would be only 0.0007 ppm.

Tests [18] with steam containing 110 ppm oxygen gave low corrosion rates for stainless steel (0.2 mils per year). Visual inspection, after 2000 Mwd operation, of the internal surfaces of the evaporator water boxes, subcoolers, and interconnected piping revealed no serious corrosion. Corrosion samples inserted into the water boxes of the evaporators (see Task 615) provide surveillance for possible corrosion problems.

6. PRIMARY AUXILIARY SYSTEMS

6.1 REACTOR WATER PURIFICATION SYSTEM (Task 401)

6.1.1 System Performance

The first six months of reactor plant operation were devoted to tests of nuclear startup from zero power operation to integrated plant operation. The greatest problem confronting the purification system was the frequent renewal of prefilters because of "crud" accumulation. Filters were changed at intervals of two or three weeks, after having processed an average of 235,000 gal of water per run. At the completion of each run the filters were coated heavily with a dark brown residue. Chemical and spectral tests identified the residue as iron oxide with small amounts of manganese, copper, nickel, and chromium. The frequent filter changes were due to the release of corrosion products into the fluid stream, caused by the frequent startups and shutdowns and the thermal cycling that occurred during the test runs.

Ion-exchangers were protected from crud contamination by the prefilters. On two occasions the units gave indication of reduced efficiencies, and resin-bed channelling was suspected. The resin was air agitated to reconstruct the bed for improved performance. In July 1963, after air agitation, the No. 2 resin-bed decontamination factor increased from 450 to 3,100. Air-agitations were then utilized whenever reduced performance indicated resin channelling. The performance of the purification systems is shown in Fig. 25. The water purity was maintained without difficulty throughout the nuclear tests and the 28-day warranty run. The water quality is indicated by the analytical averages in Table 31.

TABLE 31

WATER QUALITY

Purification flow rate, gpm	6.0
Conductivity, μ mho/cm	1.0
Dissolved solids (ionic), ppm	0.5
pH	6.5
Chlorides, ppm	0.035
Total iron, ppm	0.20
Dissolved oxygen, ppm	1.2

Calculated heat-transfer and heat-transfer-coefficient values for the purification-system heat exchanger are shown in Table 32.

6.1.2 System Analysis

Different values for reactor-water conductivity were obtained from control-room recordings and laboratory-measured primary-water samples. The instruments and the analysis techniques were then checked. A conductivity cell was constructed by field forces and operated at the purification-system cooler. The conductivity then measured agreed with the control-room recordings, thus indicating that immediate testing of carefully taken samples will provide a better check on operating data.

Most of the water impurities were non-ionic, and these non-ionic impurities imposed the most load on the purification prefilters. Frequent prefilter changes are not unusual for initial reactor testing and operation. Similar experiences were encountered with the EBWR, ALPR, VBWR, and Dresden Plants.[19] The accumulated corrosion products were released gradually from low-velocity areas in the system, and the number of filter changes was reduced (see Figs. 25 and 26).

The life expectancy of the purification resins was estimated from data obtained between June 1963 and March 1964. During this period, over 10^6 gal of reactor water were treated by each purification loop. The resin ion-exchange activity was calculated to be reduced by only 30 percent from treating water with an average conductivity of 1 μ mho (0.5 ppm). The probable life of each demineralizer was shown to be approximately 30 months. However, two other factors -- resin fouling and radiation damage -- had to be considered.

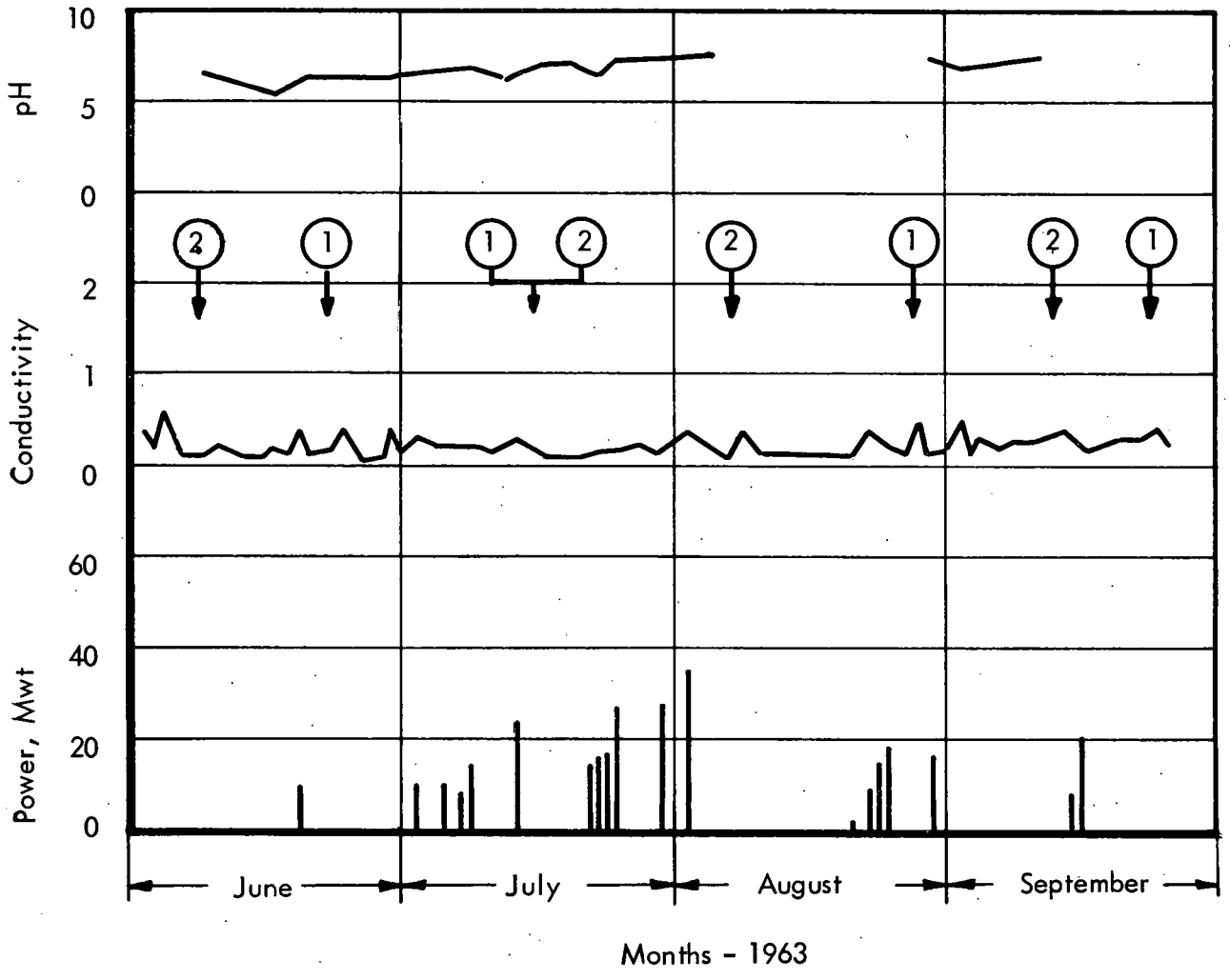

ERR PRIMARY WATER PURIFICATION (1963)

FIG. 25

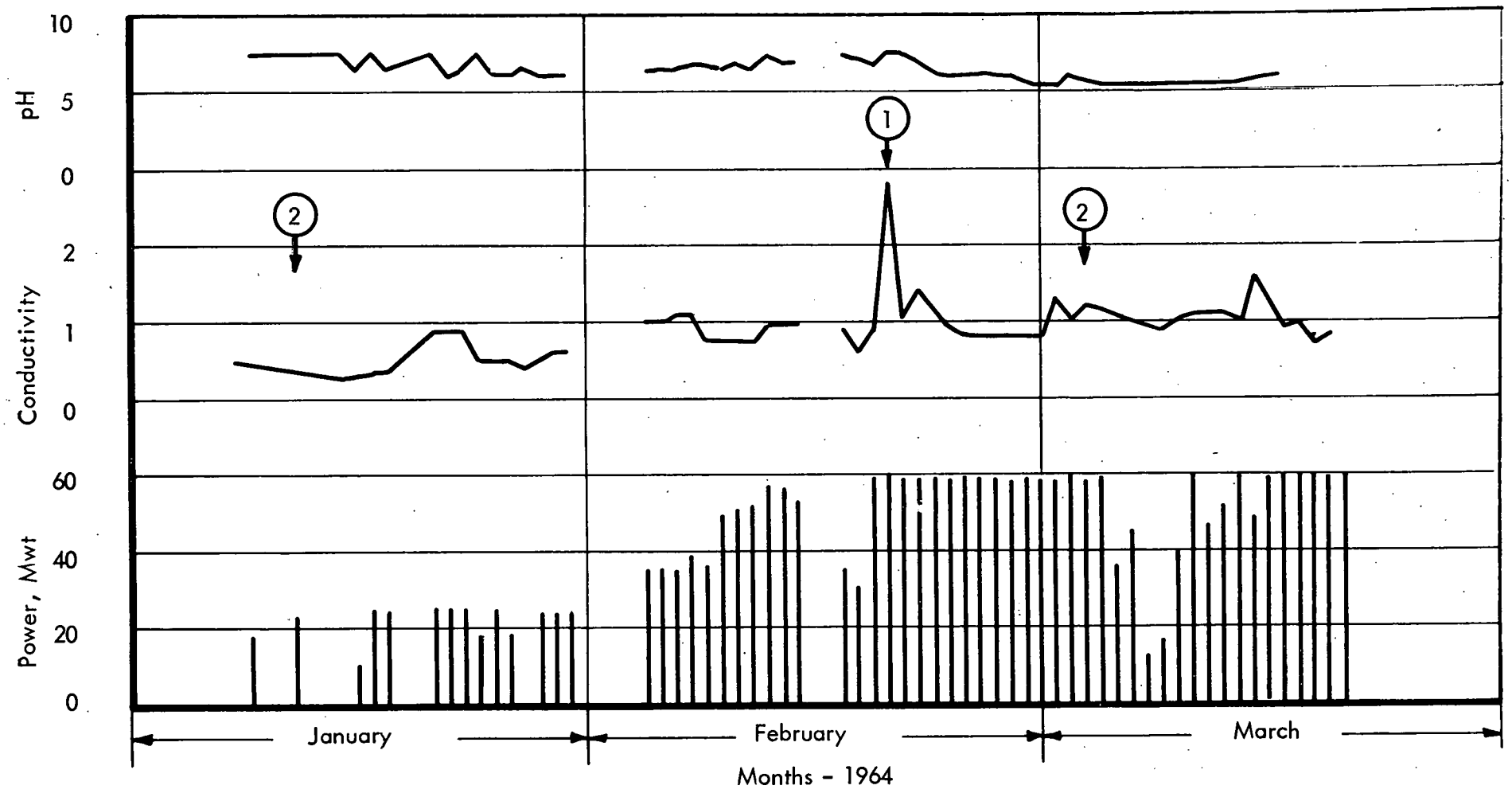

ERR PRIMARY WATER PURIFICATION (1964)

FIG. 26

TABLE 32

PURIFICATION-SYSTEM HEAT EXCHANGER HEAT BALANCE AND OVERALL HEAT-TRANSFER COEFFICIENTS

N-5 Power Level	35 Mwt	58 Mwt	58.2 Mwt	58.2 Mwt	58.2 Mwt	58.2 Mwt	58.2 Mwt	58.2 Mwt
Date Data Taken	2-5-64	2-19-64 2-20-64	3-3-64	3-3-64	3-3-64	3-19-64	3-19-64	3-19-64
Approximate Time Data Taken	0120 to 0148	1729 to 0550	1740	2240	0330	1357	1550	1848
Regenerative Heat Exchanger								
Heat Balance								
Heat in - Btu/hr	0.67×10^6	0.949×10^6	1.23×10^6	1.20×10^6	1.19×10^6	1.09×10^6	1.11×10^6	1.13×10^6
Heat out - Btu/hr	0.705×10^6	0.847×10^6	1.01×10^6	--	--	0.9×10^6	0.905×10^6	0.908×10^6
Heat Transfer Coefficient								
Based on heat in (Btu/(hr)(ft^2)($^\circ$F)	304	344	392	388	391	391	397	398
Based on heat out (Btu/(hr)(ft^2)($^\circ$F)	310	347	322	-	-	323	325	320
Purification Cooler								
Heat transmitted from primary (Btu/hr)	0.276×10^6	0.551×10^6	0.808×10^6	0.800×10^6	0.805×10^6	0.609×10^6	0.602×10^6	0.607×10^6
Overall heat transfer coefficient	48.8	141	187	185	186	132	137	139
Purification flow rates, gpm	4.0	6.0	8.0	8.0	8.0	7.0	7.0	7.0

THIS PAGE

WAS INTENTIONALLY

LEFT BLANK

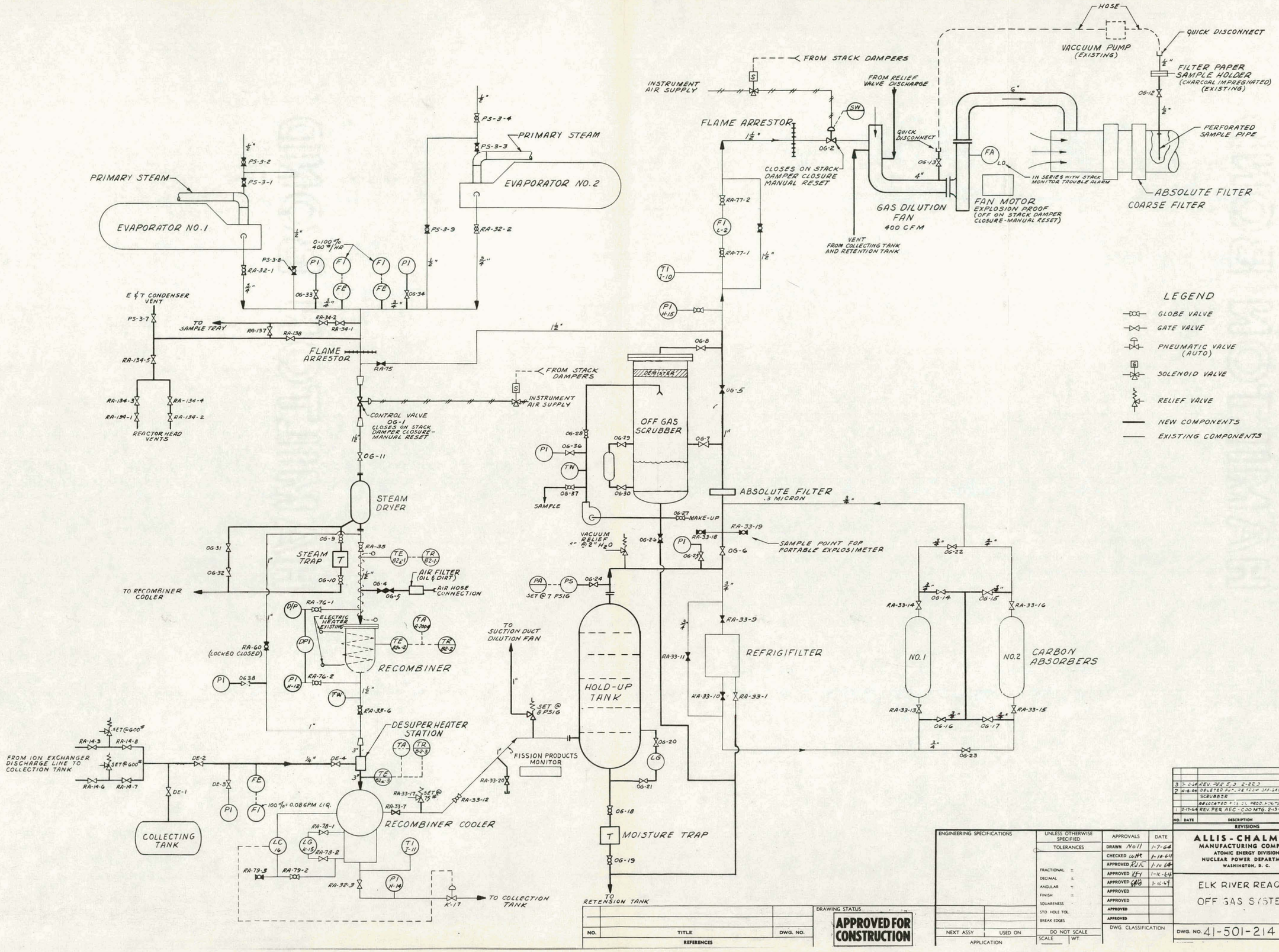

NO.	DATE	DESCRIPTION	APPD.	APPD.	APPD.
		REVISIONS			
3	7-1-64	REV. PER E.O. 2-22-3			
2	4-8-64	DELETED FUNCTIONS FROM OFF GAS SCRUBBER RELOCATED FUNCTIONS TO PROD. PIPING			
1	2-17-64	REV. PER AEC-GOO MTG. 2-13-64			

TITLE	DWG. NO.
REFERENCES	

DRAWING STATUS

APPROVED FOR CONSTRUCTION

ENGINEERING SPECIFICATIONS

UNLESS OTHERWISE SPECIFIED TOLERANCES

FRACTIONAL ±
DECIMAL ±
ANGULAR ±
FINISH
SQUARENESS
STD HOLE TOL
BREAK EDGES

DO NOT SCALE

NEXT ASSY	USED ON
APPLICATION	

SCALE WT.

APPROVALS	DATE
DRAWN NOll	1-7-64
CHECKED WHR	1-10-64
APPROVED RJK	1-10-64
APPROVED KFH	1-11-64
APPROVED GHG	1-16-64
APPROVED	
APPROVED	
APPROVED	
APPROVED	

DWG CLASSIFICATION

ALLIS-CHALMERS
MANUFACTURING COMPANY
ATOMIC ENERGY DIVISION
NUCLEAR POWER DEPARTMENT
WASHINGTON, D. C.

ELK RIVER REACTOR
OFF GAS SYSTEM

DWG. NO. 41-501-214 REV. 3

Operating experience has demonstrated that the reactor plant can be operated continuously without off-gas venting. The approval of Change Request No. 9 authorized reactor operation without routine use of the recombiner system, as long as the oxygen concentration in the primary-system steam does not exceed 400 ppm. The recombiner system may then be kept in standby during normal reactor operation.

6.4 BORON POISON SYSTEM (Task 407)

The boric acid solution was replaced[22] by sodium-pentaborate solution, a more reliable poison that can be stored at ambient temperatures without precipitation. Highly concentrated boric acid requires high-temperature storage (200 F), and failure of an electrical heating element on the tank, piping, or valves could result in cooldown, subsequent crystallization, and discharge-line clogging.

The solubilities of sodium pentaborate ($Na_2B_{10}O_{16} \cdot 10\ H_2O$) and boric acid, H_3BO_3, are compared in Fig. 28. A concentrated solution (17.85 w/o) is stored in the pressurized tank. Injection of 90 gal of this solution into the primary system reduces the reactivity by 14.5 percent. Pertinent system volumes are:

Tank volume	330 gal
Normal volume of solution	120 gal
Maximum operating volume	130 gal
Minimum volume (low-level alarm point)	107 gal

The time required for injecting 120 gal of sodium-pentaborate solution is 16.65 sec. The minimum ejection time is for the minimum volume (107 gal at 7.2 gal/sec, or 14.85 sec).

The approval of Technical Specification Change No. 5A permitted the sodium-pentaborate solution to be maintained at a temperature not less than 20 F above the crystallization temperature of the solution (i.e., 90 F).

7. OTHER PLANT SYSTEMS

7.1 SHIELD COOLING SYSTEM (Task 501)

In the absence of a flowmeter, a heat-removal estimate was made for the system, based on the circulating-pump rating of 35 gpm. A heat removal rate of 175,000 Btu/hr was calculated from the 10 F temperature difference in the cooling circuit. A water meter was installed in the service water line in April of 1964 from a recommendation made the preceding December (see Fig. 29).

The heat removal rate thus far estimated for the shield cooling system is approximately 50 percent of the design value. This value will be confirmed or corrected in the next evaluation, when metered flow rates will be used. The design rate of 350,000 Btu/hr will probably not be needed to remove heat generated in the shield.

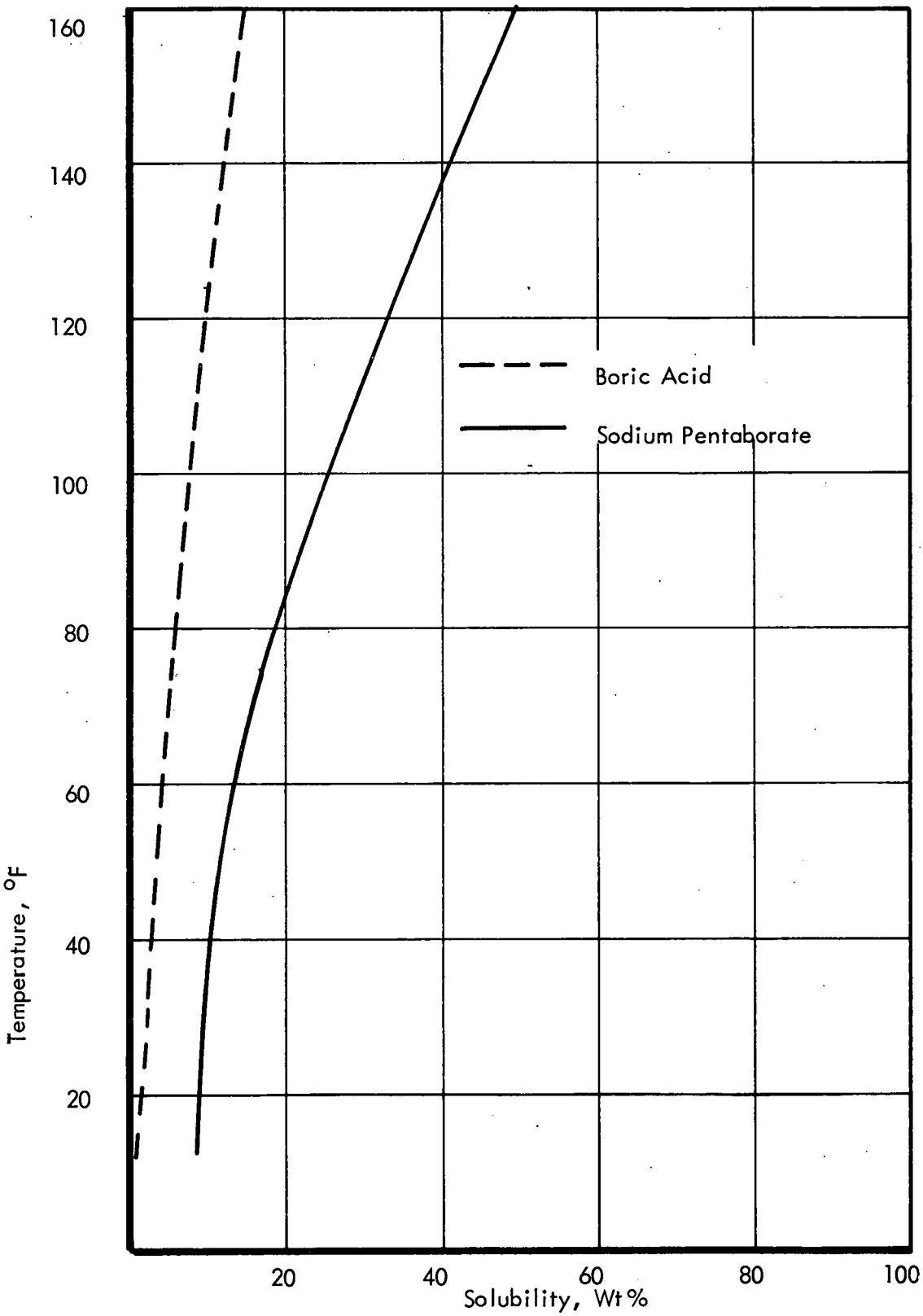

SOLUBILITY OF BORIC ACID AND SODIUM PENTABORATE FIG. 28

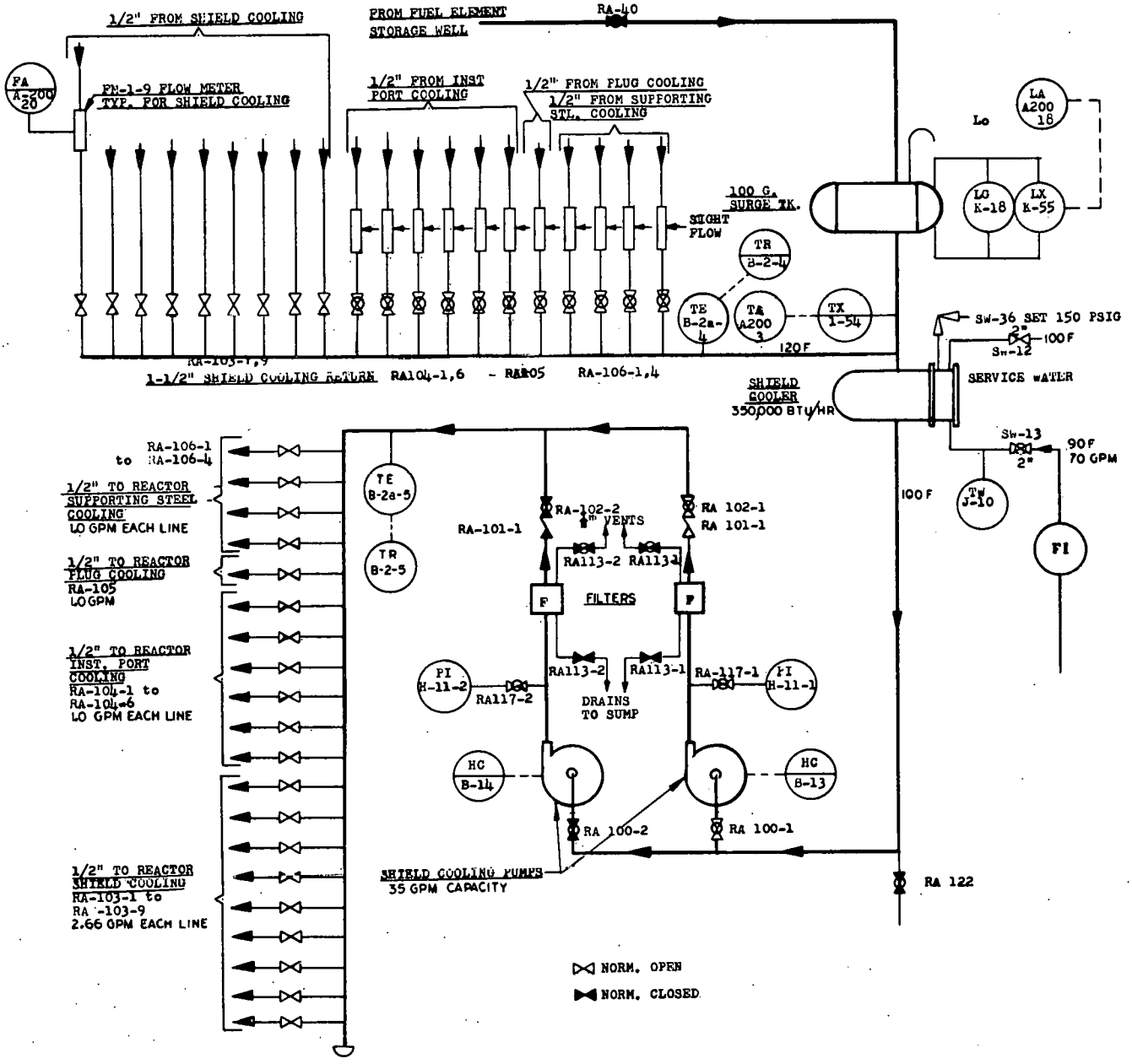

SHIELD COOLING SYSTEM FLOW DIAGRAM

FIG. 29

The reactor vessel, shielding, and shield cooling were patterned after EBWR. According to EBWR Test No. 18,[23] the shield cooling for EBWR was designed to remove 30 kw of heat (102,390 Btu/hr). Actually the equivalent of only 15 kw was removed during full-power operation.

8. MISCELLANEOUS EVALUATION

8.1 DECONTAMINATION AND WASTE DISPOSAL (Task 611)

One of the objectives of this task is to determine the long-term ERR decontamination and waste disposal requirements. Figure 30 is a schematic diagram showing the present liquid- and solid-waste disposal system. The quantities of wastes and their activity levels are estimated from plant operation through the 28-day full-power run.

8.1.1 Solid Wastes

Combustible solid wastes -- paper, rubber gloves, etc. -- are placed in plastic bags within 55-gal drums. These wastes are shipped to a burial ground for disposal. The total volume of the waste could be reduced by compressing and baling. Incineration of combustible wastes is not considered practical because of problems of controlling smoke and particulate carryover. Presently, the main problem with this type of waste is the interim storage of drums prior to shipment.

Non-combustible solid wastes consist of ion-exchange resins, filters, strainers, and contaminated items of plant equipment. These wastes have not yet created disposal problems, since their activity is low. However, higher waste-activity levels may be expected as plant operating time increases. Contaminated items of plant equipment that require external shielding would probably be imbedded in concrete and shipped to a land burial site. A large piece of equipment would have to be cut into smaller pieces before shipment and burial. The results of Task 611 indicate a need for an interim storage area for solid wastes. Wastes having an activity level too high for immediate shipment could be allowed to decay prior to disposal.

Contaminated resins and filters have been of low enough activity to be disposed of with minimal shielding. However, higher levels may occur with continued reactor operation. The radioactive isotopes responsible for the activity are Fe-59, Co-58, Co-60, Mn-56, and Cr-51. The corrosion products deposited on the filters and resin beds can be disposed of most conveniently by shipment to a burial ground in shielded casks.

8.1.2 Liquid Wastes

During normal reactor operation, the liquid waste resulting from primary system leakage should not exceed 12 gal/day. Leakages of up to 140 gal/day were handled without difficulty during the 28-day full-power run. After minor repairs to the system, leakage should be reduced by a factor of ten.

When fuel is transferred from the reactor to the fuel-element storage well, approximately 27,000 gal of water will be required to fill the reactor cavity and the fuel-element storage

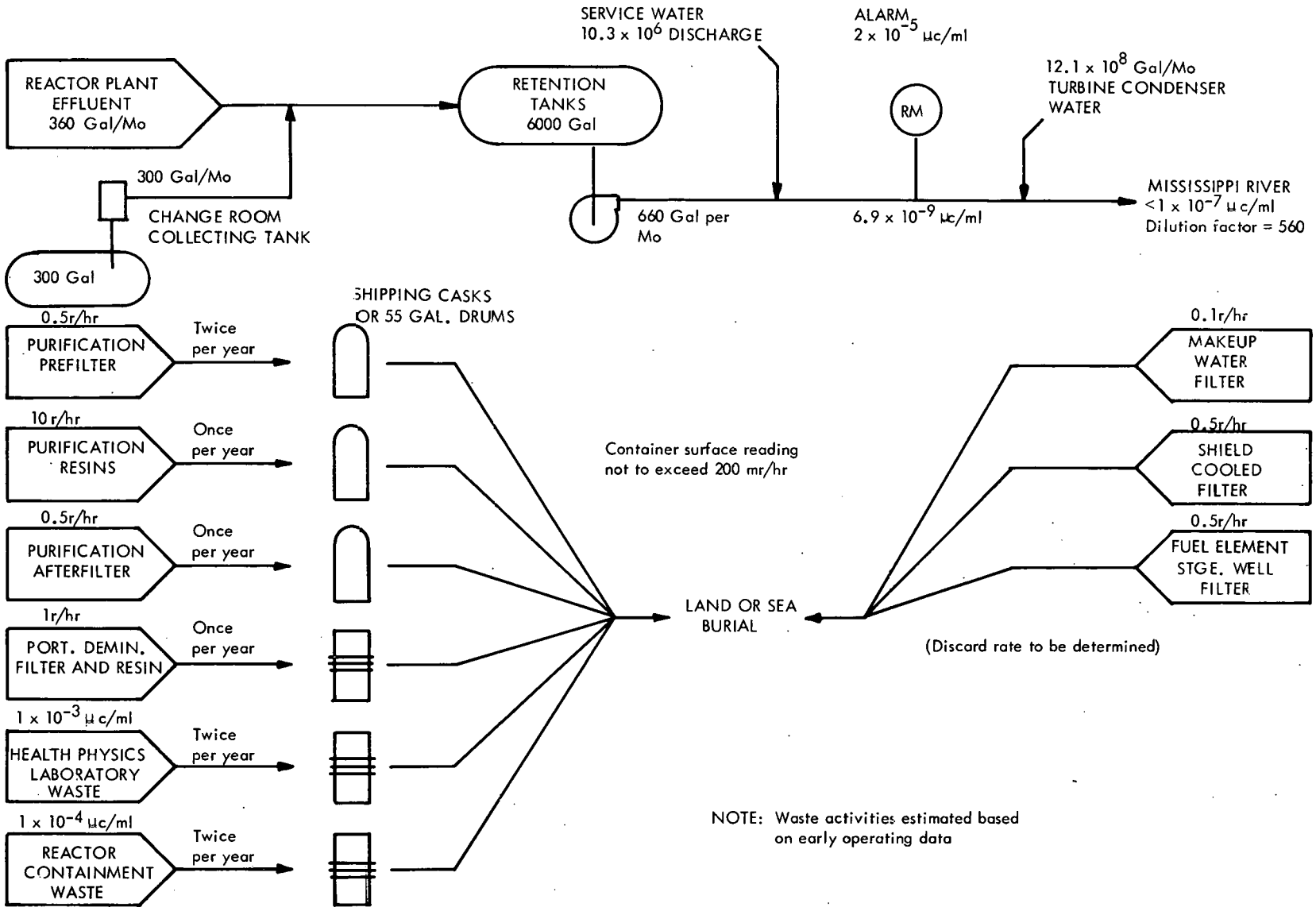

PRESENT LIQUID AND SOLID WASTE DISPOSAL SYSTEM

FIG. 30

well. The water will be supplied from the overhead storage tank and returned after the fuel transfer operations. The original plans outlined a procedure for purifying the reactor water and cavity fill water by means of the primary purification system and then transferring the decontaminated water to the overhead storage tank utilizing the decay-heat cooling pump. The fuel-element-storage-well water would be cleaned by the portable demineralizer and then pumped to the overhead storage tank by the fuel-element-storage-well pump. The volume of wastes handled during refueling should thus be much greater than for normal operation.

Consideration was given to the problems involved with this operation, particularly the waste problems that would result if the water is contaminated appreciably by the fuel-transfer operations. It was noted that if the overhead-storage-tank water is not replenished through the makeup water system, the volume would be below the 15,000 gal normally required for supplying the containment-building emergency spray system. The Hazards Reports and Operating Manuals do not indicate this specifically as a requirement during fuel transfer. However, makeup water could be added to the overhead storage tank at very low cost, and this excess water could be dumped after completion of the fuel transfer. One important consideration was the handling of contaminated reactor-cavity and storage-pool water in the event of fuel-element leaks. The initial intent was to clean the water by cyclic demineralization prior to its return to the overhead storage tank, according to the basic law of dilution:

$$C = C_o e^{-\lambda t}$$

Assuming, for example, that 20,000 gal of water are to be purified by a recirculation rate of 10 gpm to reduce the activity by a factor of 10, approximately 77 hr (3.2 days) would be required. Figure 31 illustrates the long cleanup time required for recirculation rates of 10 and 20 gpm to reduce the activity from 10^{-1} to 10^{-6}.

The simplest and most economical demineralization method would be to utilize the purification and portable systems, discharging the effluent through the retention tanks and replenishing the overhead storage tank with clean water. The pumping cost is negligible, and, at a cost of $4.76 per 1000 gal, fresh demineralized water would cost only $128.52 during each fuel-transfer operation.

8.1.3 Low Purity Aqueous Wastes

Evaporation of liquid waste is generally recommended for treating low-purity aqueous wastes (those generated by equipment decontamination, laundering operations, and laboratory operations) having total-solid concentrations between 500 and 5000 ppm. High-purity wastes are readily decontaminated by utilizing cartridge-type disposable filters and demineralizers. To date, there has been no need for waste evaporation facilities at ERR. The possibilities of such a system are being investigated as part of this task, but concentration of liquids by evaporation has not been used by either the EBWR or Dresden Plants (although both have such facilities).

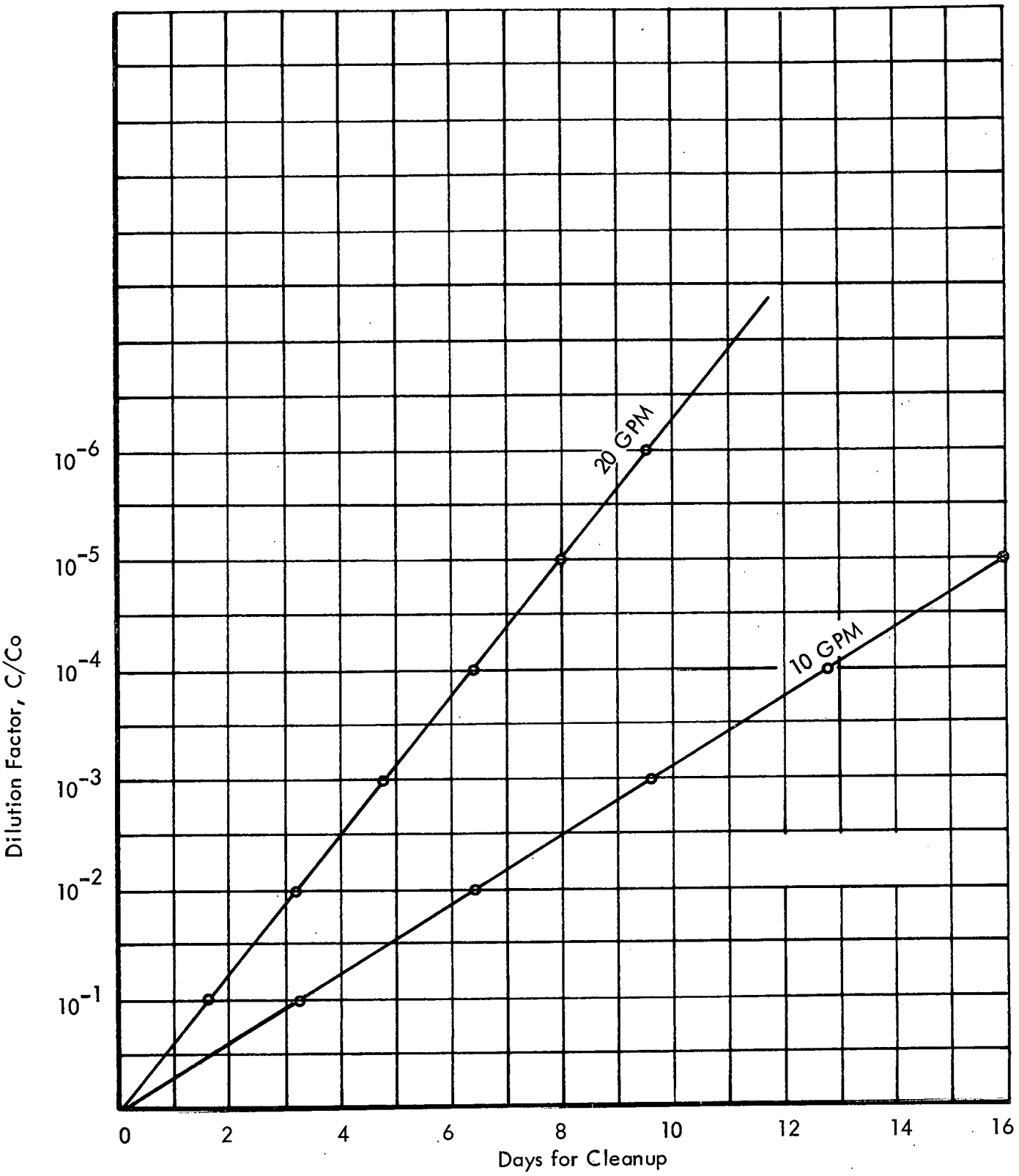

DEMINERALIZATION AND RECIRCULATION CLEANUP TIME FOR 20,000 GAL. OF ACTIVATED WATER

FIG. 31

Resin cost could be lowered by the use of regenerative-type ion exchangers. Resins can be regenerated either within a properly designed, regenerative ion-exchanger unit, or outside of the unit after the resins are sluiced to a separate vessel. Regenerative installations have the disadvantage of increasing the radioactive liquid wastes because of the caustic, acid, and rinse solutions that are used to regenerate the resins periodically. Approximately 200 gal of waste would be generated per cu ft of resin. The solids content would be between 5000 and 9000 ppm, and a waste evaporation facility would be a necessity. The estimated cost of a waste evaporation facility for the ERR is about $130,000, including a separate building of minimal-type construction. A preliminary evaluation indicates no real economic advantages for using a regenerative type resin system. The same volume of wastes is created whether the resins or the concentrated regenerants are buried, so waste storage costs would be about the same. The decreased regenerative resin cost must thus be evaluated in the light of increased capital cost for equipment and facilities.

8.1.4 Decontamination Requirements

Decontamination was required for the following:

1. decay heat pump;
2. recombiner cooler; and
3. primary water spillage in the vicinity of the purification system.

The first two involved decontamination of repairable equipment. The decay heat pump presented the biggest problem. It is a canned-rotor pump that previously had a bearing failure, which resulted in damage to the stator and rotor cans. Decontamination to acceptably low levels for return to the vendor was not possible, and "hot" machine-shop facilities had to be used to repair the pump. Possible recurrences of this type of problem are being taken into consideration, as well as decontamination problems,(e.g., fuel shipping cask decontamination,) that may arise in the future.

8.2 CASK HANDLING AND STORAGE (Task 612)

One of the objectives of this task is to evaluate the number, type, and size of all shipping containers of radioactive materials that are required for long-term ERR operation. The first containers to be studied are the resin- and filter-shipping casks. Shipment of these materials has not presented problems thusfar. Because of the low activity involved, resins and filters have been shipped in 55-gal drums. These resins were not fully depleted, however, and had not accumulated the radioactive contaminants expected for long-term reactor operation at power. The shielded shipping casks proposed previously are rather costly to be used as disposable containers since both a metal external container and a concrete inner container would have to be discarded. The following methods for cost reductions are being considered:

1. To retain the outer metal container as a shipping cask, disposing of only the concrete inner container. (The outer container is retained during shipment to comply with shipping regulations.)

2. To substitute a standard, hinged closure for the flanged and bolted head.

3. To reduce the number of welds.

4. To use an outer container suitable for accepting various concrete liners. Separate liners would be constructed for the resins and filters to be shipped.

8.3 CONTROL ROD DISPOSITION (Task 613)

The objective of this task is to establish removal and size-reduction procedures for the ERR control rods and to develop a preliminary design and cost estimate for the necessary facilities and equipment.

The following conclusions were made from a preliminary analysis of the control-rod disposition problem:

1. Control rods removed from the reactor can be stored temporarily by suspension from the lip of the pool in the fuel-element storage well, eliminating the need for special storage racks or extra provisions in the internal pool structures.

2. The size of the control rods has to be reduced before shipment. The most economical equipment for this purpose is a sawing device similar to that shown in ANL design drawing CS-2508. This sawing arrangement can be modified for use in the ERR pool, and plant air is available at the pool side to operate the saw.

3. A further reduction in control-rod size, (e.g., compacting the rod cruciform) should be considered for reducing the ultimate cost of rod disposal.

Further work in this task was deferred, pending an investigation by RCPA into the availability of a service organization for handling rod disposition.

9. REFERENCES

1. "Report on the Operation of the Elk River Reactor,"ACNP-63518, Rev. 1, August 1963

2. G.G. Bilodeau, et al., "PDQ - An IBM-704 Code to Solve the Two-dimensional Few-group Neutron Diffusion Equations," WAPD-TM-70, August 1957

3. G.D. Joanou and J.S. Dudek, "GAM-1, A Consistent P, Multigroup Code for the Calculation of Fast Neutron Spectra and Multigroup Cross Sections," GA-1850, June 1961

4. R.H. Shudde and J. Dyer, "TEMPEST-II, A Neutron Thermalization Code," AMTD-111, May 1961

5. "ERR-OAP Semiannual Progress Report,"ACNP-63605, January 1964

6. J.W. Weil, "Neutron Flux Distribution Calculation Using the P_3 Spherical Harmonic Method," KAPL-1173, July 1954

7. I. Carlvik and B. Pershagen, "Calculation of the Ratio Between the Flux at the Surface and the Average Flux for a Cylindrical Fuel Pin," AEF-68.

8. B. Pershagen and T. Carlvik, "Calculation of the Ratio Between the Flux at the Surface and the Average Flux for a Cylindrical Fuel Pin," AEF-68

9. M.N. Audi, "Non-uniform Reactivity Effects in the Elk River Reactor," ACNP-61533, August 1961

10. "Report on the Full Power Operation of the Elk River Boiling Water Reactor," ACNP-64536, June 1964

11. E.D. Kendrick, M.N. Audi, C. Ho, "Topical Report - Task 205 - Fuel Loading for Second Core," ACNP-64536, April 1964

12. J.R. Fisher and C. Ho, "Topical Report - Task 204 - Control Rod Analysis," ACNP-64568, July, 1964

13. O.J. Marlowe, et al., "WANDA, A One-dimensional Few-group Diffusion Equation Code," WAPD-TM-28, November 1956

14. "Seventeenth Monthly Operational Report - Elk River Reactor," ACNP-64537, pp. 5-7, March 1964

15. "Elk River Operations Analysis Program Semiannual Progress Report," ACNP-63605, January 1964

16. C.R. Bergen, R.B. Jerman, T.P. Kruzic, A.C. Schafer, Jr., "Interim Report, Task 615 - Corrosion Samples and Tests - Evaporator Water Boxes," ACNP-64588, July 1964

17. "Results of Testing During Elk River Reactor and Integrated Power Escalation to 25 Mwt," ACNP-64515

18. H.A. Cataldi, C.F. Cheng, V.S. Musick, "Investigation of Erosion and Corrosion of Turbine Materials in Wet Oxygenated Steam," ASME Paper No. 57-A-134, January 1958

19. C.R. Breden, "Status of the Art Report -- Water Chemistry and Corrosion," Boiling Water Technology, Vol. II, ANL-6562, February 1963

20. "Monthly Progress Report for the Elk River Reactor, October 1963,"ACNP-63618

21. "Request for Change in the Technical Specification for the Elk River Reactor, Change Request No. 9," ACNP-64539, April 1964

22. "Request for Change in the Technical Specification for the Elk River Reactor, Change Request No. 5," ACNP-63574, July 22, 1963

23. V.M. Kolba, "EBWR Test Reports," ANL-6229, November 1960

APPENDIX A

The following is a list of the presently scoped tasks and objectives for the Elk River Operations Analysis Program.

Task Number	Title	Objective
101	Control Rod Worth	To determine changes in rod worth owing to burnup. To generate up-to-date calibration curves for use in other nuclear analyses (e.g., Tasks 102, 103, 104).
102	Reactivity History	To determine the amounts of total reactivity as a function of time and to determine the reactivity in temperature, voids, Xe, and burnup, as a function of time.
103	Power Distributions	To obtain the power distributions as a function of time and rod positions. To recommend changes in rod operation if distributions indicate they may be necessary.
104	Reactivity Coefficients	To determine the temperature and void coefficients as a function of time.
105	Stability Evaluation	To monitor the reactor power as a function of time to assure stable operation.
106	NVT at Test Sample Locations	To determine the nvt, at the location of the test samples and at the vessel wall, for neutrons of energies greater than 1 Mev.
201	Fuel Cycle Studies	To define the fuel management program that meets the thorium-recycle objectives of the Elk River Reactor.
202	Scheduling of Fuel Recycle to the ERR from CNEN's PCUT Plant	Th maintain an up-to-date schedule for recycle of fuel to the ERR from CNEN's PCUT Plant in Italy
203	Fuel Element Exposure	To determine, on a monthly basis, the isotopic inventory of the core.
204	Control Rod Analysis	To investigate types and sizes of rods that might be used as replacement rods. To determine

Task Number	Title	Objective
		advantages and disadvantages of said types. To provide information for detailed procurement specifications for replacement control rods.

The objective of the following eight tasks was to determine the degree to which the operating factors of the systems studied in each task conform to the design parameters and safety factors; to project on a continuing basis, the changes in operating parameters and safety factors as a function of operating time; and to predict the effect of such changes on plant operation.

303	Technical Analysis and Evaluation of the Superheater	
304	Technical Analysis and Evaluation of the Reactor Gross Power and Plant Heat Balance	
401	Technical Analysis and Evaluation of Reactor Water Purification System	
404	Control Rod Thimble Cooling System -- Technical Analysis and Evaluation	
406	Off-gas System -- Technical Analysis and Evaluation	
407	Boron Poison System -- Technical Analysis and Evaluation	
501	Shield Cooling	
601	Radiological Physics -- Data Analysis and Evaluation	
611	Decontamination Requirements and Waste Disposal	(1) To establish the decontamination and waste disposal requirements that must be anticipated for long-term reactor operation (15 to 20 years). (2) To develop a preliminary design and cost estimate that will serve these requirements. (3) To develop procedures for the use of these facilities.

Task Number	Title	Objective
612	Cask Handling and Storage	(1) To evaluate and determine the number, type, and size of all shipping containers of radioactive materials required for long-term operation of the plant. (2) To determine the cask decontamination, handling, and storage requirements. (3) To propose procedures and facilities to meet these requirements.
613	Control Rod Disposition	To establish removal and size reduction procedures for the ERR control rods and to develop preliminary design and cost estimates for the equipment and facilities involved.
614	Development of Design of Facilities and Equipment	To complete the design, specification, and data collection needed to procure the equipment and facilities for approved ERR waste handling and decontamination facilities.
615	Corrosion Samples and Tests -- Evaporator Water Boxes	To prepare corrosion specimens for insertion into the evaporator water boxes. To evaluate the results of the corrosion tests at periodic intervals.
616	Radiolytic Gas Sampling Program	To determine the amount of hydrogen and oxygen in the primary steam and water at various points. To utilize these data for a long-term analysis of radiolytic (H_2O and O_2) gas production and to relate the information obtained to the results of the corrosion test (Task 615).